Supplement of Atmos. Chem. Phys., 25, 4477–4504, 2025
https://doi.org/10.5194/acp-25-4477-2025-supplement


Atmospheric Chemistry and Physics
Open Access

*Supplement of*

# Measurement report: A complex street-level air quality observation campaign in a heavy-traffic area utilizing the multivariate adaptive regression splines method for field calibration of low-cost sensors

**Petra Bauerová et al.**

*Correspondence to:* Petra Bauerová (petra.bauerova@chmi.cz)

This document is the Supplement containing all additional information (descriptions, tables and figures) for the "Measurement report: A complex street-level air quality observation campaign in a heavy traffic area utilizing the multivariate adaptive regression splines method for field calibration of low-cost sensors".

## S1 Introduction

**Table S1.** Summary statistics of 1-hour average NO, $NO_x$ and $NO_2$ concentrations (ppb) measured by all traffic reference monitoring (RM) stations in Prague (ALEGA = Prague 2-Legerova, AKALA = Prague 8-Karlín, AVYNA = Prague 9-Vysočany, AHOLA = Prague 7-Holešovice). Valid N = number of valid values, % valid = percentage of valid values in the dataset, CI mean = lower and upper confidence interval of mean, Min = minimum value, Max = maximum value, SD = standard deviation, CI SD = lower and upper confidence interval of standard deviation, SE = standard error of mean. Statistics done on the period from 1 June 2022 to 28 March 2023.

| Variable | Valid N | % Valid | Mean | CI mean (lower) | CI mean (upper) | Median | Min | Max | SD | CI SD (lower) | CI SD (upper) | SE mean |
|---|---|---|---|---|---|---|---|---|---|---|---|---|
| NO ALEGA[a] | 6783 | 93.90 | 27.13 | 26.40 | 27.87 | 15.30 | 0.40 | 283.57 | 30.85 | 30.34 | 31.38 | 0.37 |
| $NO_x$ ALEGA | 6783 | 93.90 | 47.38 | 46.47 | 48.28 | 36.12 | 1.62 | 326.31 | 38.08 | 37.45 | 38.73 | 0.46 |
| **$NO_2$ ALEGA** | **6783** | **93.90** | **20.20** | **19.96** | **20.45** | **18.82** | **0.52** | **63.63** | **10.37** | **10.20** | **10.55** | **0.13** |
| NO AKALA[b] | 6913 | 95.69 | 9.33 | 8.98 | 9.68 | 3.21 | 0.40 | 136.30 | 14.93 | 14.68 | 15.18 | 0.18 |
| $NO_x$ AKALA | 6913 | 95.69 | 22.92 | 22.46 | 23.38 | 16.78 | 1.78 | 161.59 | 19.70 | 19.37 | 20.03 | 0.24 |
| **$NO_2$ AKALA** | **6913** | **95.69** | **13.56** | **13.39** | **13.73** | **12.39** | **1.62** | **69.33** | **7.27** | **7.15** | **7.39** | **0.09** |
| NO AVYNA[c] | 6838 | 94.66 | 16.00 | 15.46 | 16.53 | 7.53 | 0.40 | 234.21 | 22.57 | 22.20 | 22.96 | 0.27 |
| $NO_x$ AVYNA | 6838 | 94.66 | 31.01 | 30.36 | 31.65 | 22.69 | 1.73 | 267.71 | 27.24 | 26.79 | 27.70 | 0.33 |
| **$NO_2$ AVYNA** | **6838** | **94.66** | **14.97** | **14.79** | **15.14** | **13.80** | **1.10** | **50.93** | **7.36** | **7.24** | **7.49** | **0.09** |
| NO AHOLA[d] | 6887 | 95.33 | 15.48 | 14.97 | 15.99 | 6.33 | 0.40 | 219.47 | 21.63 | 21.28 | 22.00 | 0.26 |
| $NO_x$_AHOLA | 7224 | 100.00 | 28.46 | 27.83 | 29.09 | 19.76 | 0.00 | 253.59 | 27.23 | 26.80 | 27.69 | 0.32 |
| **$NO_2$ AHOLA** | **6887** | **95.33** | **14.31** | **14.12** | **14.50** | **13.02** | **0.78** | **71.11** | **8.06** | **7.93** | **8.20** | **0.10** |

[a]coordinates: 50.0723878 N, 14.4306728 E; [b]coordinates: 50.0942383 N, 14.4420489 E; [c]coordinates: 50.1110803 N, 14.5030956 E; [d]coordinates: 50.1088447 N, 14.4436503 E.

## S2 Materials and methods

### S2.1 Study area and experimental design

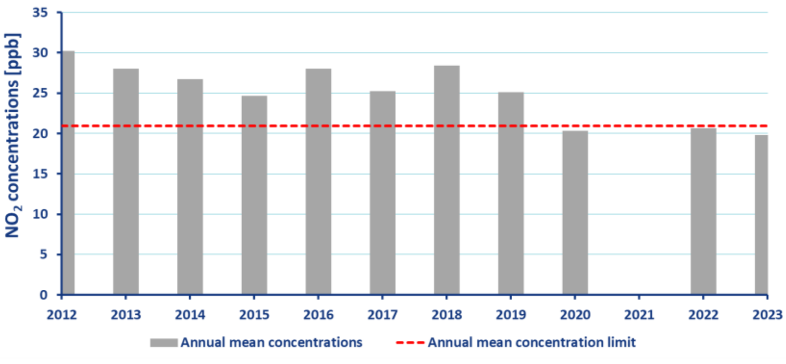


**Figure S1**. The annual mean concentrations of $NO_2$ (ppb) measured at Prague 2-Legerova AQM station (ALEGA) from 2012 to 2023. The red dashed line shows the annual EU/CZ limit value (i.e. 21 ppb ~ 40 μg·m$^{-3}$).

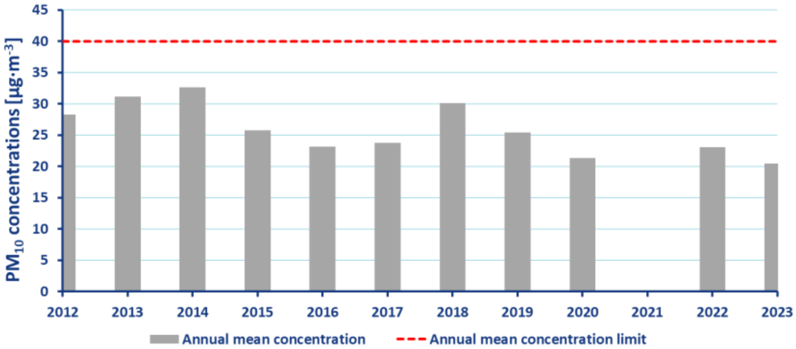


**Figure S2**. The annual mean concentrations of $PM_{10}$ ($\mu g \cdot m^{-3}$) measured at Prague 2-Legerova AQM station (ALEGA) from 2012 to 2023. The red dashed line shows the annual EU/CZ limit value (i.e. 40 $\mu g \cdot m^{-3}$).

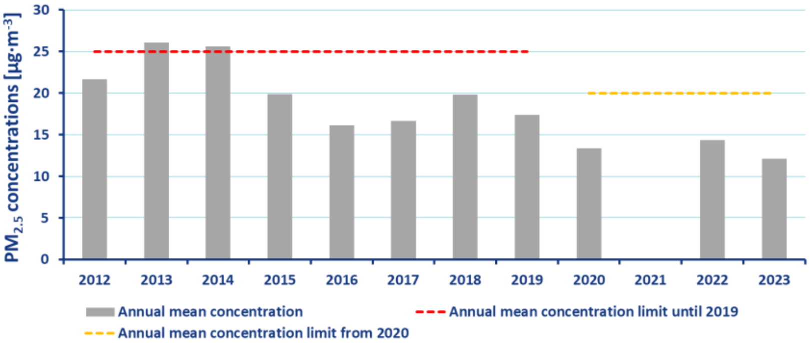


**Figure S3**. The annual mean concentrations of $PM_{2.5}$ ($\mu g \cdot m^{-3}$) measured at Prague 2-Legerova AQM station (ALEGA) from 2012 to 2023. The red dashed line shows the annual EU/CZ limit value (i.e. 40 $\mu g \cdot m^{-3}$), the yellow dashed line shows the applicable annual EU/CZ limit value from 2020.

**S2.2 Technical specification of instruments used and measurement methods**

As a supplementary non-reference meteorological measurement, the EnviMET mobile telescopic meteorological mast (further referred as MM; Envitech Bohemia, CZ) was installed on 1 June 2022 in the PVK garden (see Fig. S4a). This MM was equipped with a 2D ultrasonic anemometer WindSonic 60 (Gill Instruments, UK) for wind velocity (WV) and wind direction (WD; for technical details see Gill, 2023a) placed at a height of 7.5 m above the ground and further with the MetConnect THP weather station (Gill Instruments, UK) for temperature (TMP), relative humidity (RH) and atmospheric pressure (p) placed at 2 m above the ground (for technical details see Gill 2023b). The measurement frequency was set to 10-minute intervals in all variables and later averaged to 1-hour data.

The vertical profiles of TMP were measured with the MTP-5-He microwave radiometer (MWR; Attex, RU) installed on the roof of the Prague Karlov MS (Fig. S4b) on 23 February 2022. The MTP-5-He is a single channel passive MWR measuring at a frequency of 56.6 GHz with a maximum height range of 1,000 m and height resolution of 25 m from 0 to 100 m and 50 m from 100 to 1,000 m. The TMP accuracy is ±0.3 °C to ±1.2 °C (IFU, 2023). The measurement frequency was set to one vertical profile every 5 minutes. Beyond the measured TMPs, the mean TMP gradient and potential TMP profiles were calculated for further data processing (see section S2.3.2).

Furthermore, the radial velocity and backscatter intensity were measured by a Doppler LIDAR StreamLine XR (HALO Photonics, UK) installed on the PVK roof from 24 March 2022 (Fig. 4c). This Doppler LIDAR has an all-sky scanning head (full hemispherical coverage with 0.01° resolution in both axes) with the possibility of a variable user setting of laser pulse directions. The maximum height range is 1,200 m (highly dependent on the specific scan mode setting). The pulse rate is 10 kHz and the velocity precision <0.2 $m \cdot s^{-1}$ for signal-to-noise ratio (SNR) > -17 dB (Metek, 2023). The following three scanning modes were set: i) the VAD 6 mode with an elevation angle of 75° and azimuth step 60° for gaining processed vertical profiles of WV and WD; ii) the custom mode called “user 1” scanning a sector between azimuths of 130° to 160° while the elevation angle was gradually adjusted to values of 35° to 50° with a step of 5°; iii) the custom mode called “TKE” scanning a cone with an apex angle of 109.48° (the recommended elevation angle is 35.26°) in the continuous scanning mode (CSM; according to the method Smalikho and Banakh (2017) and the angular velocity was set to 5 deg·s$^{-1}$ (i.e. one rotation of 360° takes approximately 72 seconds). The total probing cycle for all scanning modes was set to 30 minutes, so for the TKE mode itself approximately 25 rotations were made in the meantime. The data gained were further processed before usage (see Sect. 2.3.3). In addition to the measurement listed above, TMP, RH, WD, WV and global radiation intensity (GLRD) data from MS Prague Libuš and Prague Karlov were used (especially for the correction of LCS data). The Karlov MS is also equipped with a CL51 Vaisala ceilometer (FI; Vaisala, 2022) measuring continuously the cloud base heights, backscatter intensity profile and mean mixing layer height (with a height range up to 1,500 m and measurement frequency of 16 seconds).


**Figure. S4**. Supplementary non-reference meteorological measurement used for TURBAN observation campaign: (a) mobile telescopic meteorological mast (MM, height 7.5 m) installed in PVK garden, (b) microwave radiometer MTP-5-He (MWR; for temperature profile measurement up to 1 km height) placed at the Karlov MS; (c) Doppler LIDAR StreamLine XR (for wind and backscatter intensity measurement up to 1.2 km height) placed at the PVK roof.

### S2.3 Data processing and statistical analyses

#### S2.3.1 MARS method for LCSs data correction

The Multivariate Adaptive Regression Splines (MARS) method was introduced by J.H. Friedman (1991b). The MARS algorithm is inherently nonlinear and builds model in three steps. First, it forms a set of so-called basis functions (BF). In this procedure, the range of predictor values is partitioned in several groups. For each group, a separate linear regression model is created, each with its own slope. The points of contact between the separate regression lines are referred as knots. The MARS algorithm automatically searches for the best locations to place the knots. Each knot has a pair of basis functions: $\{max(0, x - c), max(0, c - x)\}$, where $x$ denotes a continuous predictor; $c$ is an observed value of that predictor which is referred to as a knot. Basis functions are piecewise linear and each is used to model an isolated portion of the original data. For example, $max(0, x - c)$, which is symmetrical to $max(0, c - x)$, is a linear function of $x$ when $x>c$ but remains constantly zero otherwise. Suppose there are $p$ continuous predictors and they all have $n$ distinct values, then there will be such $np$ pairs of basis functions. In the second step a model-training process will iteratively select and add some of them into the model. MARS successively selects new terms into the model that minimize the sum of squared error using ordinary least squares (OLS). Initially, the basis function is added to the model and the result is a model with an intercept term. Subsequently, an original predictor or a reflected pair of hinge functions are selected and added to the model. The selected pair of basis functions (or original predictor) can enter the model directly; alternatively, they can be multiplied by an existing basis function that is already in the model and become new basis functions. The second case allows the interaction between (among) different predictors to be modelled. The reflected pair of basis functions always enter the model together (but may be removed separately in the pruning process). The training process continues until it meets one of selected conditions such as maximum number of model terms before pruning or forward stepping threshold measured by coefficient of determination ($R^2$). Finally, the very large model is built.

In the third step the pruning is applied (like for tree-based models) to avoid overfitting by iteratively removing basis functions whose contribution to the quality of the model is marginal. MARS typically applies a backward deletion procedure to prune the model. Step by step, the algorithm removes a term in the model that results in the smallest increase in the sum of squared error, obtaining an optimal model at each size. The final model is determined using generalized cross-validation (GCV) which is preferred as computationally efficient. A comprehensive and detailed description of the MARS with illustrative examples might be found in Friedman (1991a), Leathwick et al. (2006) and Everingham and Sexton (2011).

**Table S2.** Summary statistics of $NO_2$ MARS correction models performance for each LCS. Observed = $NO_2$_RM (reference concentrations), predicted = $NO_2$_SxC (corrected concentrations), independent variables: $NO_2$_SxR, TMP, RH, WV, GLRD and hour. No. of NA = number of missing values, No. of terms = number of terms used in MARS equation, No. basis functions used in MARS correction, GCV error = generalised cross validation error of MARS equation, SD = standard deviation, $R^2$ = coefficient of determination (resulting from linear regression between observed and predicted variable).

| Statistics / Sensor ID | S2 | S3[a] | S4[b] | S5 | S6 | S7 | S8[c] | S9 | S10 | S11 | S12 | S13 | S14 | S15 | S16 | S18 | S19 | S20 |
|---|---|---|---|---|---|---|---|---|---|---|---|---|---|---|---|---|---|---|
| **No. of NA** | 1029 | 149 | 212 | 196 | 197 | 197 | 294 | 264 | 197 | 231 | 197 | 197 | 197 | 937 | 197 | 197 | 264 | 678 |
| **No. of terms** | 15 | 16 | 14 | 15 | 14 | 13 | 17 | 14 | 16 | 15 | 13 | 15 | 16 | 15 | 15 | 15 | 13 | 16 |
| **No. of basis functions** | 14 | 15 | 13 | 14 | 13 | 12 | 16 | 13 | 15 | 14 | 12 | 14 | 15 | 14 | 14 | 14 | 12 | 15 |
| **GCV error** | 1.36 | 0.47 | 0.59 | 0.76 | 1.26 | 0.76 | 2.04 | 0.92 | 0.69 | 4.05 | 0.80 | 0.98 | 1.38 | 1.13 | 1.00 | 0.75 | 0.79 | 0.80 |
| **Mean (observed)** | 7.89 | 6.88 | 8.54 | 8.04 | 8.04 | 8.04 | 7.13 | 8.05 | 8.03 | 8.06 | 8.04 | 8.04 | 8.04 | 8.17 | 8.04 | 8.04 | 8.05 | 8.00 |
| **SD (observed)** | 6.21 | 5.23 | 6.81 | 6.14 | 6.14 | 6.14 | 5.04 | 6.15 | 6.14 | 6.16 | 6.14 | 6.14 | 6.14 | 6.36 | 6.14 | 6.14 | 6.15 | 6.26 |
| **Mean (predicted)** | 7.89 | 6.88 | 8.54 | 8.04 | 8.04 | 8.04 | 7.13 | 8.05 | 8.03 | 8.06 | 8.04 | 8.04 | 8.04 | 8.17 | 8.04 | 8.04 | 8.05 | 8.00 |
| **SD (predicted)** | 6.10 | 5.19 | 6.77 | 6.08 | 6.04 | 6.08 | 4.84 | 6.08 | 6.08 | 5.83 | 6.08 | 6.06 | 6.03 | 6.27 | 6.06 | 6.08 | 6.09 | 6.20 |
| **Mean (residual)** | 0.00 | 0.00 | 0.00 | 0.00 | 0.00 | 0.00 | 0.00 | 0.00 | 0.00 | 0.00 | 0.00 | 0.00 | 0.00 | 0.00 | 0.00 | 0.00 | 0.00 | 0.00 |
| **SD (residual)** | 1.15 | 0.67 | 0.76 | 0.86 | 1.12 | 0.86 | 1.42 | 0.95 | 0.82 | 2.00 | 0.89 | 0.98 | 1.17 | 1.05 | 0.99 | 0.86 | 0.88 | 0.89 |
| **$R^2$** | 0.97 | 0.98 | 0.99 | 0.98 | 0.97 | 0.98 | 0.92 | 0.98 | 0.98 | 0.89 | 0.98 | 0.97 | 0.96 | 0.97 | 0.97 | 0.98 | 0.98 | 0.98 |
| **$R^2$ adjusted** | 0.97 | 0.98 | 0.99 | 0.98 | 0.97 | 0.98 | 0.92 | 0.98 | 0.98 | 0.89 | 0.98 | 0.97 | 0.96 | 0.97 | 0.97 | 0.98 | 0.98 | 0.98 |

[a]S3 shorter validation period than other sensors (from December 16, 2021 to February 23, 2022); [b]S4 shorter validation period than other sensors (from December 16, 2021 to March 24, 2022); [c]S8 special validation dataset (from May 22, 2022 to January 31, 2023) - used as a replacement sensor for a broken one.

**Table S3.** The frequency of use of each independent variable in the $NO_2$ MARS correction equations, which sets the number of basis functions for particular sensors (i.e. the sum of frequencies for particular sensors).

| Independent variable / Sensor ID | S2 | S3[a] | S4[b] | S5 | S6 | S7 | S8[c] | S9 | S10 | S11 | S12 | S13 | S14 | S15 | S16 | S18 | S19 | S20 |
|---|---|---|---|---|---|---|---|---|---|---|---|---|---|---|---|---|---|---|
| **$NO_2$_SxR** | 3 | 3 | 2 | 4 | 2 | 3 | 2 | 3 | 3 | 3 | 3 | 4 | 3 | 2 | 3 | 3 | 4 | 4 |
| **TMP** | 3 | 4 | 3 | 3 | 4 | 3 | 4 | 4 | 2 | 2 | 3 | 3 | 4 | 3 | 2 | 3 | 3 | 3 |
| **RH** | 3 | 1 | 3 | 3 | 1 | 1 | 2 | 1 | 3 | 2 | 1 | 2 | 2 | 1 | 3 | 4 | 1 | 1 |
| **WV** | 1 | 2 | 2 | 2 | 3 | 2 | 2 | 2 | 2 | 2 | 2 | 2 | 3 | 2 | 3 | 2 | 2 | 2 |
| **GLRD** | 2 | 3 | 2 | 1 | 2 | 2 | 3 | 2 | 2 | 3 | 2 | 2 | 2 | 4 | 2 | 1 | 1 | 3 |
| **hour of the day** | 2 | 2 | 1 | 1 | 1 | 1 | 3 | 1 | 3 | 2 | 1 | 1 | 1 | 2 | 1 | 1 | 1 | 2 |

[a]S3 shorter validation period than other sensors (from December 16, 2021 to February 23, 2022); [b]S4 shorter validation period than other sensors (from December 16, 2021 to March 24, 2022); [c]S8 special validation dataset (from May 22, 2022 to January 31, 2023) - used as a replacement sensor for a broken one.

**Table S4.** Summary statistics of $O_3$ MARS correction models performance for each LCS. Observed = $O_3$_RM (reference concentrations), predicted = $O_3$_SxC (corrected concentrations), independent variables: $O_3$_SxR, ratio_$O_3$/$NO_2$_SxR, TMP, RH, WV, GLRD, hour. No. of NA = number of missing values, No. of terms = number of terms, GCV error = generalised cross validation error, SD = standard deviation, $R^2$ = coefficient of determination.

| **Variable / Sensor ID** | **S2** | **S3[a]** | **S4[b]** | **S5** | **S6** | **S7** | **S8[c]** | **S9** | **S10** | **S11** | **S12** | **S13** | **S14** | **S15** | **S16** | **S18** | **S19** | **S20** |
|---|---|---|---|---|---|---|---|---|---|---|---|---|---|---|---|---|---|---|
| **No. of NA** | 1864 | 211 | 310 | 198 | 200 | 200 | 296 | 334 | 200 | 234 | 200 | 200 | 200 | 1680 | 200 | 200 | 334 | 1162 |
| **No. of terms** | 16 | 14 | 15 | 14 | 17 | 16 | 17 | 16 | 16 | 16 | 12 | 16 | 15 | 16 | 16 | 16 | 18 | 16 |
| **No. of basis functions** | 15 | 13 | 14 | 13 | 16 | 15 | 16 | 15 | 15 | 15 | 11 | 15 | 14 | 15 | 15 | 15 | 17 | 15 |
| **GCV error** | 9.51 | 6.07 | 7.15 | 14.18 | 6.48 | 12.49 | 19.75 | 11.26 | 10.08 | 15.40 | 10.89 | 12.30 | 10.16 | 7.51 | 11.16 | 10.54 | 9.84 | 5.84 |
| **Mean (observed)** | 32.23 | 23.51 | 25.04 | 29.37 | 29.37 | 29.37 | 24.08 | 29.42 | 29.38 | 29.21 | 29.37 | 29.37 | 29.37 | 26.87 | 29.37 | 29.37 | 29.42 | 27.69 |
| **SD (observed)** | 13.00 | 9.35 | 11.13 | 13.30 | 13.30 | 13.30 | 16.53 | 13.38 | 13.30 | 13.16 | 13.30 | 13.30 | 13.30 | 11.28 | 13.30 | 13.30 | 13.38 | 11.90 |
| **Mean (predicted)** | 32.23 | 23.51 | 25.04 | 29.37 | 29.37 | 29.37 | 24.08 | 29.42 | 29.38 | 29.21 | 29.37 | 29.37 | 29.37 | 26.87 | 29.37 | 29.37 | 29.42 | 27.69 |
| **SD (predicted)** | 12.64 | 9.03 | 10.81 | 12.77 | 13.06 | 12.83 | 15.93 | 12.96 | 12.92 | 12.58 | 12.89 | 12.84 | 12.92 | 10.95 | 12.88 | 12.91 | 13.02 | 11.66 |
| **Mean (residual)** | 0.00 | 0.00 | 0.00 | 0.00 | 0.00 | 0.00 | 0.00 | 0.00 | 0.00 | 0.00 | 0.00 | 0.00 | 0.00 | 0.00 | 0.00 | 0.00 | 0.00 | 0.00 |
| **SD (residual)** | 3.05 | 2.42 | 2.64 | 3.74 | 2.52 | 3.51 | 4.42 | 3.33 | 3.15 | 3.89 | 3.28 | 3.48 | 3.16 | 2.71 | 3.31 | 3.22 | 3.11 | 2.39 |
| **$R^2$** | 0.94 | 0.93 | 0.94 | 0.92 | 0.96 | 0.93 | 0.93 | 0.94 | 0.94 | 0.91 | 0.94 | 0.93 | 0.94 | 0.94 | 0.94 | 0.94 | 0.95 | 0.96 |
| **$R^2$ adjusted** | 0.94 | 0.93 | 0.94 | 0.92 | 0.96 | 0.93 | 0.93 | 0.94 | 0.94 | 0.91 | 0.94 | 0.93 | 0.94 | 0.94 | 0.94 | 0.94 | 0.95 | 0.96 |

[a]S3 shorter validation period than other sensors (from December 16, 2021 to February 23, 2022); [b]S4 shorter validation period than other sensors (from December 16, 2021 to March 24, 2022); [c]S8 special validation dataset (from May 22, 2022 to January 31, 2023) - used as a replacement sensor for a broken one.

**Table S5.** The frequency of use of each independent variable in the $O_3$ MARS correction equations, which sets the number of basis functions for particular sensors (i.e. the sum of frequencies for particular sensors).

| **Independent variable / Sensor ID** | **S2** | **S3[a]** | **S4[b]** | **S5** | **S6** | **S7** | **S8[c]** | **S9** | **S10** | **S11** | **S12** | **S13** | **S14** | **S15** | **S16** | **S18** | **S19** | **S20** |
|---|---|---|---|---|---|---|---|---|---|---|---|---|---|---|---|---|---|---|
| **$O_3$_SxR** | 4 | 2 | 4 | 2 | 3 | 4 | 4 | 4 | 3 | 4 | 3 | 4 | 3 | 2 | 3 | 3 | 2 | 3 |
| **ratio_$O_3$/$NO_2$_SxR** | 4 | 3 | 3 | 3 | 4 | 2 | 3 | 4 | 3 | 1 | 4 | 3 | 4 | 4 | 3 | 3 | 3 | 3 |
| **TMP** | 2 | 3 | 2 | 3 | 3 | 3 | 3 | 3 | 2 | 4 | 1 | 4 | 2 | 1 | 3 | 3 | 2 | 4 |
| **RH** | 3 | 2 | 2 | 1 | 2 | 3 | 2 | 2 | 2 | 2 | 2 | 2 | 2 | 3 | 2 | 2 | 2 | 3 |
| **WV** | 2 | 2 | 2 | 1 | 2 | 2 | 0 | 2 | 2 | 2 | 1 | 2 | 2 | 2 | 2 | 2 | 3 | 0 |
| **GLRD** | 0 | 1 | 1 | 1 | 0 | 1 | 2 | 0 | 1 | 2 | 0 | 0 | 1 | 0 | 0 | 0 | 3 | 2 |
| **hour of the day** | 0 | 0 | 0 | 2 | 2 | 0 | 2 | 0 | 2 | 0 | 0 | 0 | 0 | 3 | 2 | 2 | 2 | 0 |

[a]S3 shorter validation period than other sensors (from December 16, 2021 to February 23, 2022); [b]S4 shorter validation period than other sensors (from December 16, 2021 to March 24, 2022); [c]S8 special validation dataset (from May 22, 2022 to January 31, 2023) - used as a replacement sensor for a broken one.

**Table S6.** Summary statistics of $PM_{10}$ MARS correction model performance for each LCS. Observed = $PM_{10}$_EM (reference concentrations from equivalent monitor), predicted = $PM_{10}$_SxC (corrected concentrations), independent variables: $PM_{10}$_SxR, TMP, RH, WV, GLRD, hour. No. of NA = number of missing values, No. of terms = number of terms, GCV error = generalised cross validation error, SD = standard deviation, $R^2$ = coefficient of determination.

| Variable / Sensor ID | S2 | S3[a] | S4[b] | S5 | S6 | S7 | S8[c] | S9 | S10 | S11 | S12 | S13 | S14 | S15 | S16 | S18 | S19 | S20 |
|---|---|---|---|---|---|---|---|---|---|---|---|---|---|---|---|---|---|---|
| **No. of NA** | 232 | 288 | 318 | 215 | 218 | 216 | 762 | 316 | 217 | 248 | 229 | 235 | 240 | 959 | 235 | 220 | 291 | 709 |
| **No. of terms** | 17 | 13 | 14 | 15 | 16 | 17 | 14 | 16 | 15 | 15 | 17 | 15 | 16 | 17 | 17 | 16 | 17 | 15 |
| **No. of basis functions** | 16 | 12 | 13 | 14 | 15 | 16 | 13 | 15 | 14 | 14 | 16 | 14 | 15 | 16 | 16 | 15 | 16 | 14 |
| **GCV error** | 26.21 | 7.94 | 22.66 | 28.44 | 26.28 | 26.83 | 23.51 | 29.67 | 28.11 | 31.79 | 28.38 | 38.69 | 29.17 | 30.05 | 29.01 | 32.96 | 27.66 | 27.85 |
| **Mean (observed)** | 19.29 | 12.48 | 19.00 | 19.22 | 19.23 | 19.22 | 13.98 | 19.47 | 19.23 | 19.37 | 19.28 | 19.31 | 19.33 | 18.85 | 19.31 | 19.24 | 19.36 | 18.62 |
| **SD (observed)** | 15.06 | 9.76 | 15.36 | 15.07 | 15.07 | 15.07 | 9.58 | 15.15 | 15.07 | 15.05 | 15.06 | 15.06 | 15.06 | 15.04 | 15.06 | 15.07 | 15.16 | 14.56 |
| **Mean (predicted)** | 19.29 | 12.48 | 19.00 | 19.22 | 19.23 | 19.22 | 13.98 | 19.47 | 19.23 | 19.37 | 19.28 | 19.31 | 19.33 | 18.85 | 19.31 | 19.24 | 19.36 | 18.62 |
| **SD (predicted)** | 14.18 | 9.36 | 14.62 | 14.11 | 14.18 | 14.17 | 8.28 | 14.15 | 14.12 | 13.98 | 14.11 | 13.74 | 14.07 | 14.02 | 14.08 | 13.95 | 14.23 | 13.59 |
| **Mean (residual)** | 0.00 | 0.00 | 0.00 | 0.00 | 0.00 | 0.00 | 0.00 | 0.00 | 0.00 | 0.00 | 0.00 | 0.00 | 0.00 | 0.00 | 0.00 | 0.00 | 0.00 | 0.00 |
| **SD (residual)** | 5.07 | 2.77 | 4.70 | 5.29 | 5.08 | 5.13 | 4.82 | 5.40 | 5.26 | 5.59 | 5.28 | 6.17 | 5.36 | 5.42 | 5.34 | 5.69 | 5.21 | 5.23 |
| **$R^2$** | 0.89 | 0.92 | 0.91 | 0.88 | 0.89 | 0.88 | 0.75 | 0.87 | 0.88 | 0.86 | 0.88 | 0.83 | 0.87 | 0.87 | 0.87 | 0.86 | 0.88 | 0.87 |
| **$R^2$ adjusted** | 0.89 | 0.92 | 0.91 | 0.88 | 0.89 | 0.88 | 0.75 | 0.87 | 0.88 | 0.86 | 0.88 | 0.83 | 0.87 | 0.87 | 0.87 | 0.86 | 0.88 | 0.87 |

[a]S3 shorter validation period than other sensors (from December 16, 2021 to February 23, 2022); [b]S4 shorter validation period than other sensors (from December 16, 2021 to March 24, 2022); [c]S8 special validation dataset (from May 22, 2022 to January 31, 2023) - used as a replacement sensor for a broken one.

**Table S7.** The frequency of use of each independent variable in the $PM_{10}$ MARS correction equations, which sets the number of basis functions for particular sensors (i.e. the sum of frequencies for particular sensors).

| Independent variable / Sensor ID | S2 | S3[a] | S4[b] | S5 | S6 | S7 | S8[c] | S9 | S10 | S11 | S12 | S13 | S14 | S15 | S16 | S18 | S19 | S20 |
|---|---|---|---|---|---|---|---|---|---|---|---|---|---|---|---|---|---|---|
| **$PM_{10}$_SxR** | 3 | 3 | 4 | 3 | 5 | 3 | 4 | 4 | 4 | 3 | 4 | 6 | 3 | 4 | 4 | 4 | 4 | 4 |
| **TMP** | 5 | 2 | 5 | 4 | 3 | 4 | 3 | 3 | 2 | 2 | 3 | 2 | 4 | 4 | 3 | 4 | 3 | 4 |
| **RH** | 2 | 3 | 2 | 2 | 2 | 3 | 2 | 2 | 3 | 3 | 3 | 2 | 2 | 2 | 2 | 2 | 2 | 2 |
| **WV** | 2 | 3 | 1 | 2 | 2 | 2 | 2 | 3 | 2 | 1 | 2 | 1 | 2 | 2 | 2 | 2 | 2 | 1 |
| **GLRD** | 2 | 1 | 0 | 2 | 2 | 2 | 0 | 2 | 0 | 2 | 2 | 1 | 1 | 2 | 2 | 2 | 3 | 2 |
| **hour of the day** | 2 | 0 | 1 | 1 | 1 | 2 | 2 | 1 | 3 | 3 | 2 | 2 | 3 | 2 | 3 | 1 | 2 | 1 |

[a]S3 shorter validation period than other sensors (from December 16, 2021 to February 23, 2022); [b]S4 shorter validation period than other sensors (from December 16, 2021 to March 24, 2022); [c]S8 special validation dataset (from May 22, 2022 to January 31, 2023) - used as a replacement sensor for a broken one.

**Table S8.** Summary statistics of $PM_{2.5}$ MARS correction model performance for each LCS. Observed = $PM_{2.5}$_EM (reference concentrations from equivalent monitor), predicted = $PM_{2.5}$_SxC (corrected concentrations), independent variables: $PM_{2.5}$_SxR, TMP, RH, WV, GLRD, hour. No. of NA = number of missing values, No. of terms = number of terms, GCV error = generalised cross validation error, SD = standard deviation, $R^2$ = coefficient of determination.

| Variable / Sensor ID | S2 | S3[a] | S4[b] | S5 | S6 | S7 | S8[c] | S9 | S10 | S11 | S12 | S13 | S14 | S15 | S16 | S18 | S19 | S20 |
|---|---|---|---|---|---|---|---|---|---|---|---|---|---|---|---|---|---|---|
| **No. of NA** | 243 | 302 | 333 | 236 | 231 | 224 | 764 | 335 | 225 | 267 | 245 | 245 | 250 | 966 | 254 | 229 | 302 | 726 |
| **No. of terms** | 15 | 15 | 16 | 15 | 17 | 15 | 14 | 16 | 17 | 16 | 13 | 16 | 15 | 16 | 15 | 14 | 16 | 16 |
| **No. of basis functions** | 14 | 14 | 15 | 14 | 16 | 14 | 13 | 15 | 16 | 15 | 12 | 15 | 14 | 15 | 14 | 13 | 15 | 15 |
| **GCV error** | 7.99 | 4.75 | 9.34 | 8.89 | 7.31 | 7.64 | 4.99 | 9.34 | 8.30 | 11.07 | 8.78 | 14.65 | 10.16 | 9.29 | 10.16 | 11.89 | 7.68 | 7.83 |
| **Mean (observed)** | 14.34 | 10.38 | 15.30 | 14.32 | 14.30 | 14.28 | 9.81 | 14.48 | 14.28 | 14.43 | 14.35 | 14.35 | 14.37 | 14.45 | 14.38 | 14.29 | 14.37 | 14.09 |
| **SD (observed)** | 12.48 | 9.03 | 12.80 | 12.48 | 12.48 | 12.48 | 8.02 | 12.56 | 12.48 | 12.48 | 12.48 | 12.48 | 12.48 | 12.09 | 12.48 | 12.48 | 12.57 | 11.75 |
| **Mean (predicted)** | 14.34 | 10.38 | 15.30 | 14.32 | 14.30 | 14.28 | 9.81 | 14.48 | 14.28 | 14.43 | 14.35 | 14.35 | 14.37 | 14.45 | 14.38 | 14.29 | 14.37 | 14.09 |
| **SD (predicted)** | 12.16 | 8.77 | 12.44 | 12.12 | 12.19 | 12.18 | 7.70 | 12.19 | 12.15 | 12.03 | 12.13 | 11.89 | 12.07 | 11.71 | 12.07 | 12.00 | 12.26 | 11.42 |
| **Mean (residual)** | 0.00 | 0.00 | 0.00 | 0.00 | 0.00 | 0.00 | 0.00 | 0.00 | 0.00 | 0.00 | 0.00 | 0.00 | 0.00 | 0.00 | 0.00 | 0.00 | 0.00 | 0.00 |
| **SD (residual)** | 2.80 | 2.13 | 3.01 | 2.96 | 2.68 | 2.74 | 2.22 | 3.03 | 2.86 | 3.30 | 2.94 | 3.80 | 3.16 | 3.02 | 3.16 | 3.42 | 2.75 | 2.77 |
| **$R^2$** | 0.95 | 0.94 | 0.94 | 0.94 | 0.95 | 0.95 | 0.92 | 0.94 | 0.95 | 0.93 | 0.94 | 0.91 | 0.94 | 0.94 | 0.94 | 0.92 | 0.95 | 0.94 |
| **$R^2$ adjusted** | 0.95 | 0.94 | 0.94 | 0.94 | 0.95 | 0.95 | 0.92 | 0.94 | 0.95 | 0.93 | 0.94 | 0.91 | 0.94 | 0.94 | 0.94 | 0.92 | 0.95 | 0.94 |

[a]S3 shorter validation period than other sensors (from December 16, 2021 to February 23, 2022); [b]S4 shorter validation period than other sensors (from December 16, 2021 to March 24, 2022); [c]S8 special validation dataset (from May 22, 2022 to January 31, 2023) - used as a replacement sensor for a broken one.

**Table S9.** The frequency of use of each independent variable in the $PM_{2.5}$ MARS correction equations, which sets the number of basis functions for particular sensors (i.e. the sum of frequencies for particular sensors).

| Independent variable / Sensor ID | S2 | S3[a] | S4[b] | S5 | S6 | S7 | S8[c] | S9 | S10 | S11 | S12 | S13 | S14 | S15 | S16 | S18 | S19 | S20 |
|---|---|---|---|---|---|---|---|---|---|---|---|---|---|---|---|---|---|---|
| **$PM_{2.5}$_SxR** | 3 | 4 | 5 | 3 | 4 | 6 | 4 | 5 | 4 | 5 | 4 | 3 | 5 | 5 | 4 | 5 | 5 | 5 |
| **TMP** | 3 | 2 | 3 | 4 | 2 | 2 | 4 | 2 | 2 | 2 | 2 | 2 | 2 | 1 | 3 | 2 | 2 | 2 |
| **RH** | 2 | 4 | 2 | 2 | 4 | 2 | 3 | 2 | 3 | 3 | 2 | 3 | 2 | 2 | 3 | 2 | 3 | 2 |
| **WV** | 3 | 2 | 3 | 2 | 2 | 2 | 1 | 3 | 3 | 2 | 2 | 3 | 2 | 2 | 2 | 2 | 2 | 3 |
| **GLRD** | 1 | 0 | 0 | 1 | 2 | 1 | 0 | 2 | 2 | 1 | 1 | 2 | 2 | 2 | 1 | 1 | 2 | 2 |
| **hour of the day** | 2 | 2 | 2 | 2 | 2 | 1 | 1 | 1 | 2 | 2 | 1 | 2 | 1 | 3 | 1 | 1 | 1 | 1 |

[a]S3 shorter validation period than other sensors (from December 16, 2021 to February 23, 2022); [b]S4 shorter validation period than other sensors (from December 16, 2021 to March 24, 2022); [c]S8 special validation dataset (from May 22, 2022 to January 31, 2023) - used as a replacement sensor for a broken one.

**Table S10.** Example of MARS correction equations for calculation of $NO_2$, $O_3$, $PM_{10}$ and $PM_{2.5}$ corrected concentrations in case of the LCS S2. $NO_2$_S2C, $O_3$_S2C, $PM_{10}$_S2C, $PM_{2.5}$_S2C = corrected LCSs concentrations for S2 (gases in ppb and aerosols in μg/m$^3$); $NO_2$_S2R, $O_3$_S2R, $PM_{10}$_S2R, $PM_{2.5}$_S2R = raw $NO_2$, $O_3$, $PM_{10}$ and $PM_{2.5}$ concentration measured by the LCS S2; TMP = air temperature (in °C); RH = relative humidity (in %); WV = wind velocity (in m/s); GLRD = solar radiation intensity (W/m$^2$); hour = hour of the day (UTC).

| Variable | MARS correction equation |
|---|---|
| $NO_2$_S2C | 18.91 + 1.67*MAX(0; $NO_2$_S2R-13.15) - 1.89*MAX(0; 13.15-$NO_2$_S2R) - 0.25*MAX(0; TMP-10.9) + 0.13*MAX(0; 10.9-TMP) - 0.004*MAX(0; GLRD-332.8) + 0.005*MAX(0; 332.8-GLRD) - 0.60*MAX(0; $NO_2$_S2R-5.41) + 0.03*MAX(0; 59.5-RH) + 0.19*MAX(0; hour-19) + 0.04*MAX(0; 19-hour) + 0.24*MAX(0; TMP-19.25) - 0.33*MAX(0; WV-4.5) + 0.05*MAX(0; RH-74.5) - 0.07*MAX(0; RH-86.5) |
| $O_3$_S2C | 32.50 + 0.79*MAX(0; $O_3$_S2R-23.21) - 0.79*MAX(0; 23.21-$O_3$_S2R) + 1.35*MAX(0; ratio_$O_3$_$NO_2$_S2R-3.07) - 5.92*MAX(0; 3.07-ratio_$O_3$_$NO_2$_S2R) - 0.12*MAX(0; RH-33.67) + 0.19*MAX(0; 33.67-RH) - 1.46*MAX(0; ratio_$O_3$_$NO_2$_S2R-6.61) + 0.39*MAX(0; WV-2.1) + 0.90*MAX(0; 2.1-WV) + 0.04*MAX(0; TMP-1.52) + 0.47*MAX(0; 1.52-TMP) + 0.30*MAX(0; $O_3$_S2R-32.91) - 0.65*MAX(0; $O_3$_S2R-48.38) + 3.38*MAX(0; ratio_$O_3$_$NO_2$_S2R-9.84) + 0.06*MAX(0; RH-80.17) |
| $PM_{10}$_S2C | 91.24 + 2.20*MAX(0; $PM_{10}$_S2R-48.33) - 1.51*MAX(0; 48.33-$PM_{10}$_S2R) - 0.27*MAX(0; RH-51.17) + 0.07*MAX(0; 51.17-RH) - 0.68*MAX(0; $PM_{10}$_S2R-5.70) - 0.83*MAX(0; WV-3.8) - 1.20*MAX(0; 3.8-WV) + 0.92*MAX(0; TMP-8.5) - 0.64*MAX(0; 8.5-TMP) + 0.14*MAX(0; hour-13) + 0.20*MAX(0; 13-hour) - 0.02*MAX(0; GLRD-641.1) - 0.004*MAX(0; 641.1-GLRD) - 1.19*MAX(0; TMP+0.5) + 0.56*MAX(0; TMP-4.92) - 2.69*MAX(0; TMP-26.42) |
| $PM_{2.5}$_S2C | 54.89 + 2.07*MAX(0; $PM_{2.5}$_S2R-34.98) - 1.35*MAX(0; 34.98-$PM_{2.5}$_S2R) - 0.15*MAX(0; RH-53.5) + 0.04*MAX(0; 53.5-RH) + 0.34*MAX(0; TMP-7.3) - 3.12*MAX(0; WV-5.2) - 0.97*MAX(0; 5.2-WV) - 0.60*MAX(0; $PM_{2.5}$_S2R-5.44) + 0.11*MAX(0; hour-18) + 0.06*MAX(0; 18-hour) - 0.33*MAX(0; TMP+0.5) - 0.001*MAX(0; 663.8-GLRD) + 4.39*MAX(0; WV-6.3) - 0.17*MAX(0; TMP-16.97) |

### S2.3.2 Meteorological data preparation and statistical analyses

In case of supplementary meteorological measurement the data preparation and data validation processes were as follows. All 10-minute data measured by the meteorological mast in the PVK garden (placed in 248,5 m a.s.l.), namely TMP, RH, p, WD and WV were indicatively compared to the referential data measured at the adjacent Prague Karlov MS (337 m aerial horizontal distance; 263 m a.s.l.) during the Legerova campaign (from 1 June 2022 to 19 April 2023; 322 days in total, n = 46389) by linear regression.

The vertical profiles of TMP measured by the MWR in the Prague Karlov MS were indicatively checked against TMP vertical profiles measured by radiosonde launched from the distant Prague Libuš MS during the period from 25 February 2022 to 24 March 2023 (392 days in total, n = 1172) by linear regression method. The 5-minute TMP data measured by the MWR and corresponding radiosonde data at selected heights above ground (0, 50, 100, 500, 750 and 1,000 m AGL) and selected times (times of radiosonde launching at 0, 6 and 12 UTC) were used for this comparison. Furthermore, the TMP gradients were calculated from the mean difference in 1-hour average TMPs measured by MWR between ground level and 200 m height above the ground. The interpolated meteorological profiles were later visualised with the Golden Software Surfer (version 19.4.3; Surfer, 2022). Furthermore, the profiles of the potential TMP were calculated (also from MWR data) based on Arya (2001) in the height layer between 260 and 1,260 m ASL with using the reference pressure at the Prague Karlov MS (altitude 260 m ASL) as follows:

1) $T = T_0(\frac{P}{P_0})^k$ (S1)

where $T_0$ is the temperature (TMP) corresponding to the reference pressure $P_0$ measured at the Prague Libuš MS (altitude 260 m ASL) and the exponent $k = \frac{R}{c_P} \cong 0.286$.

2) Eq. (S1) was used to relate the potential TMP $\theta$, defined as the TMP which an air parcel would have if it were brought down to a pressure of 1,000 mbar adiabatically from its innate state, to the actual TMP $T$ as

$\theta = T(\frac{1000}{P})^k$ (S2)

where $P$ is in millibars. The potential TMP has the convenient property of being conserved during vertical movements of an air parcel, provided heat is not added or removed during such excursions. Then, the parcel may be identified or labeled by its potential TMP. In an adiabatic atmosphere, potential TMP remains constant with height. For a nonadiabatic or diabatic atmosphere, it is easy to show from Eq. (S2) that, to a good approximation,

3) $\frac{\partial\theta}{\partial z} = \frac{\theta}{T}\left(\frac{\partial T}{\partial z} + \Gamma\right) \cong \frac{\partial T}{\partial z} + \Gamma$

(S3)

This approximation is particularly useful in the planetary boundary layer (PBL) where potential TMP and actual TMPs, in absolute units, do not usually differ by more than 10 %. The relationship in Eq. (S3) is often used to express the difference in the potential TMPs between any two height levels as

4) $\Delta\theta = \Delta T + \Gamma\Delta z$ (S4)

From the air TMP differences, the potential TMP differences between the individual layers were determined according to the relationship in Eq. (S4).

In the case of the Doppler LIDAR, the processed wind profile data (producing WV and WD at particular heights) from the VAD 6 scanning program were captured roughly every 33 minutes. The LIDAR wind profile data were not compared to any reference method or to the radiosonde data in this study because the comparison of winds between two distant stations (the Prague Libuš and the Prague Karlov) is inappropriate. Based on the LIDAR measurement, the turbulent kinetic energy (TKE) was calculated from the course of the radial wind component (Vr) gained during the TKE scan in the CSM regime with the elevation angle 35.26° lasting 30 minutes in a total of 25 cycles. To calculate the resulting value of TKE according to the Smalikho and Banakh (2017) method the standard deviation of Vr should be calculated for each range gate and each azimuth (from 25 values) and subsequently averaged over all azimuths. For detecting the maximum height of valuable wind profiles measured by the Doppler LIDAR (according to SNR values), two possible methods were tested. The first method was based on cutting the profile at a certain SNR threshold (i.e. cutting off the values with SNR>1.015 like in Tzadok et al., 2022; see the example in Fig. S5). The second method was based on the assumption that as the quality of the scattered LIDAR signal deteriorates (decrease in the signal-to-noise ratio), the variability of the velocity profile increases. The height level above which the variability exceeds the set limit was sought. The method was implemented in the following steps. Firstly, the standard deviation (SD) of the wind velocity (WV) was determined in a moving window over 5 height levels, starting from a level at 46.4 m AGL. Then the level of sudden increase in SD variability was sought using standardized double mass curve (DMCstd). The level of sudden increase in variability should be manifested by a break in the linear course of the DMCstd curve (Fig. S6a). A regression line (linear trend) was gradually interpolated through the DMCstd curve and the end point value of the interpolated line was determined. At a given height level, the magnitude of the deviation of the DMCstd curve value from this corresponding to the interpolated regression line was evaluated. Subsequently, the deviation was evaluated by the ratio of linear trend and DMCstd. If the linear course of the DMCstd curve was maintained (Fig. S6b), the value of this ratio was around 1. As the DMCstd deviation from the linear trend increases, this ratio also decreases. The level where we considered the deviation from the linear course to be significant was determined using the limit value of the linear trend/DMCstd ratio, e.g. 0.95. Finally, measured WV values above this level were discarded due to the high variability in the WV profile (resulting in WV cut, see Fig. S6c).

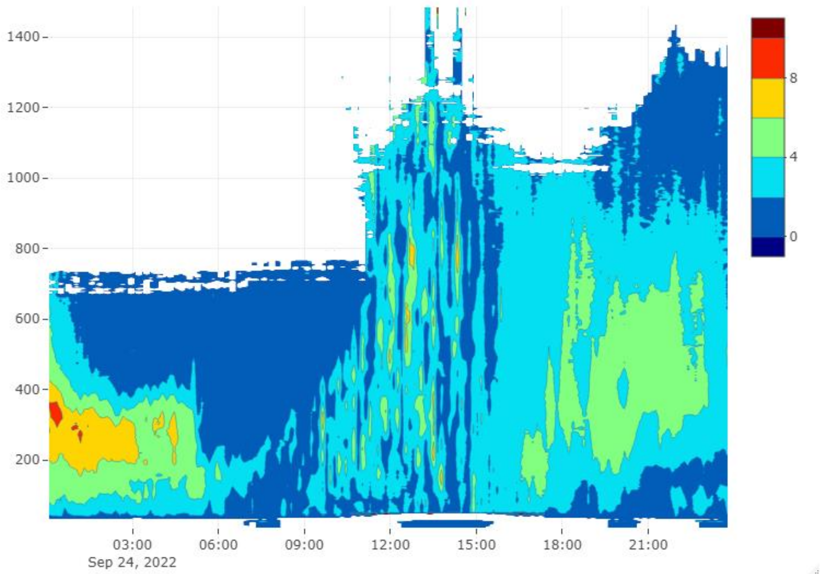


**Figure S5.** The example of adjusted wind velocity (WV; $m \cdot s^{-1}$) profile measured by doppler LIDAR on September 24, 2022 at PVK roof during measurement campaign. The values with signal-to-noise (SNR) ratio > 1.015 were cut off.

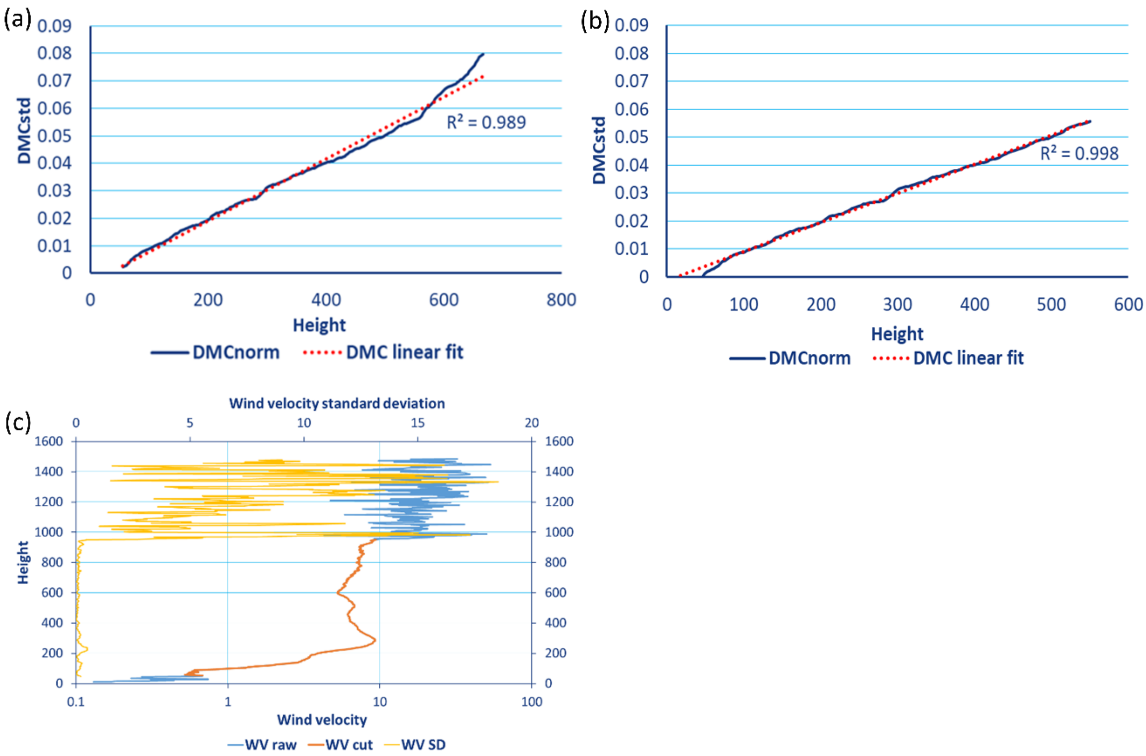


**Figure S6.** The example of cutting the raw wind profile data using standardised double mass curve (DMCstd) deviation from linear regression method; (a) example of satisfactory fitting between DMCstd and the linear trend; (b) example of DMCstd curve starting to deviate from the linear trend; (c) example of cutted wind velocity profile (WV cut) based on the variability of wind velocity standard deviation (WV SD) and DMCstd method.

## S3 Results

### S3.1 LCSs data quality and verification

#### S3.1.1 LCSs data quality during initial field comparative measurement at the Prague Libuš AQM station

**Table S11**. Descriptive statistics of all LCSs measurements during initial field comparative measurement. Shown coefficient of variation ± standard deviation of this coefficient for raw measured and MARS corrected concentrations (number of LCSs measurements compared N = 17; number of cases for mean CV and SD calculation n = 3959).

| | Raw LCS concentrations | MARS corrected LCS concentrations (COR) |
|---|---|---|
| | mean CV ± SD | mean CV ± SD |
| $NO_2$ | 27.69 ± 7.58 % | 9.25 ± 7.11 % |
| $O_3$ | 16.71 ± 2.62 % | 6.06 ± 4.90 % |
| $PM_{10}$ | 22.44 ± 9.33 % | 13.05 ± 15.29 % |
| $PM_{2.5}$ | 23.16 ± 9.94 % | 14.62 ± 15.42 % |

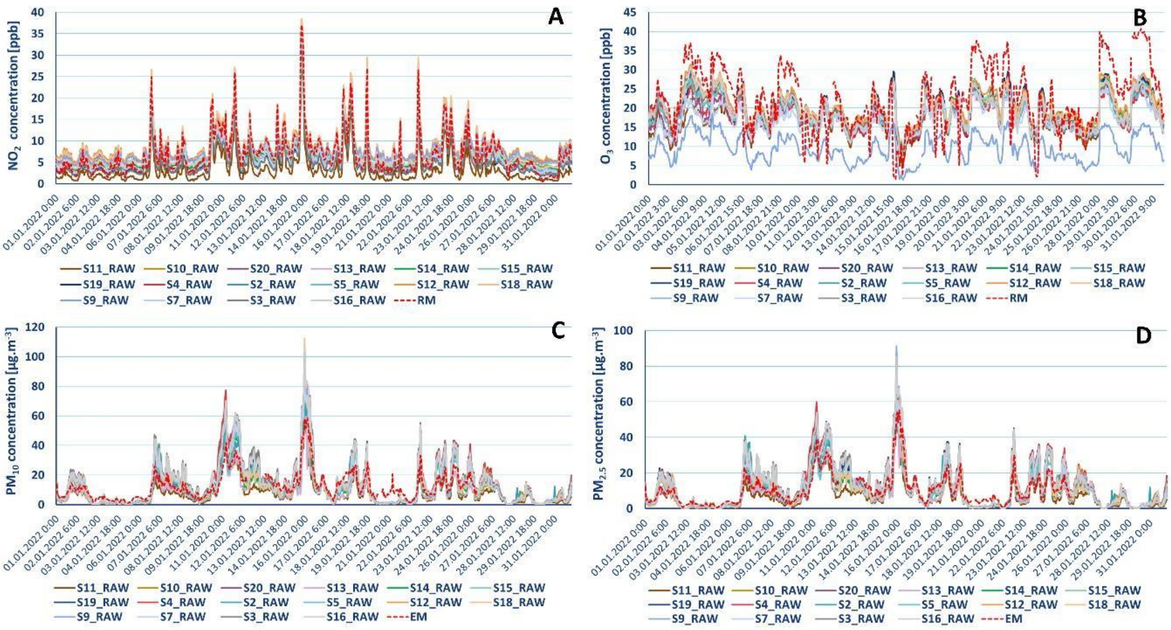


**Figure S7.** (a) Raw 1-hour average concentrations of $NO_2$, (b) $O_3$, (c) $PM_{10}$ and (d) $PM_{2.5}$ measured by all LCSs (marked as S2R, S3R, …S20R) in January 2022 during initial field comparative measurement at the Prague 4-Libuš AQM station (RM = reference monitor for gas measurement, EM = equivalent monitor for aerosol measurement).

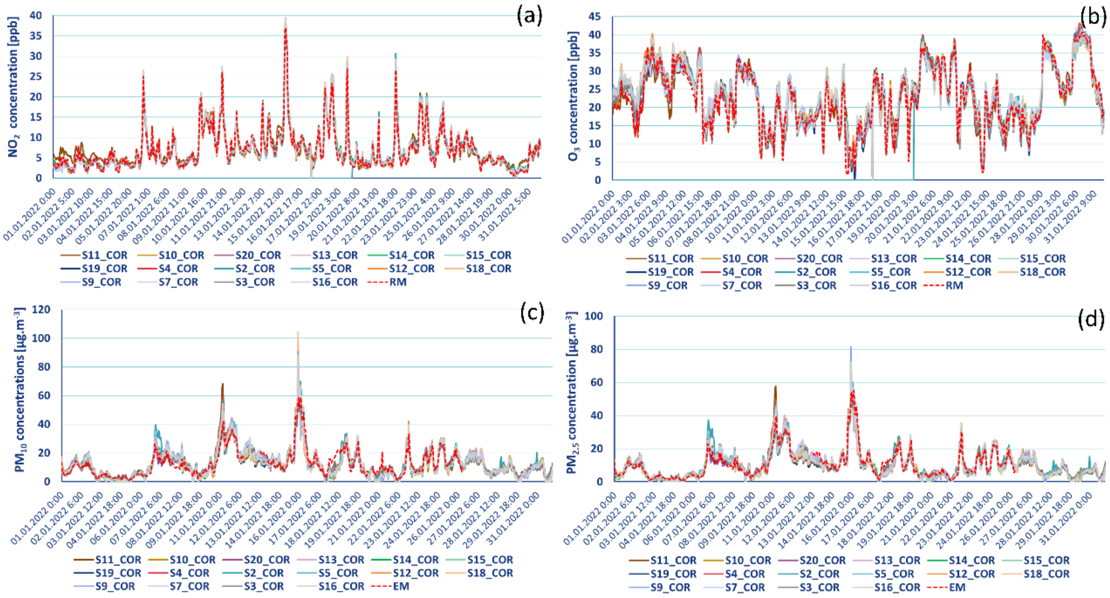


**Figure S8.** The 1-hour average concentrations of (a) $NO_2$, (b) $O_3$, (c) $PM_{10}$ and (d) $PM_{2.5}$ measured by all LCSs and corrected by MARS method (COR; marked as S2C, S3C, …S20C) in January 2022 during initial filed comparative measurement at the Prague 4-Libuš AQM station (RM = reference monitor for gas measurement, EM = equivalent monitor for aerosol measurement).

**Table S12.** Summary statistics of 1-hour average $NO_2$ concentrations measured by all LCSs during initial field comparative measurement at the Prague Libuš AQM station. Raw = original values of concentrations, cor = corrected values of concentrations (by MARS method). N valid = number of valid values, % valid = percentage of valid values in the dataset, Min = minimum value, Max = maximum value, SD = standard deviation, parameters resulting from linear regression between LCS and RM/EM concentrations: a = intercept, b = slope, SE = standard error, $R^2$ = coefficient of determination, MBE = Mean bias error, MAE = Mean absolute error, RMSE = Root mean square error.

| | Descriptive statistics | | | | | | | Linear regression | | | Williamson-York regression | | Error | |
|---|---|---|---|---|---|---|---|---|---|---|---|---|---|---|
| **Variable** | **N valid** | **% negat. values** | **Mean** | **Median** | **Min** | **Max** | **SD** | **a ± SE** | **b ± SE** | **$R^2$** | **a ± SE** | **b ± SE** | **MBE** | **RMSE** |
| **$NO_2$_raw S2** | 3122 | 0.00 | 6.98 | 5.54 | 2.21 | 42.24 | 4.62 | 1.44±0.05 | 0.70±0.00 | 0.89 | 1.82±0.04 | 0.58±0.01 | 0.90 | 2.57 |
| **$NO_2$_cor S2** | 3122 | 0.08 | 7.86 | 5.92 | -0.37 | 48.97 | 6.07 | 0.27±0.03 | 0.97±0.00 | 0.97 | -0.17±0.03 | 1.01±0.01 | 0.00 | 1.15 |
| **$NO_2$_raw S3** | 1588 | 0.00 | 5.06 | 3.68 | 1.63 | 31.04 | 3.87 | 0.06±0.04 | 0.73±0.00 | 0.96 | 0.96±0.02 | 0.55±0.01 | 1.78 | 2.41 |
| **$NO_2$_cor S3** | 1588 | 0.00 | 6.83 | 5.17 | 1.10 | 36.49 | 5.14 | 0.11±0.03 | 0.98±0.00 | 0.98 | 0.27±0.02 | 0.94±0.01 | 0.00 | 0.67 |
| **$NO_2$_raw S4** | 2253 | 0.00 | 10.03 | 7.98 | 4.66 | 45.27 | 5.56 | 3.12±0.03 | 0.81±0.00 | 0.98 | 3.60±0.02 | 0.73±0.00 | -1.53 | 2.16 |
| **$NO_2$_cor S4** | 2253 | 0.00 | 8.49 | 6.18 | 0.28 | 49.16 | 6.72 | 0.11±0.03 | 0.99±0.00 | 0.99 | 0.11±0.02 | 0.97±0.01 | 0.00 | 0.76 |
| **$NO_2$_raw S5** | 3955 | 0.00 | 7.36 | 5.71 | 2.43 | 45.52 | 4.91 | 1.08±0.03 | 0.78±0.00 | 0.95 | 1.73±0.02 | 0.65±0.00 | 0.65 | 1.84 |
| **$NO_2$_cor S5** | 3955 | 0.03 | 8.00 | 6.07 | -0.03 | 49.95 | 6.04 | 0.16±0.02 | 0.98±0.00 | 0.98 | -0.11±0.02 | 1.01±0.00 | 0.00 | 0.86 |
| **$NO_2$_raw S6** | 3954 | 0.00 | 7.16 | 5.54 | 2.18 | 42.56 | 4.51 | 1.39±0.03 | 0.72±0.00 | 0.95 | 2.06±0.02 | 0.59±0.00 | 0.85 | 2.18 |
| **$NO_2$_cor S6** | 3954 | 0.03 | 8.00 | 5.92 | -0.30 | 50.93 | 6.00 | 0.27±0.03 | 0.97±0.00 | 0.97 | 0.22±0.03 | 0.94±0.01 | 0.00 | 1.12 |
| **$NO_2$_raw S7** | 3954 | 0.00 | 8.01 | 6.43 | 2.32 | 47.21 | 5.20 | 1.63±0.05 | 0.80±0.00 | 0.88 | 1.68±0.04 | 0.70±0.01 | 0.01 | 2.23 |
| **$NO_2$_cor S7** | 3954 | 0.03 | 7.99 | 6.01 | -0.26 | 49.67 | 6.04 | 0.16±0.02 | 0.98±0.00 | 0.98 | -0.13±0.02 | 1.01±0.00 | 0.00 | 0.86 |
| **$NO_2$_raw S9** | 3887 | 0.00 | 9.27 | 7.78 | 3.88 | 41.53 | 4.48 | 3.53±0.03 | 0.72±0.00 | 0.95 | 3.81±0.02 | 0.65±0.00 | -1.24 | 2.35 |
| **$NO_2$_cor S9** | 3887 | 0.00 | 8.01 | 6.11 | 0.04 | 48.93 | 6.05 | 0.19±0.03 | 0.98±0.00 | 0.98 | -0.12±0.02 | 1.01±0.01 | 0.00 | 0.95 |
| **$NO_2$_raw S10** | 3952 | 0.00 | 8.90 | 7.24 | 3.45 | 47.80 | 5.10 | 2.41±0.03 | 0.81±0.00 | 0.94 | 2.88±0.03 | 0.70±0.01 | -0.89 | 1.93 |
| **$NO_2$_cor S10** | 3952 | 0.00 | 7.99 | 6.08 | 0.12 | 50.07 | 6.05 | 0.14±0.02 | 0.98±0.00 | 0.98 | 0.06±0.02 | 0.98±0.00 | 0.00 | 0.82 |
| **$NO_2$_raw S11** | 3918 | 0.00 | 3.48 | 1.95 | 0.04 | 40.64 | 4.21 | -1.60±0.05 | 0.63±0.00 | 0.84 | -0.45±0.02 | 0.40±0.01 | 4.56 | 5.36 |
| **$NO_2$_cor S11** | 3918 | 0.03 | 8.02 | 6.04 | -0.61 | 48.79 | 5.79 | 0.85±0.05 | 0.89±0.01 | 0.89 | 0.43±0.04 | 0.87±0.01 | 0.00 | 2.00 |
| **$NO_2$_raw S12** | 3954 | 0.00 | 10.99 | 9.50 | 4.92 | 49.07 | 5.23 | 4.46±0.04 | 0.82±0.00 | 0.91 | 4.49±0.04 | 0.75±0.01 | -2.98 | 3.57 |
| **$NO_2$_cor_S12** | 3954 | 0.05 | 8.00 | 5.99 | -0.06 | 49.13 | 6.04 | 0.17±0.02 | 0.98±0.00 | 0.98 | -0.13±0.02 | 1.01±0.00 | 0.00 | 0.89 |
| **$NO_2$_raw S13** | 3954 | 0.00 | 7.62 | 6.04 | 2.86 | 42.67 | 4.59 | 1.73±0.03 | 0.74±0.00 | 0.96 | 2.21±0.02 | 0.64±0.00 | 0.39 | 1.93 |
| **$NO_2$_cor S13** | 3954 | 0.00 | 8.00 | 6.04 | 0.26 | 50.02 | 6.02 | 0.21±0.03 | 0.97±0.00 | 0.97 | 0.19±0.02 | 0.95±0.01 | 0.00 | 0.98 |
| **$NO_2$_raw S14** | 3954 | 0.00 | 7.34 | 5.93 | 2.60 | 37.02 | 4.13 | 2.13±0.03 | 0.65±0.00 | 0.93 | 2.51±0.02 | 0.56±0.00 | 0.67 | 2.51 |
| **$NO_2$_cor S14** | 3954 | 0.28 | 8.00 | 6.17 | -0.79 | 48.52 | 6.00 | 0.29±0.03 | 0.96±0.00 | 0.96 | -0.50±0.02 | 1.07±0.01 | 0.00 | 1.17 |
| **$NO_2$_raw S15** | 3214 | 0.00 | 8.60 | 7.03 | 3.79 | 40.29 | 4.47 | 2.97±0.03 | 0.69±0.00 | 0.96 | 3.36±0.02 | 0.61±0.00 | -0.45 | 2.20 |
| **$NO_2$_cor S15** | 3214 | 0.03 | 8.13 | 6.00 | -0.27 | 49.65 | 6.24 | 0.22±0.03 | 0.97±0.00 | 0.97 | 0.18±0.03 | 0.95±0.01 | 0.00 | 1.05 |
| **$NO_2$_raw S16** | 3954 | 0.00 | 8.36 | 6.60 | 3.30 | 46.09 | 5.15 | 1.79±0.03 | 0.82±0.00 | 0.95 | 2.45±0.03 | 0.69±0.00 | -0.35 | 1.66 |
| **$NO_2$_cor S16** | 3954 | 0.08 | 7.99 | 6.13 | -0.32 | 48.42 | 6.02 | 0.21±0.03 | 0.97±0.00 | 0.97 | -0.08±0.02 | 1.00±0.01 | 0.00 | 0.99 |
| **$NO_2$_raw S18** | 3954 | 0.00 | 10.41 | 8.81 | 4.47 | 49.44 | 5.35 | 3.66±0.04 | 0.84±0.00 | 0.92 | 3.85±0.03 | 0.77±0.01 | -2.40 | 2.98 |
| **$NO_2$_cor S18** | 3954 | 0.10 | 8.00 | 5.99 | -0.54 | 49.10 | 6.04 | 0.16±0.02 | 0.98±0.00 | 0.98 | -0.18±0.02 | 1.02±0.00 | 0.00 | 0.86 |
| **$NO_2$_raw S19** | 3887 | 0.00 | 6.89 | 5.25 | 1.70 | 45.74 | 5.18 | 0.44±0.05 | 0.80±0.00 | 0.90 | 0.91±0.03 | 0.65±0.01 | 1.15 | 2.35 |
| **$NO_2$_cor S19** | 3887 | 0.00 | 8.02 | 6.08 | 0.32 | 48.69 | 6.05 | 0.17±0.02 | 0.98±0.00 | 0.98 | 0.10±0.02 | 0.97±0.00 | 0.00 | 0.88 |
| **$NO_2$_raw S20** | 3473 | 0.00 | 7.17 | 5.39 | 2.12 | 48.04 | 5.32 | 0.62±0.04 | 0.82±0.00 | 0.93 | 1.39±0.03 | 0.65±0.01 | 0.80 | 1.98 |
| **$NO_2$_cor S20** | 3473 | 0.03 | 7.95 | 5.89 | 0.00 | 49.56 | 6.17 | 0.16±0.02 | 0.98±0.00 | 0.98 | 0.12±0.02 | 0.96±0.00 | 0.00 | 0.89 |
| **$NO_2$ RM** | 3767 | 0.00 | 8.05 | 6.12 | 0.52 | 50.61 | 6.16 | | | | | | | |

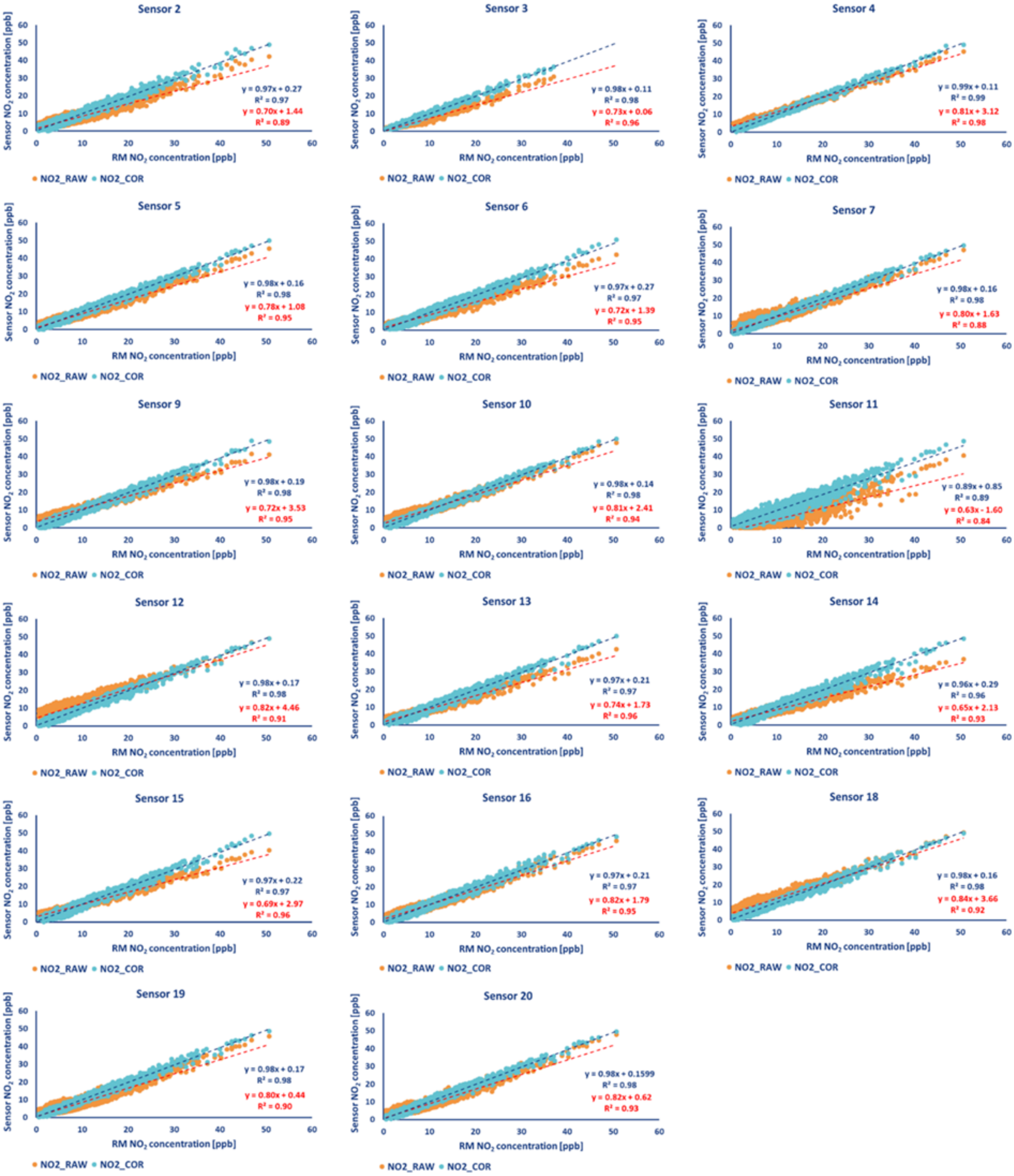


**Figure S9.** Relationship of $NO_2$ concentrations measured by LCS (the y-axis) and by reference monitor (RM; the x-axis) at the Prague Libuš air quality monitoring (AQM) station. $NO_2$_RAW = raw concentrations measured by LCSs, $NO_2$_COR = LCSs concentrations corrected by MARS method.

**Table S13.** Summary statistics of 1-hour average $O_3$ concentrations measured by all LCSs during initial field comparative measurement at the Prague Libuš AQM station. Raw = original values of concentrations, cor = corrected values of concentrations (by MARS method). N valid = number of valid values, % valid = percentage of valid values in the dataset, Min = minimum value, Max = maximum value, SD = standard deviation, parameters resulting from linear regression between LCS and RM/EM concentrations: a = intercept, b = slope, SE = standard error, $R^2$ = coefficient of determination, MBE = Mean bias error, MAE = Mean absolute error, RMSE = Root mean square error.

| | Descriptive statistics | | | | | | | Linear regression | | | Williamson-York regression | | Error | |
|---|---|---|---|---|---|---|---|---|---|---|---|---|---|---|
| **Variable** | **N valid** | **% negat. values** | **Mean** | **Median** | **Min** | **Max** | **SD** | **a ± SE** | **b ± SE** | **$R^2$** | **a ± SE** | **b ± SE** | **MBE** | **RMSE** |
| **$O_3$_raw S2** | 3122 | 0.00 | 24.89 | 23.46 | 5.71 | 54.75 | 8.61 | 5.75±0.18 | 0.60±0.01 | 0.82 | 6.30±0.13 | 0.55±0.00 | 7.14 | 9.56 |
| **$O_3$_cor S2** | 3122 | 0.00 | 32.01 | 31.84 | 1.36 | 68.52 | 12.60 | 1.78±0.15 | 0.94±0.00 | 0.94 | 0.21±0.09 | 0.98±0.00 | 0.00 | 3.05 |
| **$O_3$_raw S3** | 1588 | 0.00 | 19.78 | 19.77 | 8.64 | 30.37 | 3.86 | 12.69±0.18 | 0.30±0.01 | 0.54 | 11.40±0.16 | 0.33±0.01 | 3.69 | 7.93 |
| **$O_3$_cor S3** | 1588 | 0.00 | 23.56 | 24.30 | 2.50 | 42.24 | 9.00 | 1.58±0.16 | 0.93±0.01 | 0.93 | 1.30±0.09 | 0.92±0.01 | 0.00 | 2.42 |
| **$O_3$_raw S4** | 2253 | 0.00 | 19.86 | 19.52 | 8.07 | 47.66 | 5.15 | 11.41±0.19 | 0.34±0.01 | 0.54 | 10.21±0.15 | 0.35±0.01 | 5.07 | 9.58 |
| **$O_3$_cor S4** | 2253 | 0.00 | 24.95 | 25.11 | 0.77 | 56.67 | 10.77 | 1.41±0.14 | 0.94±0.00 | 0.94 | 0.37±0.08 | 0.96±0.01 | 0.00 | 2.64 |
| **$O_3$_raw S5** | 3955 | 0.00 | 22.31 | 20.89 | 4.46 | 55.94 | 8.28 | 6.18±0.15 | 0.55±0.00 | 0.79 | 6.38±0.11 | 0.51±0.00 | 6.90 | 9.85 |
| **$O_3$_cor S5** | 3955 | 0.00 | 29.22 | 28.55 | 3.72 | 70.57 | 12.70 | 2.32±0.14 | 0.92±0.00 | 0.92 | 2.18±0.09 | 0.89±0.00 | 0.00 | 3.74 |
| **$O_3$_raw S6** | 3954 | 0.00 | 32.53 | 30.72 | 5.26 | 74.53 | 12.45 | 8.36±0.23 | 0.83±0.01 | 0.78 | 7.23±0.17 | 0.81±0.01 | -3.41 | 7.10 |
| **$O_3$_cor S6** | 3954 | 0.00 | 29.23 | 28.54 | 1.86 | 71.20 | 12.98 | 1.06±0.10 | 0.96±0.00 | 0.96 | 0.72±0.06 | 0.96±0.00 | 0.00 | 2.52 |
| **$O_3$_raw S7** | 3954 | 0.00 | 21.44 | 20.49 | 6.64 | 45.02 | 6.78 | 8.83±0.14 | 0.43±0.00 | 0.72 | 7.82±0.12 | 0.43±0.00 | 7.78 | 11.41 |
| **$O_3$_cor S7** | 3954 | 0.00 | 29.20 | 28.56 | 1.79 | 70.06 | 12.76 | 2.04±0.13 | 0.93±0.00 | 0.93 | 0.37±0.08 | 0.96±0.00 | 0.00 | 3.50 |
| **$O_3$_raw S9** | 3887 | 0.00 | 14.75 | 12.92 | 0.55 | 48.82 | 8.39 | -1.32±0.16 | 0.55±0.00 | 0.77 | -0.37±0.08 | 0.46±0.00 | 14.52 | 16.22 |
| **$O_3$_cor S9** | 3887 | 0.00 | 29.27 | 28.57 | 4.40 | 71.64 | 12.90 | 1.82±0.13 | 0.94±0.00 | 0.94 | 2.18±0.08 | 0.89±0.00 | 0.00 | 3.33 |
| **$O_3$_raw S10** | 3952 | 0.00 | 23.77 | 22.66 | 7.43 | 54.40 | 7.60 | 8.75±0.13 | 0.52±0.00 | 0.82 | 9.15±0.10 | 0.47±0.00 | 5.48 | 9.06 |
| **$O_3$_cor S10** | 3952 | 0.00 | 29.24 | 28.39 | 2.71 | 70.61 | 12.84 | 1.65±0.12 | 0.94±0.00 | 0.94 | 0.85±0.07 | 0.95±0.00 | 0.00 | 3.15 |
| **$O_3$_raw S11** | 3952 | 0.00 | 22.92 | 20.91 | 3.05 | 60.98 | 9.83 | 3.96±0.19 | 0.65±0.01 | 0.77 | 4.41±0.12 | 0.58±0.01 | 6.28 | 9.10 |
| **$O_3$_cor S11** | 3918 | 0.00 | 29.05 | 28.66 | 3.67 | 69.80 | 12.51 | 2.55±0.15 | 0.91±0.00 | 0.91 | 1.97±0.09 | 0.90±0.00 | 0.00 | 3.89 |
| **$O_3$_raw S12** | 3954 | 0.00 | 25.81 | 24.24 | 6.68 | 61.86 | 9.07 | 7.94±0.16 | 0.61±0.00 | 0.81 | 8.76±0.12 | 0.55±0.00 | 3.40 | 7.33 |
| **$O_3$_cor S12** | 3954 | 0.00 | 29.21 | 28.51 | 2.49 | 69.01 | 12.83 | 1.79±0.13 | 0.94±0.00 | 0.94 | 0.74±0.07 | 0.95±0.00 | 0.00 | 3.28 |
| **$O_3$_raw S13** | 3954 | 0.00 | 25.81 | 24.07 | 6.90 | 64.45 | 9.46 | 7.23±0.17 | 0.64±0.01 | 0.80 | 8.29±0.12 | 0.56±0.01 | 3.40 | 7.25 |
| **$O_3$_cor S13** | 3954 | 0.00 | 29.21 | 28.63 | 3.94 | 69.47 | 12.78 | 2.01±0.13 | 0.93±0.00 | 0.93 | 1.88±0.09 | 0.90±0.00 | 0.00 | 3.48 |
| **$O_3$_raw S14** | 3954 | 0.00 | 24.44 | 23.10 | 6.17 | 54.75 | 8.24 | 8.44±0.15 | 0.55±0.00 | 0.69 | 8.24±0.12 | 0.52±0.00 | 4.78 | 8.55 |
| **$O_3$_cor S14** | 3954 | 0.00 | 29.21 | 28.37 | 2.25 | 69.98 | 12.86 | 1.66±0.12 | 0.94±0.00 | 0.94 | 0.77±0.07 | 0.95±0.00 | 0.00 | 3.16 |
| **$O_3$_raw S15** | 3214 | 0.00 | 22.36 | 21.94 | 6.30 | 52.54 | 6.16 | 10.27±0.16 | 0.46±0.01 | 0.69 | 9.78±0.12 | 0.44±0.01 | 4.38 | 8.31 |
| **$O_3$_cor S15** | 3214 | 0.00 | 26.75 | 27.02 | 1.84 | 67.25 | 10.88 | 1.55±0.12 | 0.94±0.00 | 0.94 | 0.76±0.08 | 0.95±0.00 | 0.00 | 2.71 |
| **$O_3$_raw S16** | 3954 | 0.00 | 24.23 | 22.47 | 4.74 | 61.74 | 9.54 | 5.64±0.17 | 0.64±0.01 | 0.79 | 6.35±0.12 | 0.57±0.01 | 4.97 | 8.18 |
| **$O_3$_cor S16** | 3954 | 0.00 | 29.23 | 28.51 | 4.01 | 68.70 | 12.81 | 1.82±0.13 | 0.94±0.00 | 0.94 | 1.88±0.08 | 0.91±0.00 | 0.00 | 3.31 |
| **$O_3$_raw S18** | 3954 | 0.00 | 24.86 | 23.31 | 7.24 | 57.16 | 8.45 | 8.33±0.15 | 0.57±0.00 | 0.80 | 8.87±0.12 | 0.51±0.00 | 4.35 | 8.15 |
| **$O_3$_cor S18** | 3954 | 0.00 | 29.23 | 28.53 | 3.02 | 70.72 | 12.84 | 1.72±0.12 | 0.94±0.00 | 0.94 | 1.33±0.08 | 0.93±0.00 | 0.00 | 3.22 |
| **$O_3$_raw S19** | 3887 | 0.00 | 26.39 | 24.18 | 5.15 | 67.06 | 10.52 | 6.34±0.21 | 0.69±0.01 | 0.76 | 7.01±0.15 | 0.61±0.01 | 2.82 | 7.21 |
| **$O_3$_cor S19** | 3887 | 0.05 | 29.28 | 28.60 | -1.10 | 70.07 | 12.95 | 1.59±0.12 | 0.95±0.00 | 0.95 | -1.05±0.07 | 1.03±0.00 | 0.00 | 3.11 |
| **$O_3$_raw S20** | 3473 | 0.00 | 23.42 | 21.63 | 6.17 | 62.27 | 9.07 | 6.06±0.22 | 0.63±0.01 | 0.69 | 7.21±0.15 | 0.53±0.01 | 4.13 | 7.88 |
| **$O_3$_cor S20** | 3473 | 0.00 | 27.59 | 27.64 | 0.61 | 70.57 | 11.62 | 1.12±0.10 | 0.96±0.00 | 0.96 | -0.11±0.07 | 0.99±0.00 | 0.00 | 2.39 |
| **$O_3$ RM** | 3769 | 0.00 | 29.35 | 28.71 | 0.50 | 72.66 | 13.31 | | | | | | | |

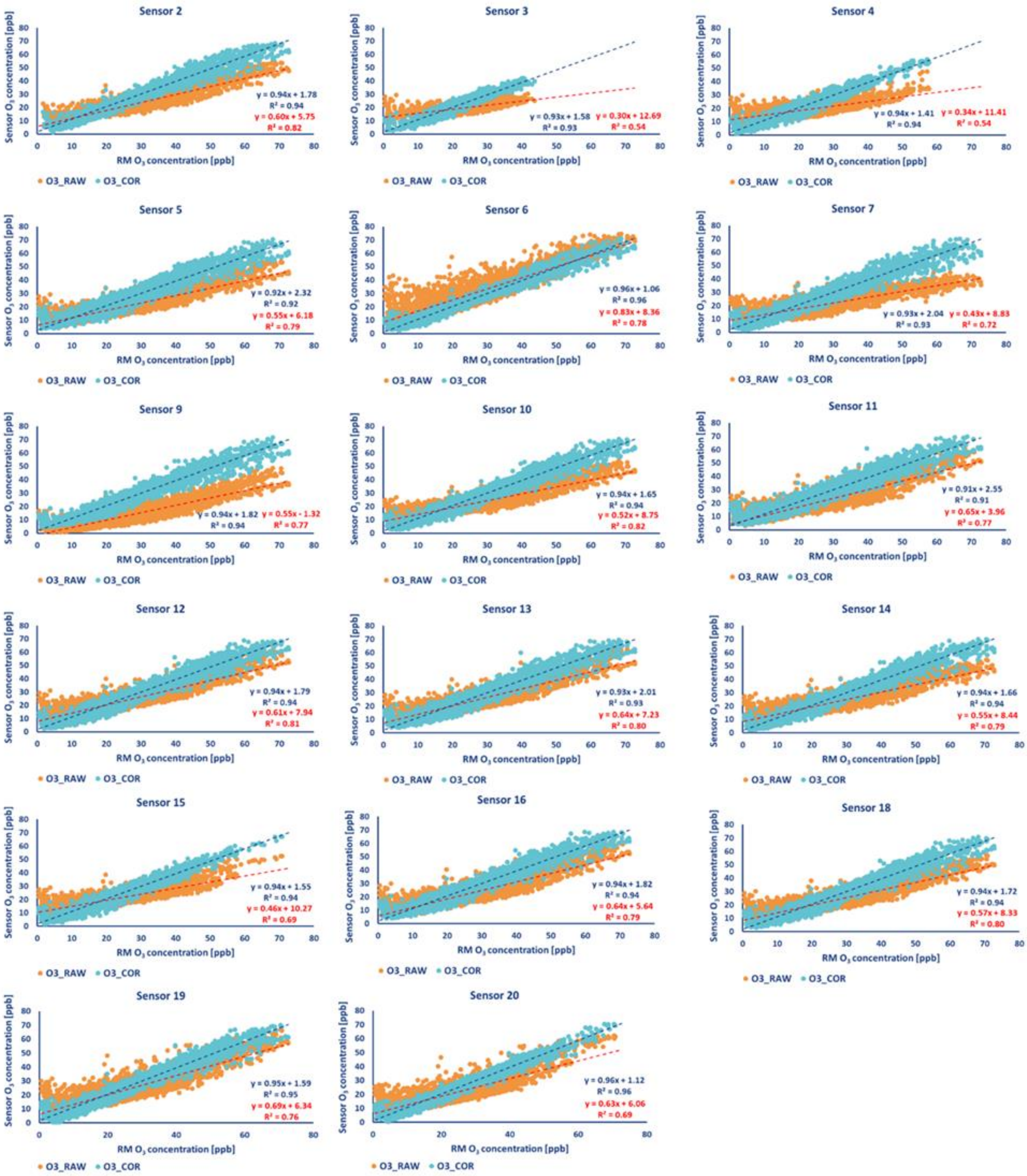


**Figure S10**. Relationship of $O_3$ concentrations measured by LCS (the y-axis) and by reference monitor (RM; the x-axis) at the Prague Libuš air quality monitoring (AQM) station. $O_3$_RAW = raw concentrations measured by LCSs, $O_3$_COR = LCSs concentrations corrected by MARS method.

**Table S14.** Summary statistics of 1-hour average $PM_{10}$ concentrations measured by all LCSs during initial field comparative measurement at the Prague Libuš AQM station. Raw = original values of concentrations, cor = corrected values of concentrations (by MARS method). N valid = number of valid values, % valid = percentage of valid values in the dataset, Min = minimum value, Max = maximum value, SD = standard deviation, parameters resulting from linear regression between LCS and RM/EM concentrations: a = intercept, b = slope, SE = standard error, $R^2$ = coefficient of determination, MBE = Mean bias error, MAE = Mean absolute error, RMSE = Root mean square error.

| | Descriptive statistics | | | | | | | Linear regression | | | Williamson-York regression | | Error | |
|---|---|---|---|---|---|---|---|---|---|---|---|---|---|---|
| **Variable** | **N valid** | **% negat. values** | **Mean** | **Median** | **Min** | **Max** | **SD** | **a ± SE** | **b ± SE** | **R2** | **a ± SE** | **b ± SE** | **MBE** | **RMSE** |
| **$PM_{10}$_raw S2** | 3933 | 0.00 | 15.13 | 9.80 | 0.04 | 125.50 | 15.54 | -1.98±0.21 | 0.91±0.01 | 0.76 | -2.34±0.06 | 0.91±0.01 | 3.68 | 8.66 |
| **$PM_{10}$_cor S2** | 3933 | 1.59 | 18.80 | 16.52 | -3.69 | 161.83 | 14.04 | 2.19±0.13 | 0.89±0.01 | 0.89 | -1.78±0.06 | 1.17±0.01 | 0.00 | 5.07 |
| **$PM_{10}$_raw S3** | 1574 | 0.00 | 15.06 | 9.05 | 0.05 | 105.32 | 17.18 | -5.45±0.27 | 1.72±0.02 | 0.89 | -3.56±0.12 | 1.56±0.03 | -3.54 | 9.92 |
| **$PM_{10}$_cor S3** | 1574 | 0.00 | 12.09 | 9.38 | 0.12 | 66.57 | 9.01 | 1.00±0.12 | 0.92±0.01 | 0.92 | -0.09±0.06 | 1.03±0.01 | 0.00 | 2.77 |
| **$PM_{10}$_raw S4** | 2241 | 0.00 | 20.90 | 14.57 | 0.03 | 101.62 | 20.58 | -1.21±0.33 | 1.23±0.01 | 0.80 | -2.44±0.08 | 1.25±0.02 | -3.07 | 10.47 |
| **$PM_{10}$_cor S4** | 2241 | 1.19 | 18.11 | 14.45 | -4.14 | 81.67 | 14.34 | 1.78±0.16 | 0.91±0.01 | 0.91 | -1.47±0.07 | 1.15±0.01 | 0.00 | 4.70 |
| **$PM_{10}$_raw S5** | 3950 | 0.00 | 15.35 | 10.16 | 0.03 | 120.32 | 15.86 | -1.96±0.21 | 0.92±0.01 | 0.75 | -1.96±0.05 | 0.87±0.01 | 3.42 | 8.80 |
| **$PM_{10}$_cor S5** | 3950 | 1.69 | 18.74 | 16.49 | -4.14 | 166.65 | 13.98 | 2.37±0.13 | 0.88±0.01 | 0.88 | -1.75±0.06 | 1.17±0.01 | 0.00 | 5.29 |
| **$PM_{10}$_raw S6** | 3947 | 0.00 | 13.21 | 8.62 | 0.03 | 103.11 | 13.34 | -1.65±0.17 | 0.79±0.01 | 0.78 | -1.60±0.04 | 0.75±0.01 | 5.62 | 9.02 |
| **$PM_{10}$_cor S6** | 3947 | 1.77 | 18.77 | 16.45 | -2.95 | 165.93 | 14.02 | 2.19±0.13 | 0.89±0.01 | 0.89 | -1.79±0.06 | 1.17±0.01 | 0.00 | 5.08 |
| **$PM_{10}$_raw S7** | 3949 | 0.00 | 17.28 | 11.73 | 0.05 | 135.87 | 16.98 | -1.18±0.23 | 0.99±0.01 | 0.75 | -2.12±0.06 | 1.00±0.01 | 1.46 | 8.78 |
| **$PM_{10}$_cor S7** | 3949 | 2.10 | 18.73 | 16.35 | -5.48 | 161.12 | 14.05 | 2.23±0.13 | 0.88±0.01 | 0.88 | -1.80±0.06 | 1.17±0.01 | 0.00 | 5.13 |
| **$PM_{10}$_raw S9** | 3849 | 0.00 | 17.44 | 11.04 | 0.04 | 146.43 | 18.21 | -2.10±0.26 | 1.03±0.01 | 0.72 | -2.98±0.08 | 1.05±0.01 | 1.49 | 9.93 |
| **$PM_{10}$_cor S9** | 3849 | 2.32 | 18.94 | 16.59 | -7.05 | 159.39 | 14.05 | 2.48±0.14 | 0.87±0.01 | 0.87 | -2.20±0.07 | 1.21±0.01 | 0.00 | 5.40 |
| **$PM_{10}$_raw S10** | 3946 | 0.00 | 17.86 | 11.97 | 0.03 | 135.08 | 17.72 | -1.07±0.25 | 1.01±0.01 | 0.72 | -2.19±0.06 | 1.02±0.01 | 0.88 | 9.54 |
| **$PM_{10}$_cor S10** | 3946 | 2.58 | 18.74 | 16.53 | -7.66 | 163.50 | 14.01 | 2.34±0.13 | 0.88±0.01 | 0.88 | -1.92±0.06 | 1.19±0.01 | 0.00 | 5.26 |
| **$PM_{10}$_raw S11** | 3915 | 0.00 | 11.26 | 7.43 | 0.03 | 89.49 | 11.79 | -2.00±0.15 | 0.71±0.01 | 0.79 | -1.92±0.04 | 0.68±0.01 | 7.71 | 10.45 |
| **$PM_{10}$_cor S11** | 3915 | 0.66 | 18.84 | 16.25 | -1.74 | 151.66 | 13.83 | 2.68±0.14 | 0.86±0.01 | 0.86 | -0.89±0.07 | 1.10±0.01 | 0.00 | 5.59 |
| **$PM_{10}$_raw S12** | 3936 | 0.00 | 17.68 | 12.00 | 0.03 | 133.72 | 17.49 | -1.25±0.24 | 1.01±0.01 | 0.74 | -2.51±0.07 | 1.05±0.01 | 1.07 | 9.13 |
| **$PM_{10}$_cor S12** | 3936 | 2.05 | 18.77 | 16.40 | -5.54 | 162.02 | 14.00 | 2.37±0.13 | 0.88±0.01 | 0.88 | -1.86±0.07 | 1.18±0.01 | 0.00 | 5.28 |
| **$PM_{10}$_raw S13** | 3930 | 0.00 | 10.85 | 7.47 | 0.03 | 99.29 | 11.36 | -1.48±0.16 | 0.65±0.01 | 0.73 | -1.51±0.04 | 0.63±0.01 | 8.16 | 11.39 |
| **$PM_{10}$_cor S13** | 3930 | 1.14 | 18.81 | 16.55 | -3.89 | 165.35 | 13.64 | 3.24±0.15 | 0.83±0.01 | 0.83 | -1.37±0.06 | 1.14±0.01 | 0.00 | 6.17 |
| **$PM_{10}$_raw S14** | 3925 | 0.00 | 15.70 | 10.33 | 0.04 | 137.91 | 16.26 | -2.14±0.22 | 0.95±0.01 | 0.76 | -2.62±0.06 | 0.95±0.01 | 3.07 | 8.70 |
| **$PM_{10}$_cor S14** | 3925 | 1.54 | 18.77 | 16.26 | -4.55 | 162.12 | 13.96 | 2.45±0.13 | 0.87±0.01 | 0.87 | -1.75±0.06 | 1.16±0.01 | 0.00 | 5.36 |
| **$PM_{10}$_raw S15** | 3206 | 0.00 | 17.40 | 11.74 | 0.05 | 96.05 | 17.37 | -1.23±0.25 | 1.03±0.01 | 0.76 | -2.41±0.06 | 1.05±0.01 | 0.75 | 8.65 |
| **$PM_{10}$_cor S15** | 3206 | 1.77 | 18.21 | 14.61 | -5.72 | 69.63 | 13.87 | 2.45±0.15 | 0.87±0.01 | 0.87 | -1.77±0.07 | 1.18±0.01 | 0.00 | 5.42 |
| **$PM_{10}$_raw S16** | 3930 | 0.00 | 19.46 | 12.76 | 0.03 | 155.50 | 19.47 | -1.50±0.27 | 1.12±0.01 | 0.73 | -3.01±0.08 | 1.17±0.01 | -0.80 | 10.39 |
| **$PM_{10}$_cor S16** | 3930 | 2.30 | 18.77 | 16.33 | -5.64 | 159.70 | 13.97 | 2.43±0.13 | 0.87±0.01 | 0.87 | -2.02±0.07 | 1.19±0.01 | 0.00 | 5.34 |
| **$PM_{10}$_raw S18** | 3945 | 0.00 | 16.46 | 10.12 | 0.04 | 144.81 | 17.37 | -2.09±0.25 | 0.99±0.01 | 0.72 | -2.25±0.06 | 0.94±0.01 | 2.22 | 9.55 |
| **$PM_{10}$_cor S18** | 3945 | 1.87 | 18.69 | 16.35 | -6.57 | 156.53 | 13.85 | 2.75±0.14 | 0.86±0.01 | 0.86 | -1.70±0.06 | 1.17±0.01 | 0.00 | 5.69 |
| **$PM_{10}$_raw S19** | 3874 | 0.00 | 20.03 | 13.52 | 0.03 | 160.50 | 19.68 | -1.37±0.26 | 1.14±0.01 | 0.75 | -3.01±0.08 | 1.21±0.01 | -1.37 | 10.18 |
| **$PM_{10}$_cor S19** | 3874 | 1.62 | 18.79 | 16.17 | -4.13 | 159.87 | 14.12 | 2.29±0.13 | 0.88±0.01 | 0.88 | -1.63±0.06 | 1.16±0.01 | 0.00 | 5.21 |
| **$PM_{10}$_raw S20** | 3456 | 0.00 | 16.82 | 10.70 | 0.03 | 94.34 | 17.27 | -2.21±0.24 | 1.06±0.01 | 0.77 | -2.58±0.06 | 1.05±0.01 | 1.16 | 8.54 |
| **$PM_{10}$_cor S20** | 3456 | 1.31 | 18.05 | 14.82 | -4.29 | 69.41 | 13.44 | 2.40±0.14 | 0.87±0.01 | 0.87 | -1.56±0.06 | 1.16±0.01 | 0.00 | 5.23 |
| **$PM_{10}$ EM** | 3753 | 0.00 | 19.22 | 15.60 | 0.60 | 164.85 | 15.10 | | | | | | | |

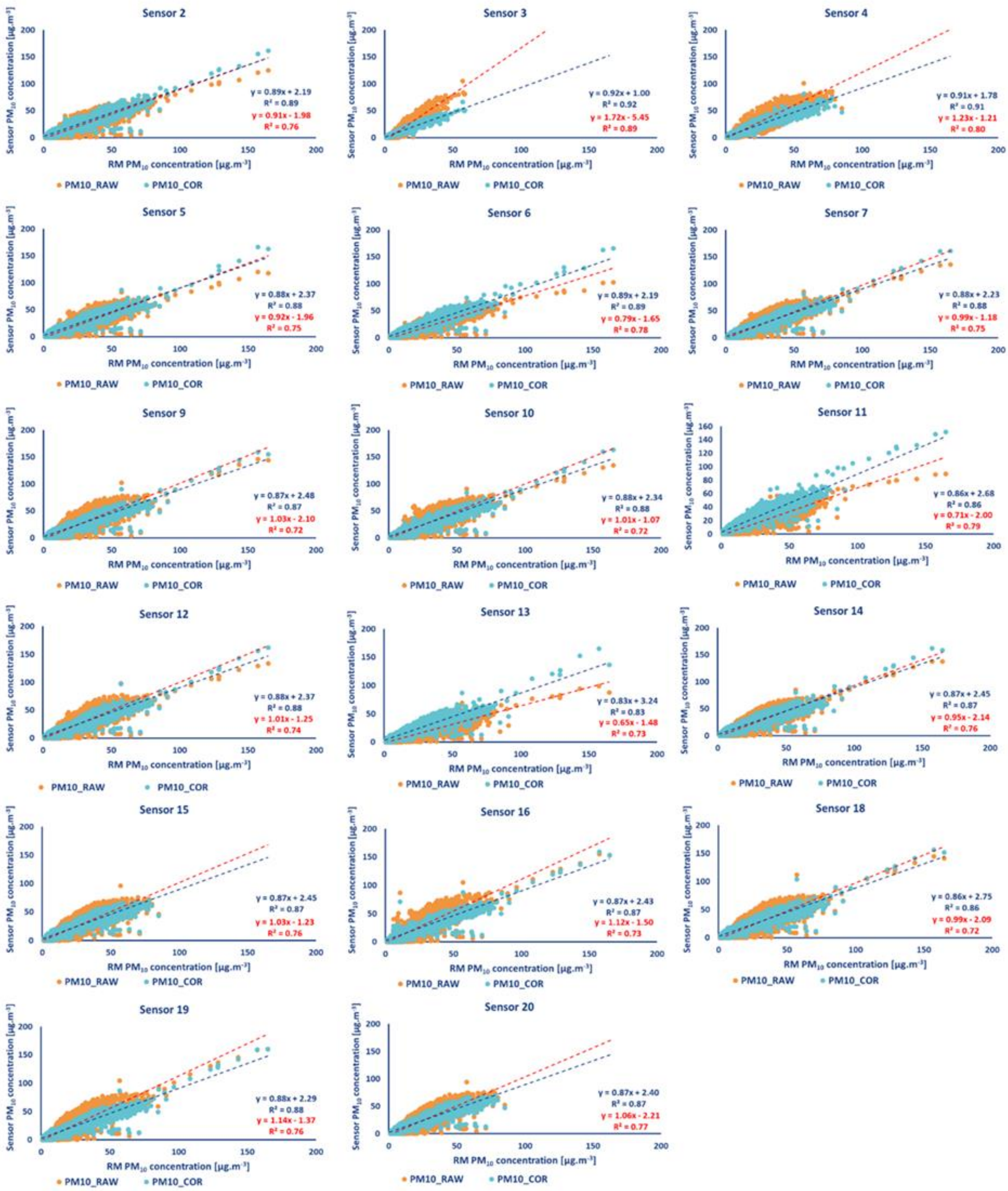


**Figure S11**. Relationship of $PM_{10}$ concentrations measured by LCS (the y-axis) and by reference monitor (RM; the x-axis) at the Prague Libuš air quality monitoring (AQM) station. $PM_{10}$_RAW = raw concentrations measured by LCSs, $PM_{10}$_COR = LCSs concentrations corrected by MARS method.

**Table S15.** Summary statistics of 1-hour average $PM_{2.5}$ concentrations measured by all LCSs during initial field comparative measurement at the Prague Libuš AQM station. Raw = original values of concentrations, cor = corrected values of concentrations (by MARS method). N valid = number of valid values, % valid = percentage of valid values in the dataset, Min = minimum value, Max = maximum value, SD = standard deviation, parameters resulting from linear regression between LCS and RM/EM concentrations: a = intercept, b = slope, SE = standard error, $R^2$ = coefficient of determination, MBE = Mean bias error, MAE = Mean absolute error, RMSE = Root mean square error.

| | Descriptive statistics | | | | | | | Linear regression | | | Williamson-York regression | | Error | |
|---|---|---|---|---|---|---|---|---|---|---|---|---|---|---|
| **Variable** | **N valid** | **% negat. values** | **Mean** | **Median** | **Min** | **Max** | **SD** | **a ± SE** | **b ± SE** | **R2** | **a ± SE** | **b ± SE** | **MBE** | **RMSE** |
| **$PM_{2.5}$_raw S2** | 3922 | 0.00 | 13.70 | 9.20 | 0.03 | 118.92 | 13.43 | -0.49±0.12 | 1.02±0.01 | 0.87 | -1.75±0.03 | 1.08±0.01 | 0.22 | 4.82 |
| **$PM_{2.5}$_cor S2** | 3922 | 1.64 | 14.01 | 11.23 | -3.30 | 151.71 | 11.98 | 0.72±0.07 | 0.95±0.00 | 0.95 | -1.23±0.04 | 1.16±0.01 | 0.00 | 2.80 |
| **$PM_{2.5}$_raw S3** | 1560 | 0.00 | 12.83 | 8.31 | 0.03 | 84.18 | 13.75 | -1.98±0.18 | 1.51±0.01 | 0.91 | -2.20±0.07 | 1.51±0.02 | -3.27 | 7.03 |
| **$PM_{2.5}$_cor S3** | 1560 | 0.13 | 9.99 | 7.77 | -0.77 | 60.35 | 8.43 | 0.58±0.09 | 0.94±0.01 | 0.94 | -0.23±0.04 | 1.05±0.01 | 0.00 | 2.13 |
| **$PM_{2.5}$_raw S4** | 2226 | 0.00 | 17.94 | 13.52 | 0.03 | 84.06 | 16.57 | -0.02±0.20 | 1.24±0.01 | 0.88 | -1.75±0.05 | 1.33±0.01 | -3.63 | 7.48 |
| **$PM_{2.5}$_cor S4** | 2226 | 1.09 | 14.56 | 11.90 | -2.96 | 62.54 | 12.19 | 0.85±0.10 | 0.94±0.01 | 0.94 | -1.04±0.04 | 1.14±0.01 | 0.00 | 3.01 |
| **$PM_{2.5}$_raw S5** | 3929 | 0.00 | 12.88 | 8.85 | 0.03 | 108.85 | 12.85 | -0.71±0.11 | 0.98±0.01 | 0.88 | -1.52±0.03 | 0.99±0.01 | 1.04 | 4.68 |
| **$PM_{2.5}$_cor S5** | 3929 | 1.31 | 13.98 | 11.26 | -2.45 | 148.20 | 11.97 | 0.80±0.07 | 0.94±0.00 | 0.94 | -1.03±0.03 | 1.13±0.01 | 0.00 | 2.96 |
| **$PM_{2.5}$_raw S6** | 3934 | 0.00 | 11.85 | 7.88 | 0.03 | 97.39 | 11.61 | -0.45±0.10 | 0.89±0.01 | 0.88 | -1.21±0.02 | 0.89±0.01 | 2.09 | 4.77 |
| **$PM_{2.5}$_cor S6** | 3934 | 1.54 | 13.98 | 11.29 | -3.43 | 147.28 | 12.01 | 0.66±0.07 | 0.95±0.00 | 0.95 | -1.10±0.03 | 1.15±0.01 | 0.00 | 2.68 |
| **$PM_{2.5}$_raw S7** | 3941 | 0.00 | 15.13 | 10.82 | 0.03 | 127.71 | 14.10 | 0.28±0.12 | 1.07±0.01 | 0.88 | -1.55±0.03 | 1.17±0.01 | -1.27 | 5.25 |
| **$PM_{2.5}$_cor S7** | 3941 | 2.12 | 13.92 | 11.30 | -3.55 | 144.40 | 12.03 | 0.69±0.07 | 0.95±0.00 | 0.95 | -1.11±0.03 | 1.15±0.01 | 0.00 | 2.74 |
| **$PM_{2.5}$_raw S9** | 3830 | 0.00 | 15.69 | 10.62 | 0.03 | 140.47 | 15.43 | -0.51±0.15 | 1.15±0.01 | 0.86 | -2.26±0.04 | 1.25±0.01 | -1.68 | 6.41 |
| **$PM_{2.5}$_cor S9** | 3830 | 2.40 | 14.11 | 11.58 | -4.19 | 142.67 | 12.05 | 0.84±0.07 | 0.94±0.00 | 0.94 | -1.40±0.04 | 1.19±0.01 | 0.00 | 3.03 |
| **$PM_{2.5}$_raw S10** | 3938 | 0.00 | 15.53 | 11.04 | 0.04 | 126.71 | 14.61 | 0.29±0.14 | 1.10±0.01 | 0.86 | -1.64±0.03 | 1.19±0.01 | -1.66 | 5.94 |
| **$PM_{2.5}$_cor S10** | 3938 | 2.37 | 13.94 | 11.39 | -4.17 | 150.45 | 12.00 | 0.75±0.07 | 0.95±0.00 | 0.95 | -1.23±0.03 | 1.16±0.01 | 0.00 | 2.86 |
| **$PM_{2.5}$_raw S11** | 3896 | 0.00 | 10.42 | 7.04 | 0.03 | 84.28 | 10.52 | -0.79±0.09 | 0.80±0.00 | 0.88 | -1.54±0.02 | 0.83±0.01 | 3.64 | 5.71 |
| **$PM_{2.5}$_cor S11** | 3896 | 0.58 | 14.05 | 11.05 | -1.34 | 149.03 | 11.86 | 1.01±0.08 | 0.93±0.00 | 0.93 | -0.67±0.03 | 1.09±0.01 | 0.00 | 3.30 |
| **$PM_{2.5}$_raw S12** | 3920 | 0.00 | 15.83 | 11.35 | 0.03 | 127.45 | 14.72 | 0.39±0.14 | 1.11±0.01 | 0.87 | -1.87±0.04 | 1.25±0.01 | -1.95 | 5.96 |
| **$PM_{2.5}$_cor S12** | 3920 | 1.64 | 14.00 | 11.31 | -3.97 | 146.89 | 11.97 | 0.80±0.07 | 0.94±0.00 | 0.94 | -1.06±0.04 | 1.14±0.01 | 0.00 | 2.94 |
| **$PM_{2.5}$_raw S13** | 3920 | 0.00 | 10.18 | 7.22 | 0.03 | 94.68 | 10.19 | -0.63±0.09 | 0.77±0.00 | 0.87 | -1.19±0.02 | 0.78±0.01 | 3.90 | 6.12 |
| **$PM_{2.5}$_cor S13** | 3920 | 1.06 | 14.00 | 11.04 | -1.82 | 149.71 | 11.75 | 1.33±0.09 | 0.91±0.00 | 0.91 | -0.95±0.03 | 1.13±0.01 | 0.00 | 3.80 |
| **$PM_{2.5}$_raw S14** | 3915 | 0.00 | 14.09 | 9.71 | 0.03 | 131.18 | 13.83 | -0.55±0.12 | 1.05±0.01 | 0.88 | -1.99±0.03 | 1.13±0.01 | -0.22 | 4.85 |
| **$PM_{2.5}$_cor S14** | 3915 | 1.82 | 13.97 | 11.11 | -2.46 | 142.72 | 11.91 | 0.92±0.08 | 0.94±0.00 | 0.94 | -1.30±0.04 | 1.17±0.01 | 0.00 | 3.16 |
| **$PM_{2.5}$_raw S15** | 3199 | 0.00 | 15.35 | 10.98 | 0.05 | 81.62 | 14.42 | -0.52±0.14 | 1.14±0.01 | 0.89 | -1.62±0.03 | 1.17±0.01 | -1.49 | 5.40 |
| **$PM_{2.5}$_cor S15** | 3199 | 1.24 | 13.96 | 10.87 | -3.01 | 59.78 | 11.55 | 0.90±0.08 | 0.94±0.00 | 0.94 | -0.88±0.03 | 1.12±0.01 | 0.00 | 3.02 |
| **$PM_{2.5}$_raw S16** | 3911 | 0.00 | 17.04 | 11.92 | 0.04 | 146.14 | 16.06 | 0.29±0.15 | 1.20±0.01 | 0.86 | -2.25±0.04 | 1.37±0.01 | -3.21 | 7.38 |
| **$PM_{2.5}$_cor S16** | 3930 | 1.57 | 13.94 | 11.34 | -2.94 | 146.13 | 11.92 | 0.92±0.08 | 0.94±0.00 | 0.94 | -1.04±0.04 | 1.14±0.01 | 0.00 | 3.16 |
| **$PM_{2.5}$_raw S18** | 3936 | 0.00 | 14.38 | 9.31 | 0.03 | 136.71 | 14.44 | -0.62±0.14 | 1.08±0.01 | 0.85 | -1.59±0.03 | 1.08±0.01 | -0.56 | 5.71 |
| **$PM_{2.5}$_cor S18** | 3936 | 1.69 | 13.90 | 11.37 | -3.40 | 143.59 | 11.86 | 1.08±0.08 | 0.92±0.00 | 0.92 | -0.98±0.04 | 1.14±0.01 | 0.00 | 3.42 |
| **$PM_{2.5}$_raw S19** | 3863 | 0.00 | 17.69 | 12.85 | 0.03 | 151.69 | 16.43 | 0.47±0.14 | 1.24±0.01 | 0.88 | -2.13±0.04 | 1.41±0.01 | -3.92 | 7.57 |
| **$PM_{2.5}$_cor S19** | 3863 | 1.06 | 13.95 | 10.98 | -2.34 | 142.67 | 12.10 | 0.69±0.07 | 0.95±0.00 | 0.95 | -0.86±0.03 | 1.12±0.01 | 0.00 | 2.75 |
| **$PM_{2.5}$_raw S20** | 3439 | 0.00 | 15.00 | 10.20 | 0.03 | 80.20 | 14.38 | -1.00±0.13 | 1.17±0.01 | 0.90 | -1.89±0.03 | 1.20±0.01 | -1.46 | 5.31 |
| **$PM_{2.5}$_cor S20** | 3439 | 0.81 | 13.66 | 10.53 | -1.63 | 59.85 | 11.27 | 0.78±0.07 | 0.94±0.00 | 0.94 | -0.78±0.03 | 1.11±0.01 | 0.00 | 2.77 |
| **$PM_{2.5}$EM** | 3753 | 0.00 | 14.25 | 10.87 | 0.38 | 151.18 | 12.50 | | | | | | | |

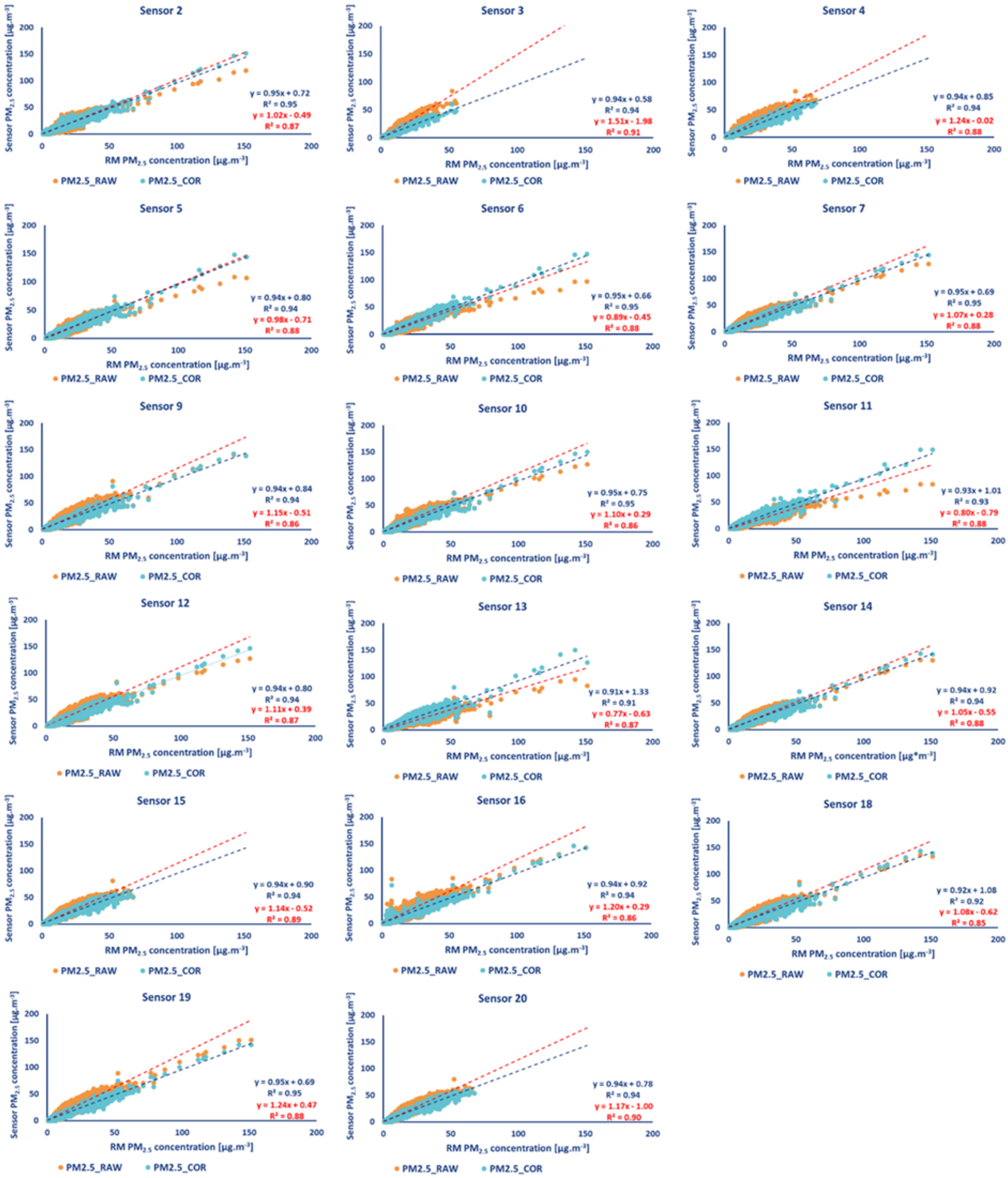


**Figure S12**. Relationship of $PM_{2.5}$ concentrations measured by LCS (the y-axis) and by reference monitor (RM; the x-axis) at the Prague 4-Libuš air quality monitoring (AQM) station. $PM_{2.5}$_RAW = raw concentrations measured by LCSs, $PM_{2.5}$_COR = LCSs concentrations corrected by MARS method.

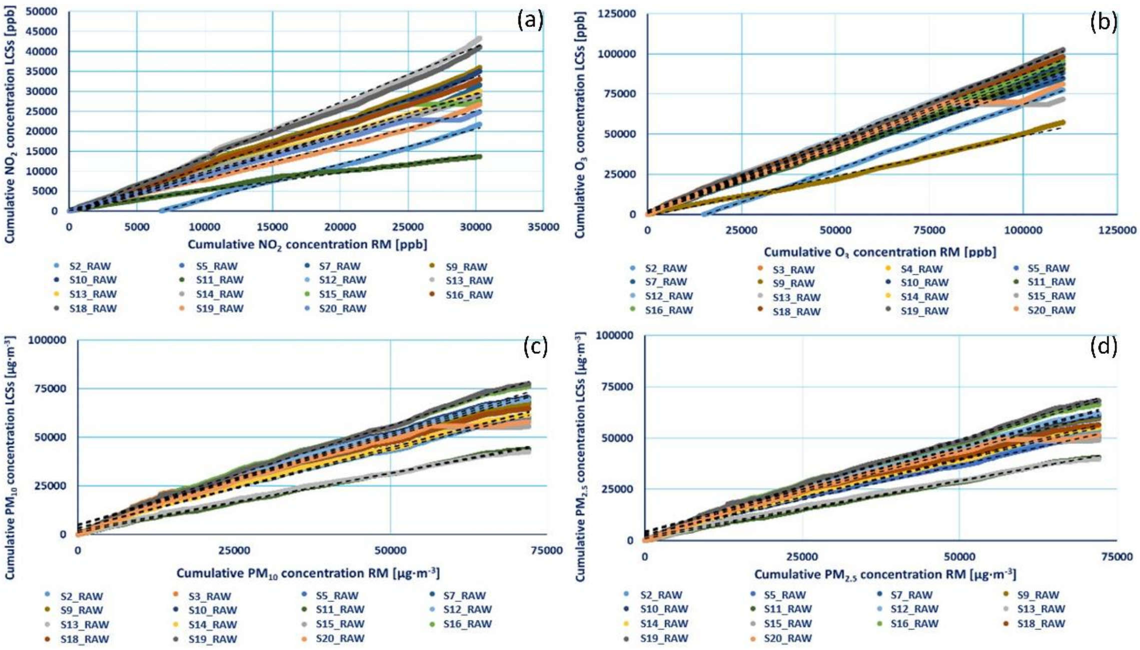


**Figure S13.** The Double Mass Curve (DMC) method for data continuity check and data drift identification. Showed on the relationships of (a) $NO_2$, (b) $O_3$, (c) $PM_{10}$ and (d) $PM_{2.5}$ cumulative raw concentrations measured by all LCS (the y-axis) and by reference and equivalent monitors (RMs and EMs; the x-axis) during the initial field comparative measurement at the Prague 4-Libuš AQM station. Dashed lines are the linear fits of each regression. The data gaps are shown by a change to a horizontal line, the LCS S2 has shifted zero point in case of $NO_2$ and $O_3$ due to the later start of LCSs measurement.

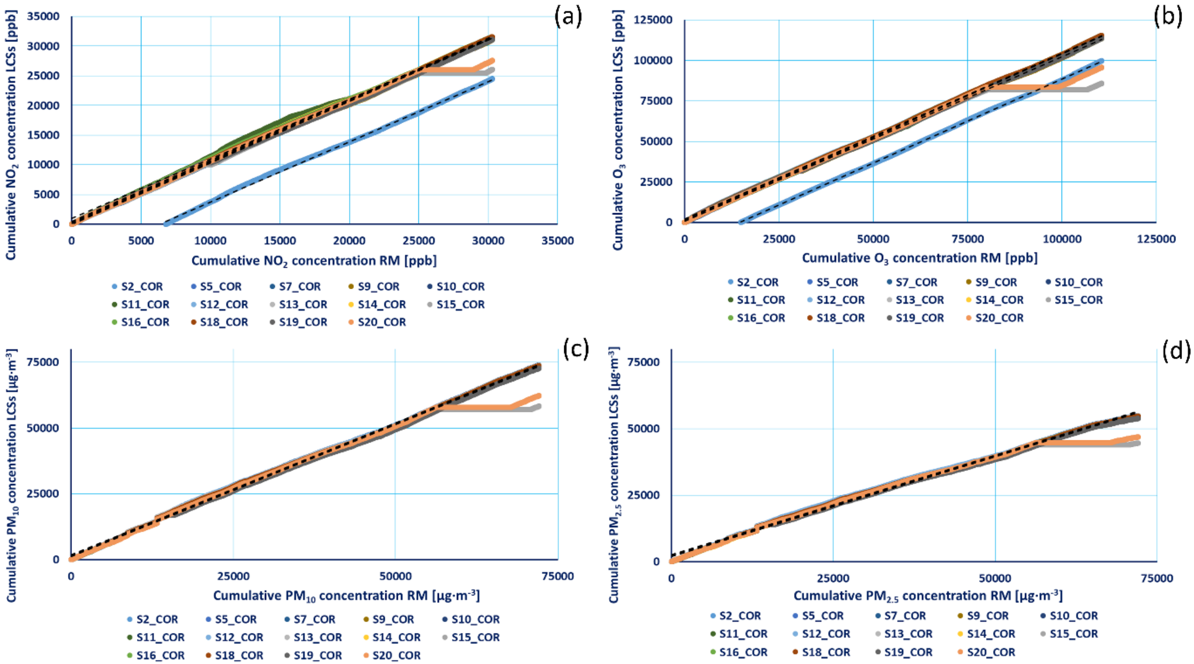


**Figure S14.** Double Mass Curve (DMC) method for data continuity check and data drift identification. Showed on the relationships of (a) $NO_2$, (b) $O_3$, (c) $PM_{10}$ and (d) $PM_{2.5}$ cumulative MARS corrected concentrations of all LCS (the y-axis) and reference or equivalent monitors (RMs and EMs; the x-axis) at the Prague 4-Libuš AQM station during initial field comparative measurement. Dashed lines are the linear fits of each regression. The data gaps are shown by a change to a horizontal line, the LCS S2 has shifted zero point in case of $NO_2$ and $O_3$ due to the later start of LCSs measurement.

### S3.1.2 LCSs data quality during Legerova campaign

Mutual comparison of the data from LCSs installed in pairs at the same locations but at different height levels above the ground during the Legerova campaign (i.e. S11 + S10, S20 + S13, S14 + S15, S2 + S5, S12 + S18, S9 + S7, always mentioned as lower + higher elevation) and the LCS S4 collocated with the Prague Legerova AQM, installed in the same height as the control monitor throughout the campaign.

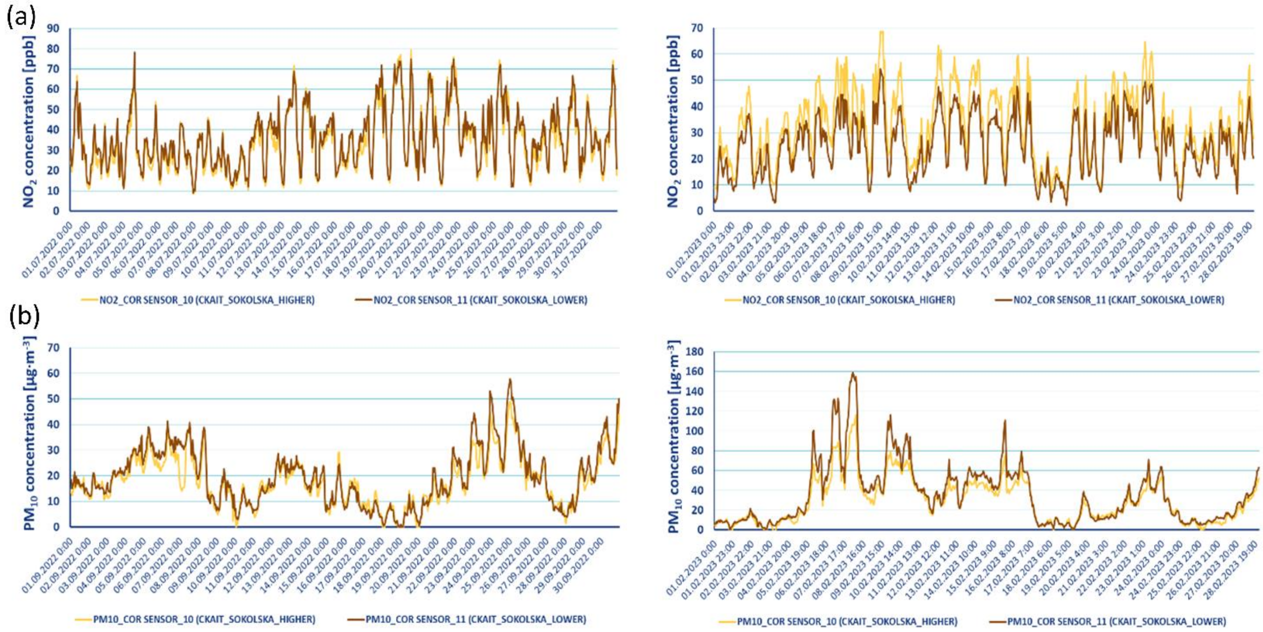


**Figure S15.** The course of 1-hour average MARS corrected concentrations from the pair of LCSs S10 and S11 during Legerova campaign (both installed at CKAIT Sokolská locality in different height levels); (a) $NO_2$ concentrations (ppb) during July 2022 and February 2023, (b) $PM_{10}$ concentrations ($\mu g \cdot m^{-3}$) during September 2022 and February 2023.

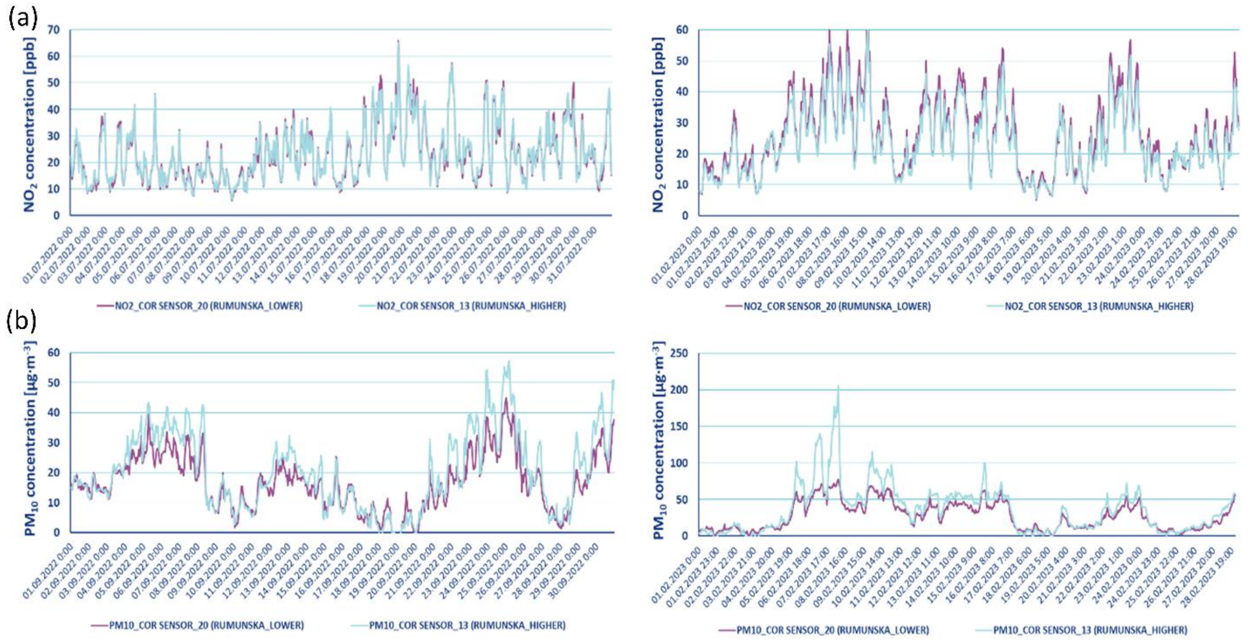


**Figure S16.** The course of 1-hour average MARS corrected concentrations from the pair of LCSs S20 and S13 during Legerova campaign (both installed at Rumunská locality in different height levels); (a) $NO_2$ concentrations (ppb) during July 2022 and February 2023, (b) $PM_{10}$ concentrations ($\mu g \cdot m^{-3}$) during September 2022 and February 2023.

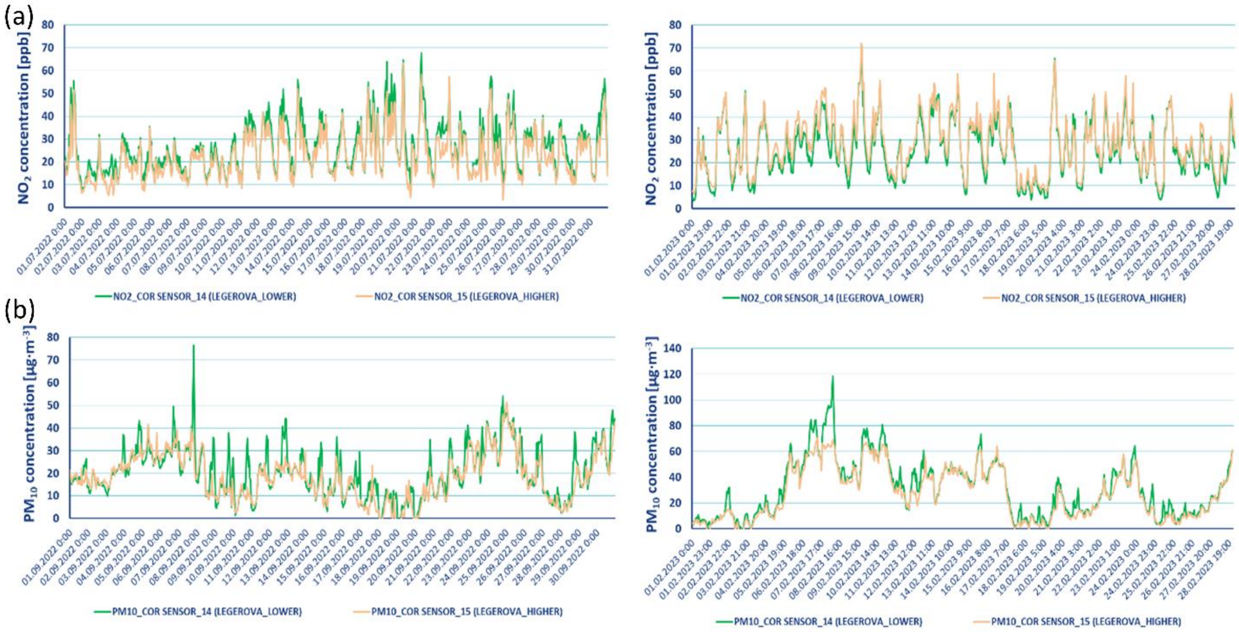


**Figure S17.** The course of 1-hour average MARS corrected concentrations from the pair of LCSs S14 and S15 during Legerova campaign (both installed at Legerova locality in different height levels); (a) $NO_2$ concentrations (ppb) during July 2022 and February 2023, (b) $PM_{10}$ concentrations ($\mu g \cdot m^{-3}$) during September 2022 and February 2023.

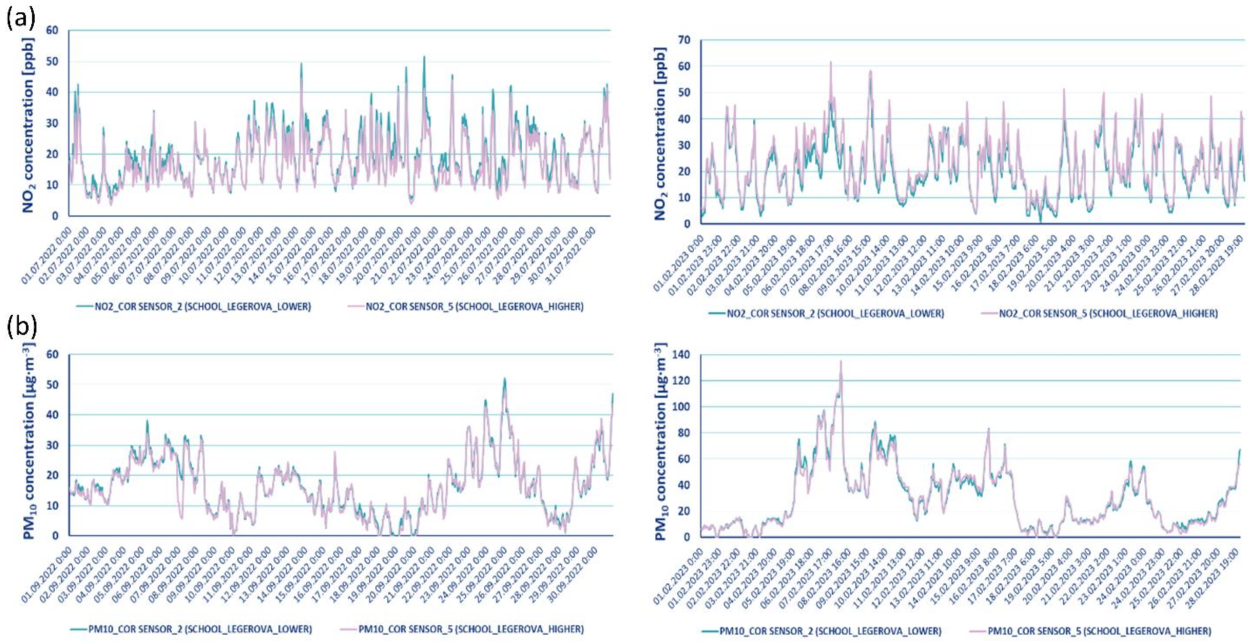


**Figure S18.** The course of 1-hour average MARS corrected concentrations from the pair of LCSs S2 and S5 during Legerova campaign (both installed at School Legerova locality in different height levels); (a) $NO_2$ concentrations (ppb) during July 2022 and February 2023, (b) $PM_{10}$ concentrations ($\mu g \cdot m^{-3}$) during September 2022 and February 2023.

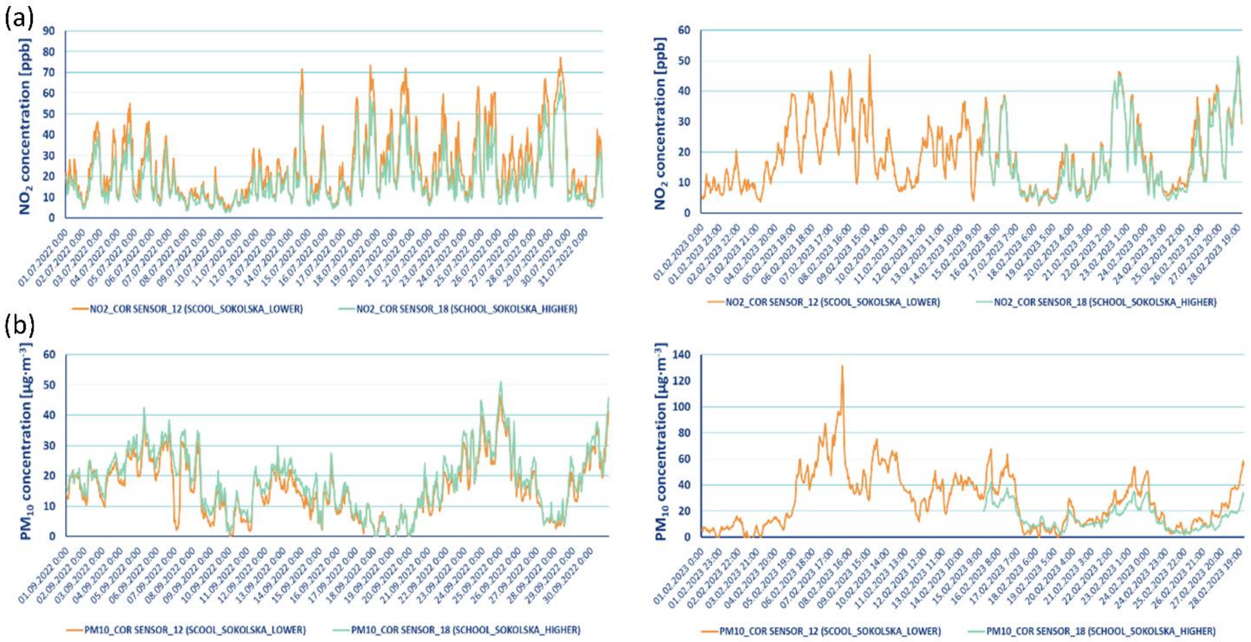


**Figure S19.** The course of 1-hour average MARS corrected concentrations from the pair of LCSs S12 and S18 during Legerova campaign (both installed at School Sokolská locality in different height levels); (a) $NO_2$ concentrations (ppb) during July 2022 and February 2023, (b) $PM_{10}$ concentrations (µg·m$^{-3}$) during September 2022 and February 2023.

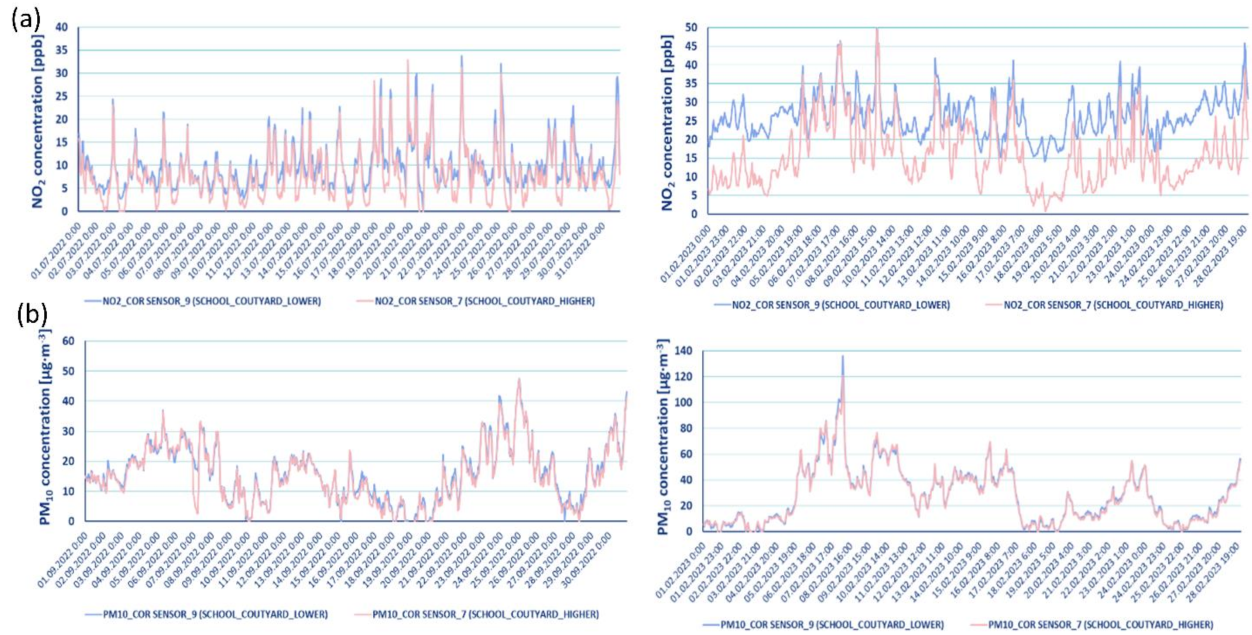


**Figure S20.** The course of 1-hour average MARS corrected concentrations from the pair of LCSs S9 and S7 during Legerova campaign (both installed at School courtyard locality in different height levels); (a) $NO_2$ concentrations (ppb) during July 2022 and February 2023, (b) $PM_{10}$ concentrations (µg·m$^{-3}$) during September 2022 and February 2023.

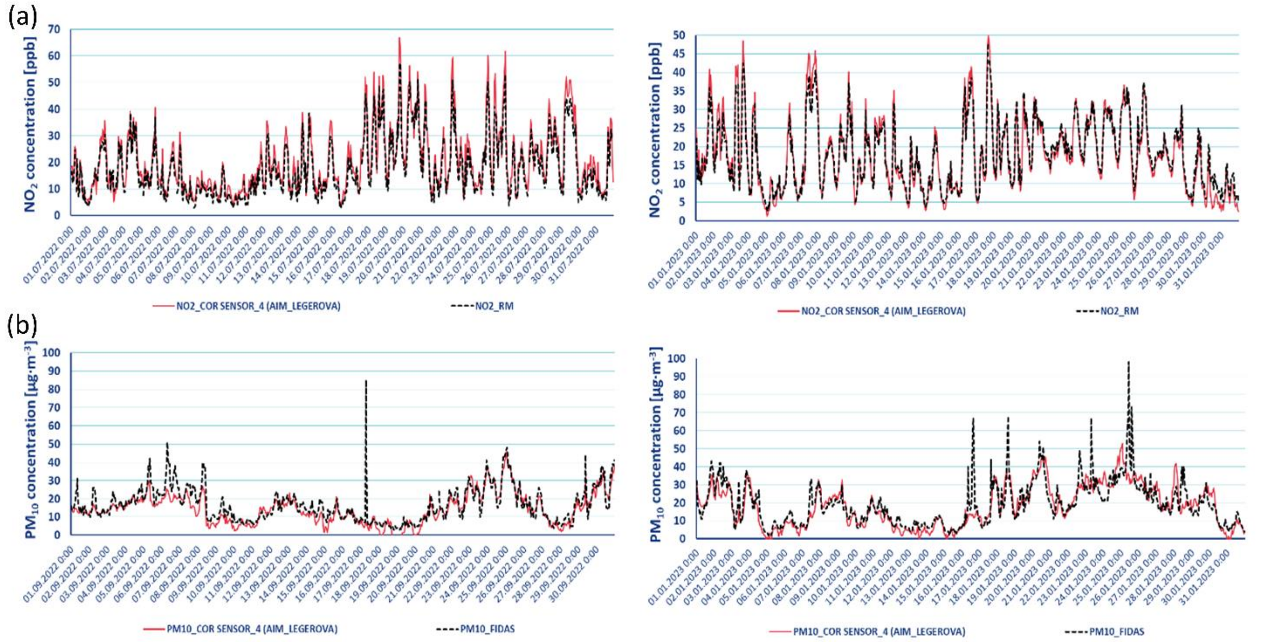


**Figure S21.** The course of 1-hour average MARS corrected concentrations from the LCS S4 and RM or EM (Fidas) during Legerova campaign (both installed at the Legerova AQM station); (a) $NO_2$ concentrations (ppb) during July 2022 and February 2023, (b) $PM_{10}$ concentrations ($\mu g \cdot m^{-3}$) during September 2022 and February 2023.

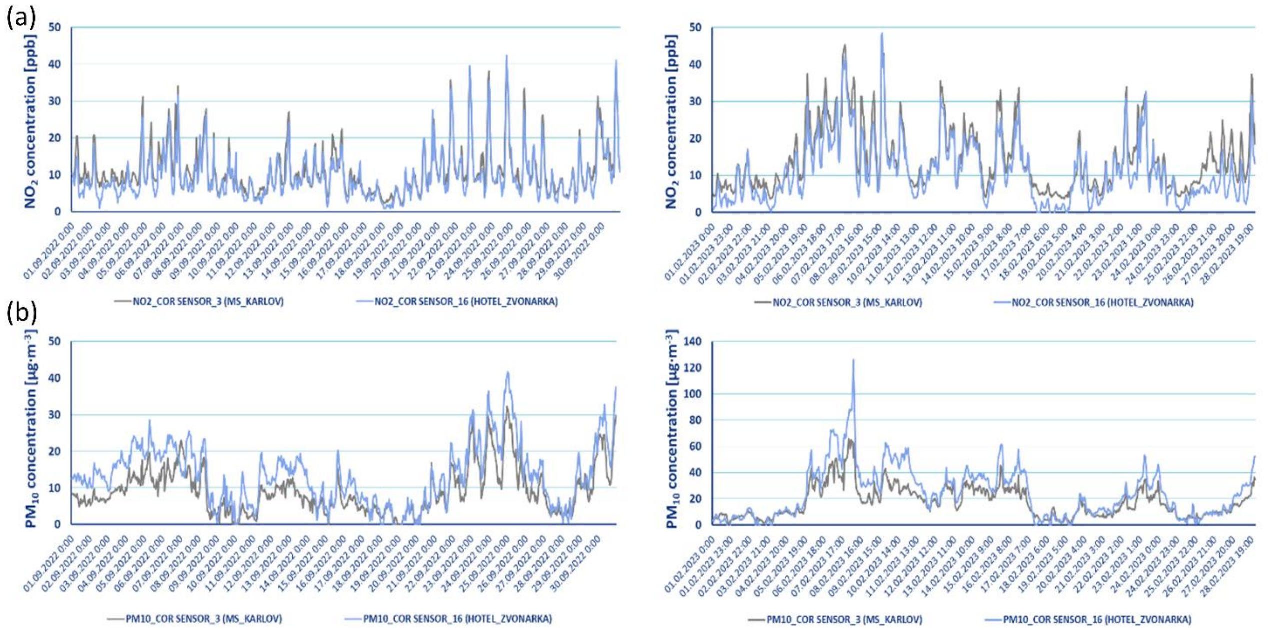


**Figure S22.** The course of 1-hour average MARS corrected concentrations from the pair of LCSs S3 and S16 during Legerova campaign (installed at the Prague Karlov MS roof and at the Hotel Zvonařka roof, both classified as background LCSs stations); (a) $NO_2$ concentrations (ppb) during July 2022 and February 2023, (b) $PM_{10}$ concentrations ($\mu g \cdot m^{-3}$) during September 2022 and February 2023.

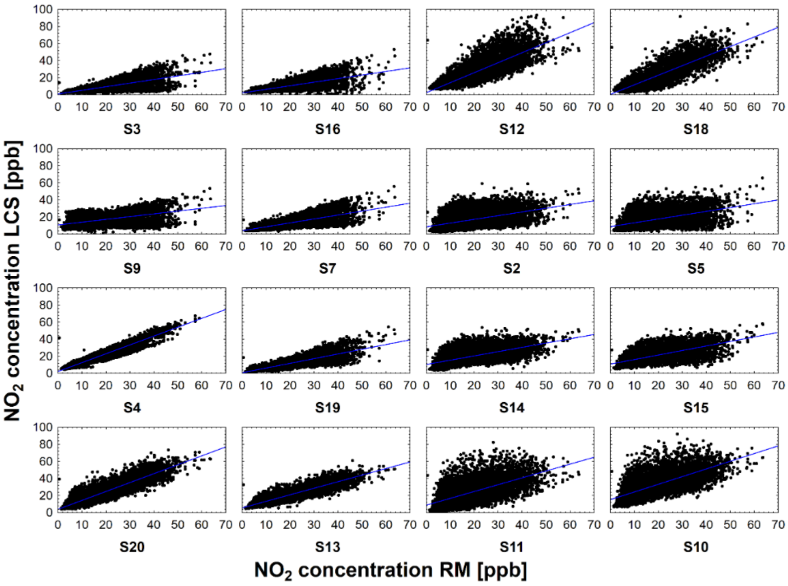


**Figure S23.** Relationships of the MARS corrected $NO_2$ LCSs concentrations (the y-axis) and $NO_2$ concentrations measured by the RM Legerova (the x- axis; during the Legerova measurement campaign from May 30, 2022 to March 28, 2023). Only the LCS S4 was collocated with the RM Legerova, other LCSs were installed at different distances from the RM Legerova. Similar patterns were observed in pairs placed at the same locations (S12 + S18, S9 + S7, S2 + S5, S14 + S15, S20 + S13, S11 + S10).

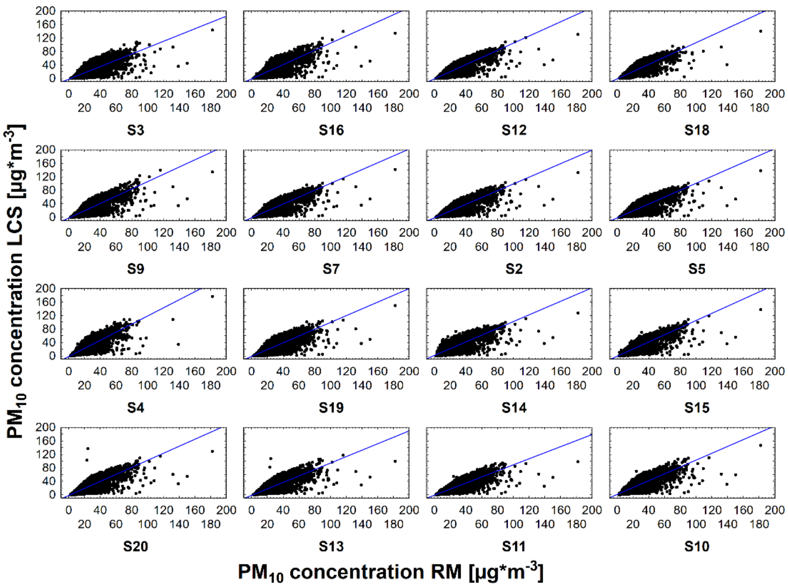


**Figure S24.** Relationships of the MARS corrected $PM_{10}$ LCSs concentrations (the y-axis) and $PM_{10}$ concentrations measured by the RM Legerova (the x-axis; during the Legerova measurement campaign from May 30, 2022 to March 28, 2023). Only the LCS S4 was collocated with the RM Legerova, other LCSs were installed at different distances from the RM Legerova. Similar patterns were observed in pairs placed at the same locations (S12 + S18, S9 + S7, S2 + S5, S14 + S15, S20 + S13, S11 + S10).

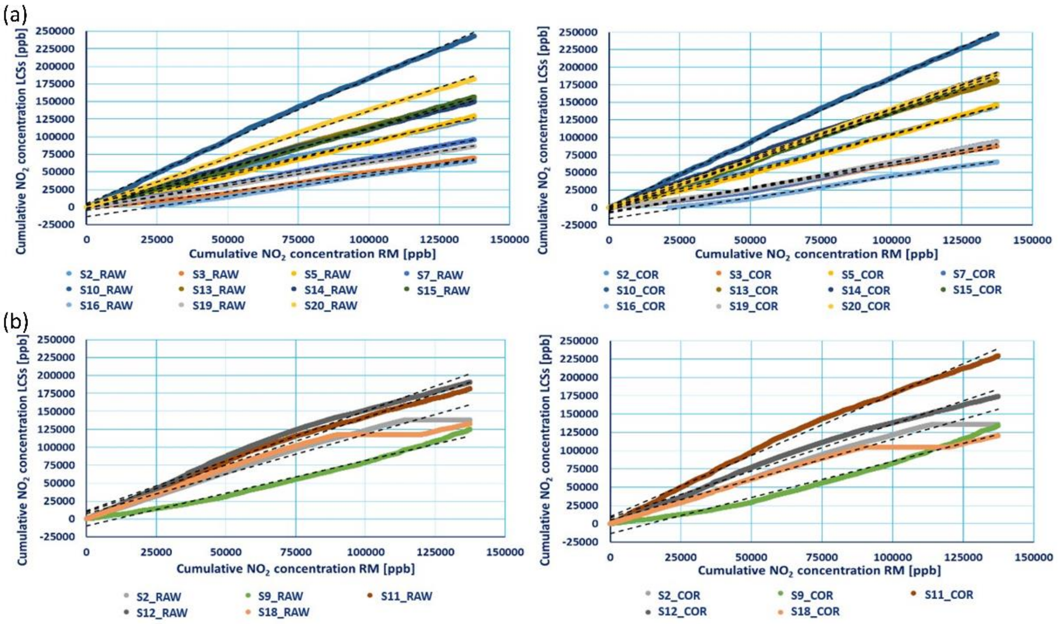


**Figure S25.** The Double Mass Curve (DMC) method for data continuity check and data drift identification. Showed on the relationships of $NO_2$ cumulative LCS concentrations (the y-axis) and $NO_2$ cumulative concentrations measured by RM Legerova (the x-axis) during the Legerova campaign. Dashed lines are the linear fits of each regression. (a) LCSs identified without any data drifts in raw (on the left) or MARS corrected (on the right) $NO_2$ LCS concentrations, (b) LCSs with identified data gaps (S4 and S18) and data drifts in raw (on the left) or MARS corrected (on the right) $NO_2$ concentrations (in case of S11, S12 and S9).

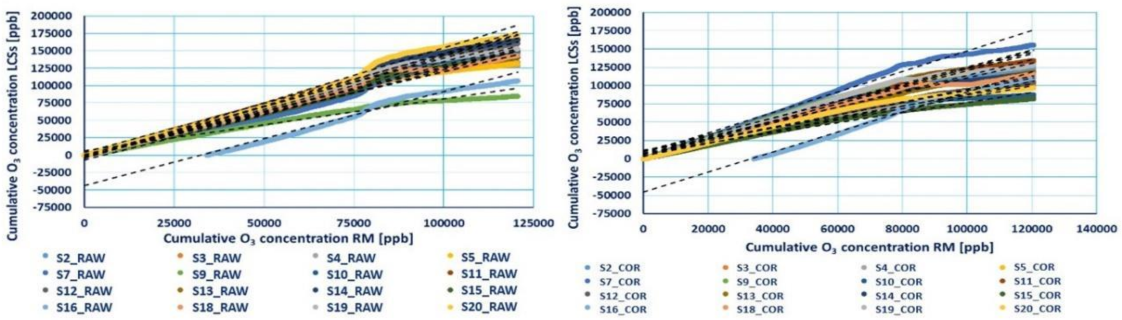


**Figure S26.** The Double Mass Curve (DMC) method for data continuity check and data drift identification. Showed on the relationships of $O_3$, cumulative LCS concentrations (the y-axis) and $O_3$ cumulative concentrations measured by RM Vysočany (the x-axis) during the Legerova campaign. Dashed lines are the linear fits of each regression. The difference between raw (on the left) and MARS corrected (on the right) LCS $O_3$ concentrations is shown. A partial data drift was identified in all LCSs during the October and November 2022 (around the value of 80,000 ppb measured by the RM).

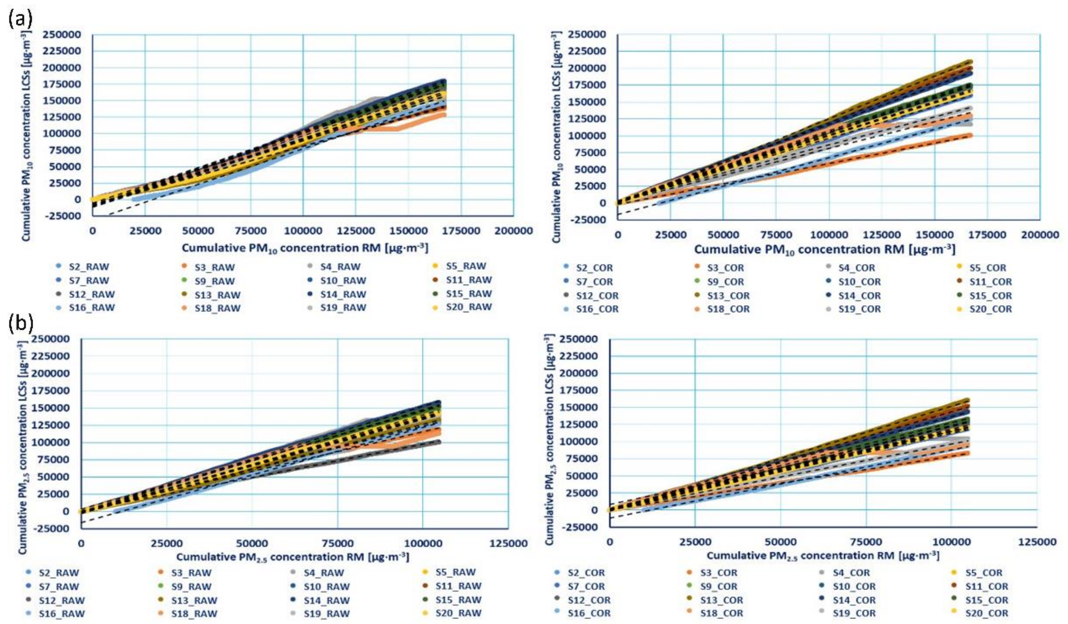

**Figure S27.** The Double Mass Curve (DMC) method for data continuity check and data drift identification. Showed on the relationships of (a) $PM_{10}$ cumulative LCS concentrations (the y-axis) and $PM_{10}$ cumulative concentrations measured by RM Legerova (the x-axis); (b) $PM_{2.5}$ cumulative LCS concentrations (the y-axis) and $PM_{2.5}$ cumulative concentrations measured by RM Legerova (the x-axis) during the Legerova campaign. Dashed lines are the linear fits of each regression. The difference between raw (on the left) and MARS corrected (on the right) LCS concentrations is shown. No significant data drifts were identified. Data gaps are shown in case of S4 and S18.

### S3.1.3 LCSs data quality during final field comparative measurement at the Prague Libuš AQM station

Results of the final field comparative measurement of all LCSs at the Prague Libuš AQM station lasting from 9 May 2023 to 14 June 2023 (37 days).

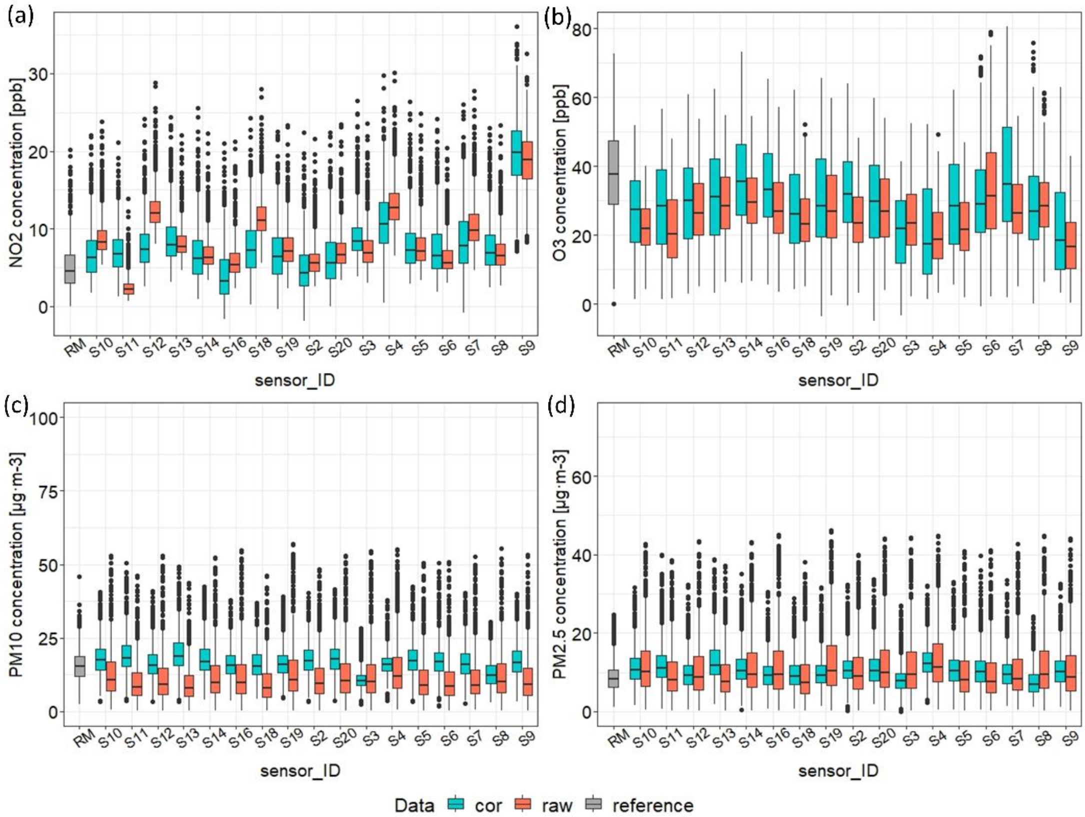


**Figure S28**. Boxplot showing medians and ranges of (a) $NO_2$, (b) $O_3$, (c) $PM_{10}$ and (d) $PM_{2.5}$ 1-hourly averaged concentrations originally measured by LCSs (raw; red colour), corrected by the MARS method (corrected; blue colour) and by reference or equivalent method (RM; grey colour) during the final field comparative measurement at the Prague Libuš RM station from 9 May 2023 to 14 June 2023. Black dots show the deviated concentrations. Some weakly negative values are shown in MARS corrected data (less than 1 % of the whole dataset for both gases and aerosols).

**Table S16.** Summary statistics of 1-hour average $NO_2$ concentrations measured by all LCSs during final field comparative measurement at the Prague Libuš AQM station. Raw = original values of concentrations, cor = corrected values of concentrations (by MARS method). N valid = number of valid values, % valid = percentage of valid values in the dataset, Min = minimum value, Max = maximum value, SD = standard deviation, parameters resulting from linear regression between LCS and RM/EM concentrations: a = intercept, b = slope, SE = standard error, $R^2$ = coefficient of determination, MBE = Mean bias error, MAE = Mean absolute error, RMSE = Root mean square error.

| | **Descriptive statistics** | | | | | | **Linear regression** | | | **Williamson-York regression** | | **Error** | |
|---|---|---|---|---|---|---|---|---|---|---|---|---|---|
| **Variable** | **N valid** | **Mean** | **Median** | **Min** | **Max** | **SD** | **a ± SE** | **b ± SE** | **R2** | **a ± SE** | **b ± SE** | **MBE** | **RMSE** |
| **$NO_2$_raw S2** | 862 | 6.01 | 5.53 | 2.54 | 21.53 | 2.35 | 2.85±0.10 | 0.59±0.02 | 0.63 | 2.84±0.10 | 0.48±0.02 | -0.68 | 2.05 |
| **$NO_2$_cor S2** | 862 | 5.01 | 4.30 | -1.87 | 22.43 | 3.28 | -0.27±0.07 | 0.99±0.01 | 0.90 | -1.31±0.07 | 1.18±0.02 | 0.33 | 1.08 |
| **$NO_2$_raw S3** | 862 | 7.46 | 6.91 | 3.00 | 23.55 | 2.71 | 3.74±0.11 | 0.70±0.02 | 0.66 | 3.59±0.11 | 0.60±0.02 | -2.14 | 2.83 |
| **$NO_2$_cor S3** | 862 | 9.10 | 8.39 | 3.77 | 26.45 | 3.06 | 4.60±0.10 | 0.84±0.02 | 0.76 | 4.50±0.11 | 0.77±0.02 | -3.77 | 4.09 |
| **$NO_2$_raw S4** | 862 | 13.04 | 12.66 | 6.52 | 30.11 | 2.97 | 9.36±0.14 | 0.69±0.02 | 0.54 | 9.07±0.16 | 0.61±0.03 | -7.71 | 8.03 |
| **$NO_2$_cor S4** | 862 | 10.83 | 10.58 | 0.45 | 29.76 | 4.01 | 5.67±0.18 | 0.97±0.03 | 0.58 | 2.04±0.19 | 1.46±0.05 | -5.48 | 6.07 |
| **$NO_2$_raw S5** | 862 | 7.82 | 7.11 | 3.38 | 24.91 | 2.91 | 3.53±0.10 | 0.80±0.02 | 0.76 | 3.53±0.10 | 0.70±0.02 | -2.49 | 2.94 |
| **$NO_2$_cor S5** | 862 | 8.01 | 7.17 | 2.89 | 26.35 | 3.61 | 2.21±0.08 | 1.09±0.01 | 0.90 | 1.95±0.08 | 1.07±0.02 | -2.67 | 2.92 |
| **$NO_2$_raw S6** | 862 | 6.30 | 5.58 | 3.01 | 20.36 | 2.36 | 2.60±0.06 | 0.69±0.01 | 0.86 | 2.86±0.06 | 0.60±0.01 | -0.97 | 1.63 |
| **$NO_2$_cor S6** | 862 | 7.40 | 6.54 | 1.88 | 24.16 | 3.63 | 1.59±0.08 | 1.09±0.01 | 0.89 | 1.04±0.09 | 1.13±0.02 | -2.06 | 2.40 |
| **$NO_2$_raw S7** | 862 | 10.43 | 9.83 | 4.60 | 27.76 | 3.14 | 6.32±0.14 | 0.77±0.02 | 0.60 | 5.89±0.15 | 0.70±0.03 | -5.11 | 5.53 |
| **$NO_2$_cor S7** | 862 | 8.54 | 7.85 | -0.86 | 26.07 | 4.08 | 2.84±0.16 | 1.07±0.03 | 0.68 | -0.49±0.16 | 1.59±0.04 | -3.19 | 3.94 |
| **$NO_2$_raw S9** | 862 | 18.71 | 18.89 | 8.23 | 32.54 | 3.79 | 16.59±0.25 | 0.40±0.04 | 0.11 | 15.01±0.30 | 0.36±0.05 | -13.38 | 13.98 |
| **$NO_2$_cor S9** | 862 | 19.73 | 19.89 | 7.10 | 36.07 | 4.67 | 16.43±0.29 | 0.61±0.05 | 0.17 | 13.87±0.35 | 0.64±0.07 | -14.39 | 15.05 |
| **$NO_2$_raw S10** | 862 | 8.96 | 8.30 | 5.38 | 23.81 | 2.60 | 5.01±0.08 | 0.74±0.01 | 0.81 | 5.18±0.08 | 0.65±0.02 | -3.63 | 3.89 |
| **$NO_2$_cor S10** | 862 | 6.91 | 6.22 | 1.70 | 22.04 | 3.28 | 1.51±0.05 | 1.01±0.01 | 0.94 | 0.99±0.06 | 1.08±0.02 | -1.57 | 1.76 |
| **$NO_2$_raw S11** | 697 | 2.56 | 2.18 | 0.66 | 13.89 | 1.57 | 0.47±0.07 | 0.38±0.01 | 0.61 | 0.61±0.06 | 0.26±0.01 | 2.92 | 3.67 |
| **$NO_2$_cor S11** | 697 | 7.18 | 6.72 | 1.25 | 21.07 | 2.85 | 2.82±0.09 | 0.79±0.01 | 0.81 | 2.11±0.10 | 0.85±0.02 | -1.70 | 2.20 |
| **$NO_2$_raw S12** | 862 | 12.58 | 12.01 | 7.98 | 28.78 | 2.75 | 8.80±0.11 | 0.71±0.02 | 0.66 | 8.82±0.11 | 0.63±0.02 | -7.25 | 7.48 |
| **$NO_2$_cor S12** | 862 | 7.89 | 7.26 | 2.58 | 24.11 | 3.10 | 2.84±0.06 | 0.94±0.01 | 0.92 | 2.48±0.06 | 0.98±0.02 | -2.54 | 2.70 |
| **$NO_2$_raw S13** | 862 | 8.32 | 7.65 | 4.68 | 22.01 | 2.29 | 4.85±0.07 | 0.65±0.01 | 0.80 | 5.05±0.07 | 0.57±0.01 | -3.00 | 3.35 |
| **$NO_2$_cor S13** | 862 | 8.73 | 7.96 | 3.09 | 24.43 | 3.12 | 3.65±0.06 | 0.95±0.01 | 0.92 | 3.50±0.07 | 0.94±0.02 | -3.39 | 3.50 |
| **$NO_2$_raw S14** | 862 | 6.91 | 6.30 | 3.35 | 22.26 | 2.47 | 3.40±0.09 | 0.66±0.01 | 0.71 | 3.48±0.09 | 0.56±0.02 | -1.58 | 2.33 |
| **$NO_2$_cor S14** | 862 | 6.84 | 6.12 | 0.88 | 25.61 | 3.68 | 1.13±0.10 | 1.07±0.02 | 0.84 | 0.01±0.10 | 1.20±0.03 | -1.50 | 2.11 |
| **$NO_2$_raw S16** | 862 | 5.95 | 5.32 | 2.32 | 21.27 | 2.42 | 2.35±0.08 | 0.68±0.01 | 0.77 | 2.49±0.08 | 0.57±0.02 | -0.62 | 1.67 |
| **$NO_2$_cor S16** | 862 | 4.09 | 3.18 | -1.64 | 20.94 | 3.49 | -1.52±0.08 | 1.05±0.01 | 0.90 | -2.42±0.08 | 1.26±0.03 | 1.26 | 1.68 |
| **$NO_2$_raw S18** | 862 | 11.51 | 11.11 | 5.62 | 28.03 | 2.93 | 7.77±0.13 | 0.70±0.02 | 0.57 | 7.46±0.15 | 0.62±0.03 | -6.18 | 6.54 |
| **$NO_2$_cor S18** | 862 | 7.66 | 7.22 | 0.24 | 24.27 | 3.52 | 2.74±0.14 | 0.92±0.02 | 0.68 | -0.03±0.15 | 1.34±0.04 | -2.32 | 3.06 |
| **$NO_2$_raw S19** | 862 | 7.56 | 7.10 | 2.32 | 23.33 | 2.80 | 4.00±0.13 | 0.67±0.02 | 0.56 | 3.38±0.14 | 0.60±0.03 | -2.24 | 3.09 |
| **$NO_2$_cor S19** | 862 | 6.84 | 6.35 | -0.41 | 22.54 | 3.57 | 1.85±0.14 | 0.93±0.02 | 0.68 | -0.93±0.15 | 1.39±0.04 | -1.50 | 2.51 |
| **$NO_2$_raw S20** | 697 | 7.31 | 6.58 | 3.32 | 23.45 | 2.81 | 3.18±0.11 | 0.75±0.02 | 0.75 | 3.40±0.11 | 0.62±0.02 | -1.83 | 2.44 |
| **$NO_2$_cor S20** | 697 | 6.30 | 5.62 | -0.05 | 22.43 | 3.66 | 0.28±0.07 | 1.10±0.01 | 0.94 | -0.80±0.07 | 1.30±0.02 | -0.82 | 1.24 |
| **$NO_2$ RM** | 825 | 5.30 | 4.50 | 0.00 | 20.18 | 3.17 | | | | | | | |

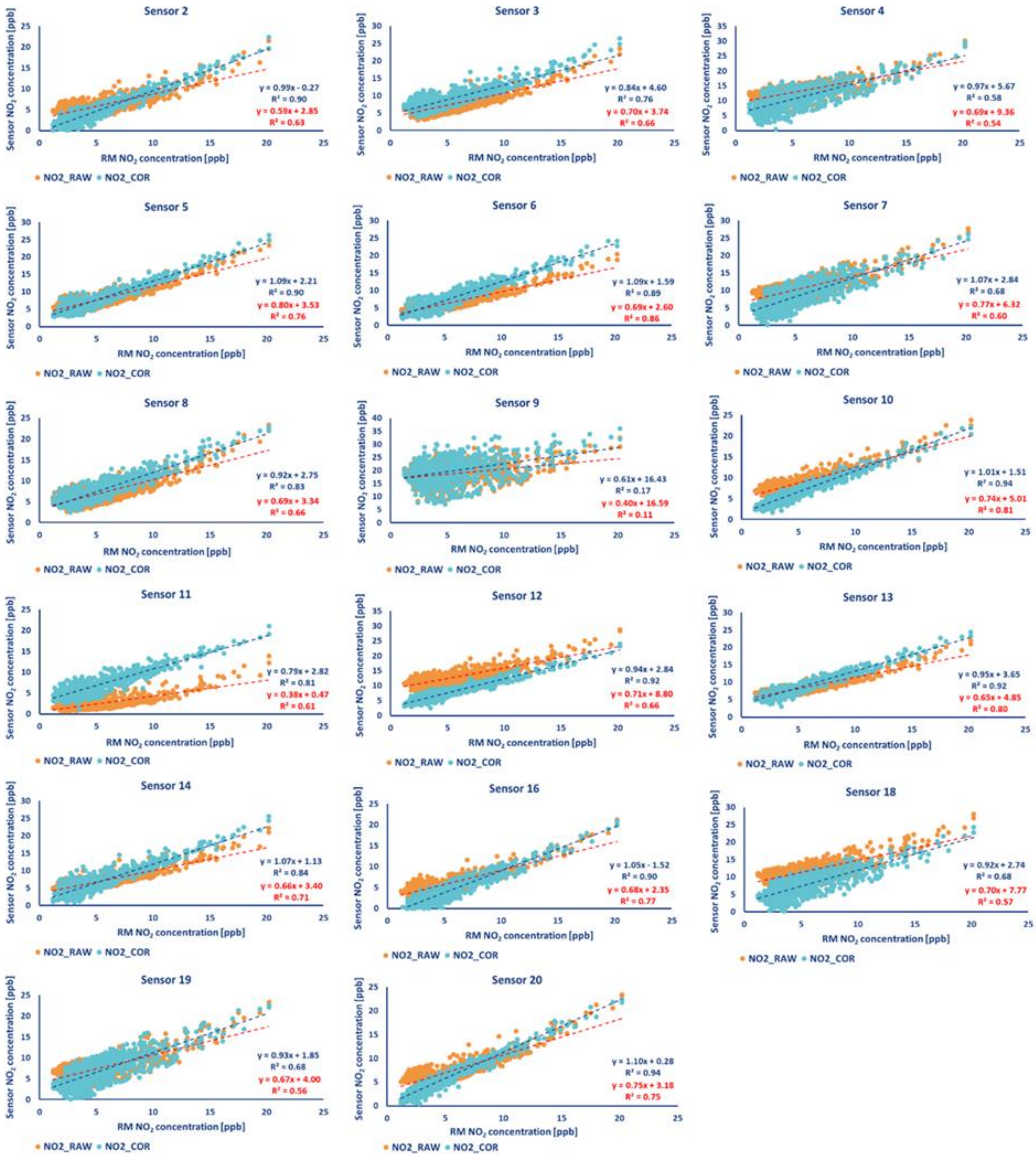


**Figure S29**. Relationship of $NO_2$ concentrations measured by LCS (the y-axis) and by reference monitor (RM; the x-axis) at the Prague Libuš air quality monitoring (AQM) station during final field comparative measurement. $NO_2$_RAW = raw concentrations measured by LCSs, $NO_2$_COR = LCSs concentrations corrected by MARS method.

**Table S17.** Summary statistics of 1-hour average $O_3$ concentrations measured by all LCSs during final field comparative measurement at the Prague 4-Libuš AQM station. Raw = original values of concentrations, cor = corrected values of concentrations (by MARS method). N valid = number of valid values, % valid = percentage of valid values in the dataset, Min = minimum value, Max = maximum value, SD = standard deviation, parameters resulting from linear regression between LCS and RM/EM concentrations: a = intercept, b = slope, SE = standard error, $R^2$ = coefficient of determination, MBE = Mean bias error, MAE = Mean absolute error, RMSE = Root mean square error.

| | **Descriptive statistics** | | | | | | **Linear regression** | | | **Williamson-York regression** | | **Error** | |
|---|---|---|---|---|---|---|---|---|---|---|---|---|---|
| **Variable** | **N valid** | **Mean** | **Median** | **Min** | **Max** | **SD** | **a ± SE** | **b ± SE** | **R2** | **a ± SE** | **b ± SE** | **MBE** | **RMSE** |
| **$O_3$_raw S2** | 862 | 24.05 | 23.40 | 3.33 | 48.26 | 9.18 | -1.06±0.25 | 0.67±0.01 | 0.93 | 0.01±0.14 | 0.63±0.01 | 13.34 | 14.24 |
| **$O_3$_cor S2** | 862 | 31.61 | 31.94 | -0.33 | 63.98 | 13.17 | -4.86±0.30 | 0.98±0.01 | 0.95 | -5.41±0.13 | 0.98±0.01 | 5.73 | 6.43 |
| **$O_3$_raw S3** | 862 | 23.90 | 23.39 | 2.29 | 52.47 | 9.76 | -2.49±0.31 | 0.71±0.01 | 0.91 | -1.24±0.15 | 0.65±0.01 | 13.49 | 14.36 |
| **$O_3$_cor S3** | 862 | 20.39 | 22.00 | -3.42 | 41.35 | 11.08 | -9.04±0.41 | 0.79±0.01 | 0.88 | -9.45±0.20 | 0.78±0.01 | 17.00 | 17.67 |
| **$O_3$_raw S4** | 862 | 20.20 | 18.87 | 3.31 | 49.14 | 9.05 | -3.99±0.32 | 0.65±0.01 | 0.89 | -0.90±0.16 | 0.54±0.01 | 17.19 | 18.07 |
| **$O_3$_cor S4** | 862 | 21.75 | 17.40 | 1.37 | 52.10 | 14.62 | -16.10±0.62 | 1.02±0.02 | 0.84 | -6.03±0.38 | 0.66±0.02 | 15.45 | 16.55 |
| **$O_3$_raw S5** | 862 | 22.13 | 21.74 | 2.03 | 46.89 | 9.46 | -3.49±0.29 | 0.69±0.01 | 0.91 | -1.82±0.14 | 0.62±0.01 | 15.25 | 16.04 |
| **$O_3$_cor S5** | 862 | 29.15 | 28.57 | 5.52 | 62.19 | 13.62 | -7.67±0.43 | 0.99±0.01 | 0.91 | -3.01±0.26 | 0.82±0.01 | 8.13 | 9.11 |
| **$O_3$_raw S6** | 862 | 33.42 | 31.33 | 2.23 | 78.97 | 15.67 | -8.74±0.52 | 1.13±0.01 | 0.90 | -3.40±0.22 | 0.95±0.01 | 3.81 | 6.51 |
| **$O_3$_cor S6** | 862 | 30.27 | 29.07 | -0.65 | 71.82 | 15.25 | -11.49±0.42 | 1.12±0.01 | 0.93 | -6.83±0.19 | 0.96±0.01 | 6.99 | 8.20 |
| **$O_3$_raw S7** | 862 | 27.27 | 26.34 | 5.20 | 54.62 | 9.68 | 1.10±0.31 | 0.70±0.01 | 0.91 | 1.88±0.18 | 0.67±0.01 | 10.08 | 11.21 |
| **$O_3$_cor S7** | 862 | 36.70 | 34.83 | 2.02 | 80.53 | 17.68 | -11.53±0.51 | 1.29±0.01 | 0.93 | -6.71±0.32 | 1.12±0.01 | 0.45 | 6.22 |
| **$O_3$_raw S9** | 861 | 16.75 | 16.60 | 0.21 | 42.99 | 8.63 | -6.75±0.27 | 0.63±0.01 | 0.91 | -4.26±0.13 | 0.54±0.01 | 20.71 | 21.44 |
| **$O_3$_cor S9** | 861 | 21.53 | 18.60 | 3.25 | 62.81 | 12.93 | -12.91±0.49 | 0.92±0.01 | 0.87 | -4.04±0.28 | 0.62±0.01 | 15.79 | 16.49 |
| **$O_3$_raw S10** | 862 | 21.97 | 21.85 | 4.22 | 40.16 | 7.19 | 2.38±0.21 | 0.53±0.01 | 0.92 | 2.08±0.13 | 0.53±0.00 | 15.48 | 16.83 |
| **$O_3$_cor S10** | 862 | 26.41 | 27.35 | 1.46 | 51.83 | 11.38 | -4.56±0.34 | 0.83±0.01 | 0.92 | -3.78±0.15 | 0.79±0.01 | 10.96 | 11.64 |
| **$O_3$_raw S11** | 697 | 21.63 | 20.32 | 1.66 | 48.02 | 10.58 | -5.56±0.32 | 0.73±0.01 | 0.93 | -2.59±0.16 | 0.62±0.01 | 15.96 | 16.68 |
| **$O_3$_cor S11** | 697 | 28.39 | 28.52 | 1.42 | 56.54 | 13.33 | -6.32±0.34 | 0.92±0.01 | 0.95 | -3.93±0.14 | 0.84±0.01 | 9.18 | 9.74 |
| **$O_3$_raw S12** | 862 | 27.05 | 26.49 | 4.95 | 53.82 | 9.95 | 0.21±0.32 | 0.72±0.01 | 0.91 | 1.09±0.21 | 0.68±0.01 | 10.34 | 11.41 |
| **$O_3$_cor S12** | 862 | 29.16 | 29.92 | 2.87 | 60.75 | 13.20 | -6.69±0.41 | 0.96±0.01 | 0.91 | -4.37±0.23 | 0.87±0.01 | 8.19 | 9.08 |
| **$O_3$_raw S13** | 862 | 28.82 | 28.59 | 6.28 | 54.76 | 9.92 | 1.98±0.32 | 0.72±0.01 | 0.91 | 2.42±0.20 | 0.69±0.01 | 8.58 | 9.82 |
| **$O_3$_cor S13** | 862 | 30.88 | 31.14 | 3.14 | 62.48 | 13.81 | -6.66±0.42 | 1.01±0.01 | 0.92 | -3.96±0.22 | 0.90±0.01 | 6.43 | 7.57 |
| **$O_3$_raw S14** | 862 | 29.66 | 29.41 | 6.70 | 54.61 | 9.37 | 4.15±0.28 | 0.68±0.01 | 0.92 | 3.94±0.19 | 0.68±0.01 | 7.73 | 9.19 |
| **$O_3$_cor S14** | 862 | 35.98 | 35.53 | 6.00 | 73.25 | 14.33 | -3.57±0.35 | 1.06±0.01 | 0.95 | -1.79±0.22 | 0.99±0.01 | 1.30 | 3.65 |
| **$O_3$_raw S16** | 862 | 27.34 | 26.85 | 3.41 | 57.05 | 10.28 | -0.42±0.33 | 0.74±0.01 | 0.91 | 0.09±0.18 | 0.71±0.01 | 10.03 | 11.05 |
| **$O_3$_cor S16** | 862 | 33.49 | 33.27 | 5.68 | 65.26 | 12.32 | -0.11±0.35 | 0.90±0.01 | 0.93 | -0.60±0.22 | 0.90±0.01 | 3.85 | 5.27 |
| **$O_3$_raw S18** | 862 | 24.45 | 23.31 | 5.14 | 52.15 | 9.08 | 0.59±0.36 | 0.64±0.01 | 0.86 | 2.11±0.19 | 0.58±0.01 | 12.95 | 14.23 |
| **$O_3$_cor S18** | 862 | 27.89 | 26.15 | 4.19 | 62.03 | 13.42 | -7.50±0.51 | 0.95±0.01 | 0.87 | -3.32±0.32 | 0.79±0.01 | 9.38 | 10.60 |
| **$O_3$_raw S19** | 862 | 27.73 | 26.81 | 2.39 | 59.68 | 11.82 | -4.37±0.35 | 0.86±0.01 | 0.92 | -2.22±0.18 | 0.78±0.01 | 9.58 | 10.32 |
| **$O_3$_cor S19** | 862 | 29.55 | 28.36 | -3.57 | 65.49 | 15.11 | -11.77±0.42 | 1.11±0.01 | 0.93 | -9.47±0.19 | 1.02±0.01 | 7.68 | 8.76 |
| **$O_3$_raw S20** | 697 | 27.51 | 26.77 | 4.12 | 53.94 | 10.66 | -0.03±0.31 | 0.73±0.01 | 0.93 | 0.83±0.18 | 0.70±0.01 | 10.10 | 11.12 |
| **$O_3$_cor S20** | 697 | 29.17 | 29.77 | -4.83 | 59.80 | 14.23 | -8.07±0.33 | 0.99±0.01 | 0.96 | -9.72±0.14 | 1.03±0.01 | 8.39 | 8.89 |
| **$O_3$ RM** | 825 | 37.49 | 37.78 | 0.00 | 72.66 | 13.43 | | | | | | | |

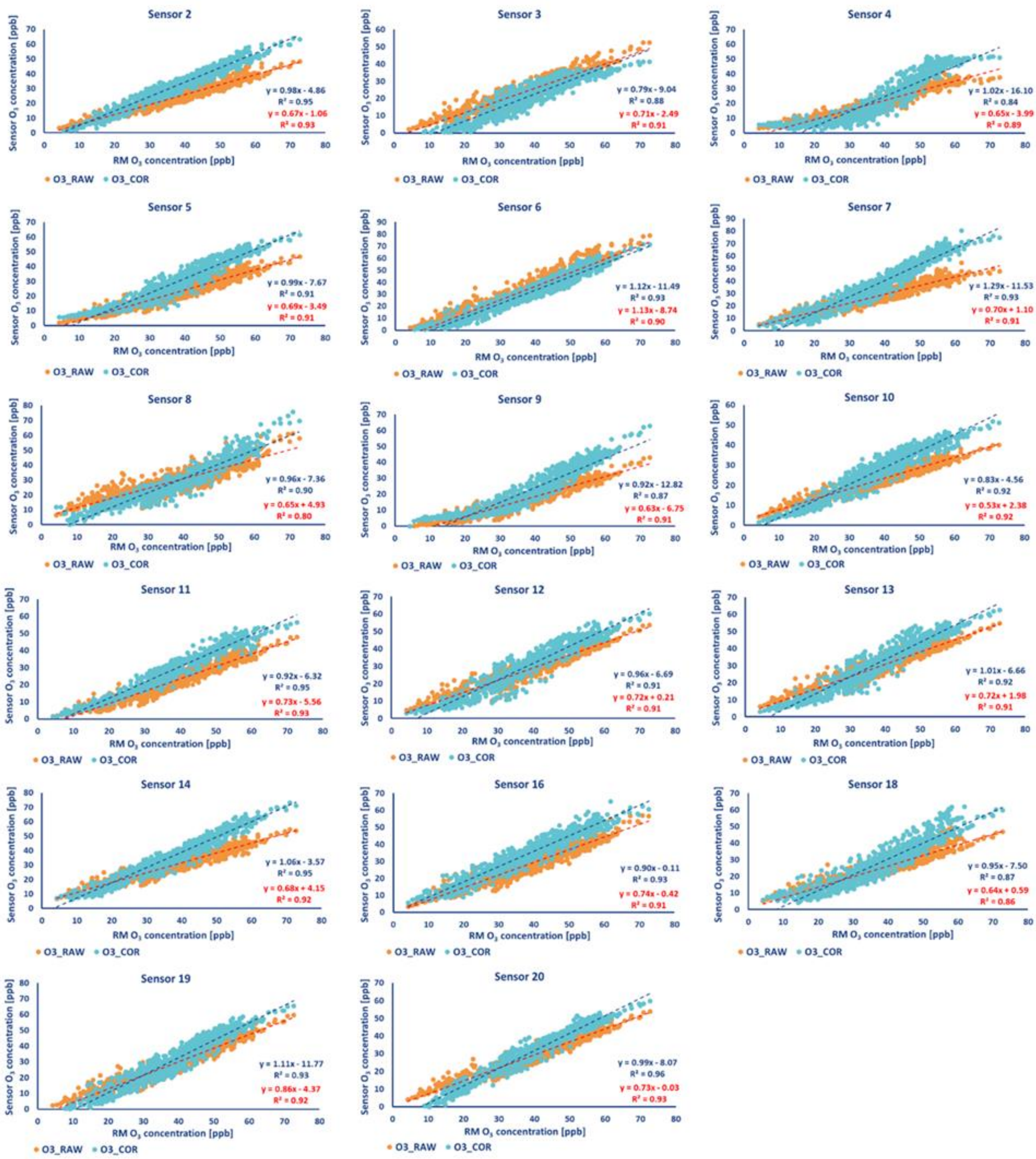


**Figure S30**. Relationship of $O_3$ concentrations measured by LCS (the y-axis) and by reference monitor (RM; the x-axis) at the Prague Libuš air quality monitoring (AQM) station during final field comparative measurement. O3_RAW = raw concentrations measured by LCSs, O3_COR = LCSs concentrations corrected by MARS method.

**Table S18.** Summary statistics of 1-hour average $PM_{10}$ concentrations measured by all LCSs during final field comparative measurement at the Prague 4-Libuš AQM station. Raw = original values of concentrations, cor = corrected values of concentrations (by MARS method). N valid = number of valid values, % valid = percentage of valid values in the dataset, Min = minimum value, Max = maximum value, SD = standard deviation, parameters resulting from linear regression between LCS and RM/EM concentrations: a = intercept, b = slope, SE = standard error, $R^2$ = coefficient of determination, MBE = Mean bias error, MAE = Mean absolute error, RMSE = Root mean square error.

| | Descriptive statistics | | | | | | Linear regression | | | Williamson-York regression | | Error | |
|---|---|---|---|---|---|---|---|---|---|---|---|---|---|
| **Variable** | **N valid** | **Mean** | **Median** | **Min** | **Max** | **SD** | **a ± SE** | **b ± SE** | **R2** | **a ± SE** | **b ± SE** | **MBE** | **RMSE** |
| **$PM_{10}$_raw S2** | 862 | 11.45 | 9.41 | 0.28 | 48.19 | 8.00 | -1.46±0.72 | 0.82±0.04 | 0.30 | -6.95±0.51 | 1.19±0.04 | 4.29 | 8.02 |
| **$PM_{10}$_cor S2** | 862 | 18.08 | 17.18 | 3.47 | 40.33 | 5.79 | 4.98±0.40 | 0.83±0.02 | 0.58 | 1.30±0.28 | 1.05±0.02 | -2.34 | 4.49 |
| **$PM_{10}$_raw S3** | 862 | 12.37 | 9.96 | 0.33 | 54.34 | 8.93 | -1.57±0.81 | 0.89±0.05 | 0.28 | -8.11±0.60 | 1.34±0.05 | 3.37 | 8.32 |
| **$PM_{10}$_cor S3** | 862 | 10.94 | 10.54 | 2.32 | 28.14 | 3.68 | 3.27±0.28 | 0.49±0.02 | 0.50 | 0.89±0.19 | 0.63±0.01 | 4.80 | 6.11 |
| **$PM_{10}$_raw S4** | 862 | 14.36 | 11.96 | 0.55 | 55.12 | 9.42 | -0.71±0.84 | 0.96±0.05 | 0.29 | -7.43±0.58 | 1.39±0.05 | 1.38 | 8.04 |
| **$PM_{10}$_cor S4** | 862 | 16.16 | 16.00 | 3.70 | 37.85 | 4.36 | 7.35±0.34 | 0.56±0.02 | 0.47 | 3.27±0.27 | 0.80±0.02 | -0.42 | 3.97 |
| **$PM_{10}$_raw S5** | 862 | 11.14 | 8.92 | 0.36 | 50.48 | 8.09 | -1.34±0.74 | 0.79±0.04 | 0.27 | -7.23±0.54 | 1.20±0.05 | 4.60 | 8.36 |
| **$PM_{10}$_cor S5** | 862 | 18.06 | 17.34 | 3.35 | 42.45 | 5.98 | 4.48±0.41 | 0.86±0.02 | 0.59 | 1.03±0.28 | 1.07±0.02 | -2.31 | 4.55 |
| **$PM_{10}$_raw S6** | 862 | 10.52 | 8.43 | 0.27 | 50.89 | 7.83 | -1.71±0.71 | 0.78±0.04 | 0.28 | -6.75±0.50 | 1.12±0.04 | 5.23 | 8.55 |
| **$PM_{10}$_cor S6** | 862 | 17.64 | 17.00 | 1.70 | 50.60 | 6.41 | 3.26±0.45 | 0.91±0.03 | 0.57 | -0.34±0.26 | 1.13±0.02 | -1.89 | 4.62 |
| **$PM_{10}$_raw S7** | 862 | 11.25 | 8.88 | 0.44 | 52.75 | 8.30 | -1.20±0.76 | 0.79±0.05 | 0.26 | -7.19±0.55 | 1.20±0.05 | 4.50 | 8.52 |
| **$PM_{10}$_cor S7** | 862 | 16.54 | 15.94 | 2.64 | 40.39 | 5.66 | 4.26±0.41 | 0.78±0.02 | 0.54 | 0.04±0.30 | 1.03±0.02 | -0.79 | 4.11 |
| **$PM_{10}$_raw S9** | 862 | 11.23 | 9.09 | 0.19 | 53.12 | 8.33 | -1.93±0.75 | 0.84±0.05 | 0.28 | -7.88±0.57 | 1.26±0.05 | 4.51 | 8.41 |
| **$PM_{10}$_cor S9** | 862 | 17.36 | 16.45 | 3.36 | 39.86 | 5.67 | 4.38±0.38 | 0.82±0.02 | 0.60 | 0.85±0.27 | 1.03±0.02 | -1.61 | 4.05 |
| **$PM_{10}$_raw S10** | 862 | 12.97 | 10.86 | 0.56 | 52.89 | 8.96 | -1.93±0.79 | 0.95±0.05 | 0.32 | -7.51±0.57 | 1.32±0.05 | 2.78 | 7.92 |
| **$PM_{10}$_cor S10** | 862 | 18.11 | 17.40 | 3.19 | 40.47 | 5.81 | 4.47±0.38 | 0.87±0.02 | 0.63 | 1.14±0.27 | 1.06±0.02 | -2.36 | 4.32 |
| **$PM_{10}$_raw S11** | 697 | 10.40 | 8.41 | 0.12 | 46.00 | 7.55 | -2.56±0.75 | 0.79±0.04 | 0.32 | -5.90±0.44 | 1.00±0.04 | 6.01 | 8.72 |
| **$PM_{10}$_cor S11** | 697 | 19.53 | 18.09 | 3.74 | 50.59 | 6.97 | 4.09±0.58 | 0.94±0.03 | 0.53 | 0.54±0.36 | 1.14±0.03 | -3.12 | 5.71 |
| **$PM_{10}$_raw S12** | 862 | 11.28 | 9.07 | 0.25 | 52.86 | 8.49 | -1.92±0.77 | 0.84±0.05 | 0.28 | -8.10±0.59 | 1.28±0.05 | 4.46 | 8.54 |
| **$PM_{10}$_cor S12** | 862 | 16.45 | 15.61 | 3.41 | 41.03 | 5.52 | 3.93±0.38 | 0.79±0.02 | 0.59 | 0.69±0.27 | 0.99±0.02 | -0.71 | 3.78 |
| **$PM_{10}$_raw S13** | 862 | 9.52 | 7.84 | 0.12 | 43.56 | 6.53 | -1.77±0.56 | 0.72±0.03 | 0.34 | -5.19±0.38 | 0.94±0.03 | 6.22 | 8.31 |
| **$PM_{10}$_cor S13** | 862 | 20.14 | 18.82 | 3.43 | 49.31 | 6.89 | 4.46±0.47 | 1.00±0.03 | 0.59 | 1.03±0.31 | 1.19±0.02 | -4.40 | 6.23 |
| **$PM_{10}$_raw S14** | 862 | 12.05 | 9.79 | 0.16 | 52.46 | 8.45 | -1.35±0.76 | 0.85±0.05 | 0.29 | -7.41±0.55 | 1.26±0.05 | 3.69 | 8.07 |
| **$PM_{10}$_cor S14** | 862 | 18.07 | 16.96 | 4.08 | 42.36 | 6.01 | 4.20±0.40 | 0.88±0.02 | 0.61 | 1.19±0.28 | 1.06±0.02 | -2.33 | 4.47 |
| **$PM_{10}$_raw S16** | 862 | 12.30 | 9.93 | 0.22 | 54.92 | 9.20 | -1.93±0.84 | 0.90±0.05 | 0.27 | -9.07±0.66 | 1.41±0.06 | 3.45 | 8.58 |
| **$PM_{10}$_cor S16** | 862 | 16.22 | 15.51 | 3.51 | 37.81 | 5.27 | 4.13±0.35 | 0.77±0.02 | 0.60 | 0.87±0.26 | 0.96±0.02 | -0.48 | 3.58 |
| **$PM_{10}$_raw S18** | 862 | 9.72 | 7.96 | 0.22 | 46.16 | 7.19 | -1.97±0.64 | 0.74±0.04 | 0.30 | -6.73±0.48 | 1.08±0.04 | 6.02 | 8.61 |
| **$PM_{10}$_cor S18** | 862 | 16.34 | 15.46 | 4.35 | 36.77 | 5.40 | 4.17±0.37 | 0.77±0.02 | 0.58 | 0.97±0.29 | 0.96±0.02 | -0.60 | 3.76 |
| **$PM_{10}$_raw S19** | 862 | 13.49 | 10.86 | 0.35 | 57.08 | 9.70 | -1.85±0.87 | 0.97±0.05 | 0.29 | -9.01±0.67 | 1.48±0.06 | 2.25 | 8.50 |
| **$PM_{10}$_cor S19** | 862 | 16.63 | 15.90 | 4.43 | 39.20 | 5.32 | 4.39±0.36 | 0.78±0.02 | 0.60 | 1.99±0.26 | 0.91±0.02 | -0.89 | 3.65 |
| **$PM_{10}$_raw S20** | 697 | 12.54 | 10.27 | 0.29 | 52.82 | 9.26 | -3.42±0.92 | 0.97±0.05 | 0.32 | -7.77±0.58 | 1.26±0.05 | 3.87 | 8.55 |
| **$PM_{10}$_cor S20** | 697 | 18.40 | 17.81 | 3.72 | 41.63 | 6.16 | 4.11±0.48 | 0.87±0.03 | 0.59 | 0.70±0.33 | 1.06±0.02 | -1.99 | 4.49 |
| **$PM_{10}$ FIDAS** | 862 | 15.74 | 15.20 | 2.50 | 45.90 | 5.32 | | | | | | | |

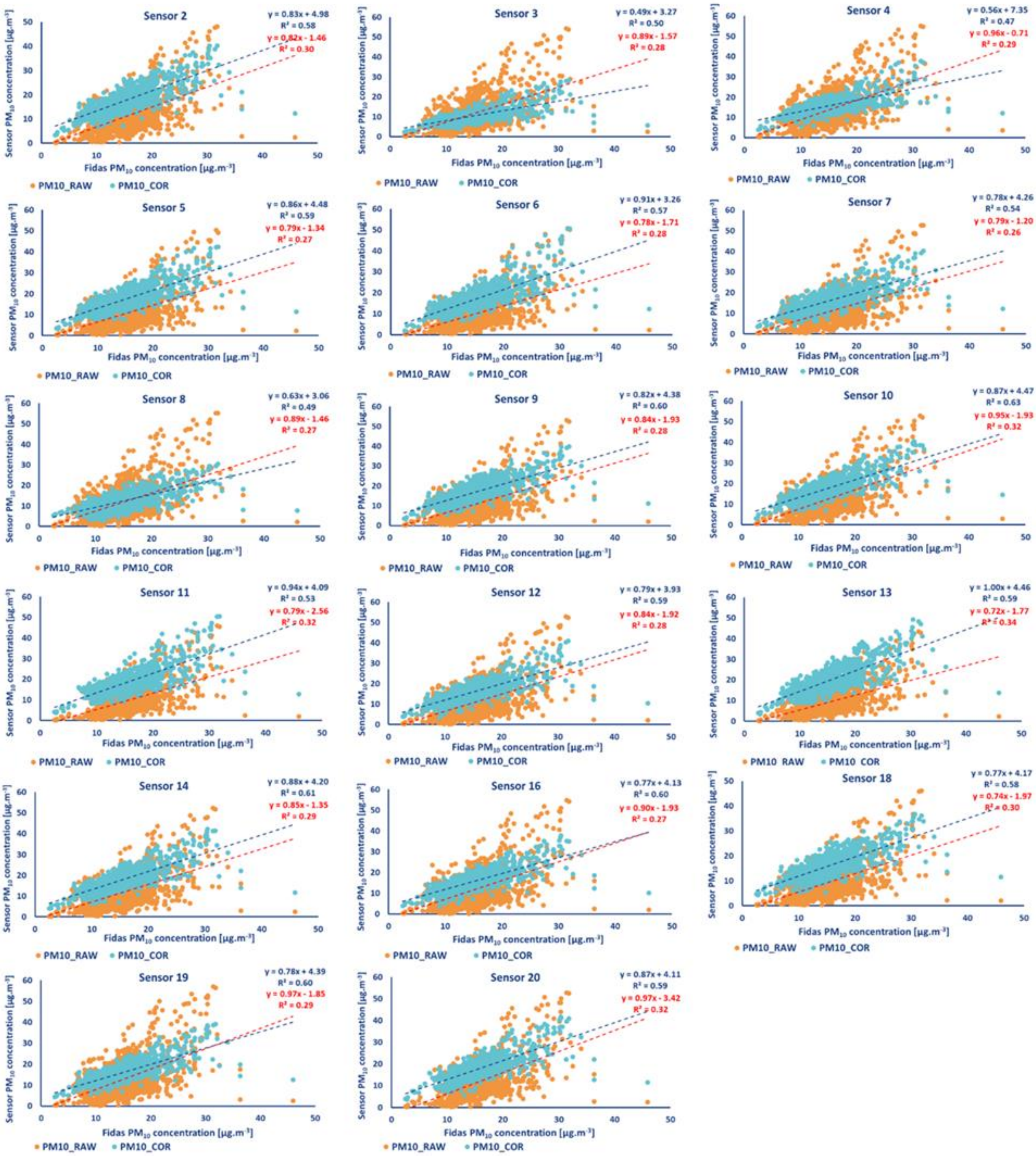


**Figure S31**. Relationship of $PM_{10}$ concentrations measured by LCS (the y-axis) and by reference monitor (RM; the x-axis) at the Prague Libuš air quality monitoring (AQM) station during final field comparative measurement. $PM_{10}$_RAW = raw concentrations measured by LCSs, $PM_{10}$_COR = LCSs concentrations corrected by MARS method.

**Table S19.** Summary statistics of 1-hour average $PM_{2.5}$ concentrations measured by all LCSs during final field comparative measurement at the Prague 4-Libuš AQM station. Raw = original values of concentrations, cor = corrected values of concentrations (by MARS method). N valid = number of valid values, % valid = percentage of valid values in the dataset, Min = minimum value, Max = maximum value, SD = standard deviation, parameters resulting from linear regression between LCS and RM/EM concentrations: a = intercept, b = slope, SE = standard error, $R^2$ = coefficient of determination, MBE = Mean bias error, MAE = Mean absolute error, RMSE = Root mean square error.

| | Descriptive statistics | | | | | | Linear regression | | | Williamson-York regression | | Error | |
|---|---|---|---|---|---|---|---|---|---|---|---|---|---|
| **Variable** | **N valid** | **Mean** | **Median** | **Min** | **Max** | **SD** | **a ± SE** | **b ± SE** | **R2** | **a ± SE** | **b ± SE** | **MBE** | **RMSE** |
| **$PM_{2.5}$_raw S2** | 862 | 10.74 | 8.91 | 0.20 | 39.93 | 7.23 | -3.78±0.30 | 1.65±0.03 | 0.76 | -3.21±0.15 | 1.54±0.03 | -1.95 | 4.75 |
| **$PM_{2.5}$_cor S2** | 862 | 11.21 | 10.44 | 0.20 | 32.33 | 4.56 | 1.29±0.13 | 1.13±0.01 | 0.89 | -0.32±0.08 | 1.33±0.01 | -2.42 | 2.88 |
| **$PM_{2.5}$_raw S3** | 862 | 11.40 | 9.32 | 0.26 | 44.34 | 7.88 | -3.36±0.39 | 1.68±0.04 | 0.66 | -3.64±0.20 | 1.67±0.04 | -2.60 | 5.89 |
| **$PM_{2.5}$_cor S3** | 862 | 8.12 | 7.81 | -0.03 | 27.03 | 3.96 | 0.11±0.16 | 0.91±0.02 | 0.77 | -1.58±0.10 | 1.12±0.02 | 0.68 | 2.05 |
| **$PM_{2.5}$_raw S4** | 862 | 13.30 | 11.29 | 0.49 | 44.84 | 8.23 | -3.21±0.35 | 1.88±0.04 | 0.76 | -3.40±0.18 | 1.86±0.03 | -4.51 | 6.93 |
| **$PM_{2.5}$_cor S4** | 862 | 12.94 | 12.29 | 2.24 | 32.06 | 4.28 | 3.97±0.15 | 1.02±0.02 | 0.83 | 2.25±0.13 | 1.21±0.02 | -4.15 | 4.52 |
| **$PM_{2.5}$_raw S5** | 862 | 9.90 | 7.99 | 0.23 | 40.89 | 7.07 | -3.94±0.32 | 1.57±0.03 | 0.72 | -3.16±0.16 | 1.44±0.03 | -1.11 | 4.47 |
| **$PM_{2.5}$_cor S5** | 862 | 11.14 | 10.30 | 0.49 | 32.93 | 5.01 | 0.32±0.15 | 1.23±0.02 | 0.88 | -0.60±0.09 | 1.34±0.01 | -2.35 | 3.06 |
| **$PM_{2.5}$_raw S6** | 862 | 9.56 | 7.68 | 0.22 | 41.15 | 6.86 | -3.60±0.33 | 1.50±0.03 | 0.69 | -2.93±0.15 | 1.37±0.03 | -0.76 | 4.32 |
| **$PM_{2.5}$_cor S6** | 862 | 10.81 | 10.13 | -0.01 | 39.73 | 5.10 | 0.00±0.17 | 1.23±0.02 | 0.84 | -0.86±0.09 | 1.33±0.02 | -2.01 | 2.98 |
| **$PM_{2.5}$_raw S7** | 862 | 10.34 | 8.34 | 0.34 | 42.80 | 7.28 | -2.93±0.38 | 1.51±0.04 | 0.62 | -3.20±0.18 | 1.50±0.03 | -1.54 | 5.10 |
| **$PM_{2.5}$_cor S7** | 862 | 9.95 | 9.41 | 1.44 | 33.46 | 4.43 | 1.20±0.20 | 1.00±0.02 | 0.73 | -0.01±0.13 | 1.12±0.02 | -1.16 | 2.56 |
| **$PM_{2.5}$_raw S9** | 862 | 10.70 | 8.77 | 0.17 | 44.03 | 7.57 | -3.82±0.36 | 1.65±0.04 | 0.69 | -3.55±0.18 | 1.58±0.03 | -1.91 | 5.24 |
| **$PM_{2.5}$_cor S9** | 862 | 10.63 | 10.07 | 1.12 | 32.60 | 4.59 | 1.07±0.17 | 1.09±0.02 | 0.82 | -0.28±0.12 | 1.24±0.02 | -1.84 | 2.71 |
| **$PM_{2.5}$_raw S10** | 862 | 11.81 | 10.01 | 0.44 | 42.77 | 7.78 | -3.58±0.34 | 1.75±0.04 | 0.74 | -3.32±0.18 | 1.68±0.03 | -3.01 | 5.76 |
| **$PM_{2.5}$_cor S10** | 862 | 11.32 | 10.57 | 1.46 | 31.71 | 4.89 | 1.02±0.17 | 1.17±0.02 | 0.84 | -0.09±0.12 | 1.29±0.02 | -2.53 | 3.28 |
| **$PM_{2.5}$_raw S11** | 697 | 9.83 | 8.04 | 0.09 | 38.52 | 6.90 | -3.78±0.32 | 1.49±0.03 | 0.75 | -2.60±0.13 | 1.31±0.02 | -0.69 | 4.02 |
| **$PM_{2.5}$_cor S11** | 697 | 12.31 | 11.11 | 0.74 | 39.92 | 5.88 | 0.00±0.22 | 1.35±0.02 | 0.85 | -0.02±0.11 | 1.33±0.02 | -3.17 | 4.16 |
| **$PM_{2.5}$_raw S12** | 862 | 10.57 | 8.65 | 0.20 | 43.31 | 7.58 | -3.54±0.38 | 1.60±0.04 | 0.65 | -3.63±0.19 | 1.58±0.03 | -1.78 | 5.33 |
| **$PM_{2.5}$_cor S12** | 862 | 9.79 | 9.15 | 0.44 | 32.24 | 4.46 | 0.62±0.17 | 1.04±0.02 | 0.79 | -0.72±0.10 | 1.20±0.02 | -1.00 | 2.26 |
| **$PM_{2.5}$_raw S13** | 862 | 9.13 | 7.55 | 0.12 | 37.17 | 6.10 | -3.40±0.24 | 1.42±0.02 | 0.79 | -2.48±0.12 | 1.28±0.02 | -0.34 | 3.24 |
| **$PM_{2.5}$_cor S13** | 862 | 13.23 | 11.85 | 1.92 | 38.83 | 5.84 | 0.59±0.17 | 1.44±0.02 | 0.88 | 0.57±0.11 | 1.42±0.02 | -4.44 | 5.16 |
| **$PM_{2.5}$_raw S14** | 862 | 11.35 | 9.32 | 0.12 | 43.21 | 7.59 | -3.52±0.34 | 1.69±0.04 | 0.72 | -3.36±0.17 | 1.63±0.03 | -2.56 | 5.43 |
| **$PM_{2.5}$_cor S14** | 862 | 11.35 | 10.42 | 0.49 | 35.12 | 4.95 | 0.68±0.15 | 1.21±0.02 | 0.87 | -0.37±0.08 | 1.34±0.01 | -2.56 | 3.21 |
| **$PM_{2.5}$_raw S16** | 862 | 11.46 | 9.33 | 0.18 | 45.08 | 8.18 | -3.88±0.41 | 1.74±0.04 | 0.66 | -4.06±0.21 | 1.73±0.04 | -2.67 | 6.14 |
| **$PM_{2.5}$_cor S16** | 862 | 9.70 | 9.16 | 0.73 | 30.36 | 4.25 | 0.81±0.15 | 1.01±0.02 | 0.82 | -0.11±0.10 | 1.11±0.02 | -0.90 | 2.01 |
| **$PM_{2.5}$_raw S18** | 862 | 8.98 | 7.34 | 0.18 | 38.06 | 6.47 | -3.51±0.30 | 1.42±0.03 | 0.70 | -3.00±0.15 | 1.33±0.03 | -0.19 | 3.89 |
| **$PM_{2.5}$_cor S18** | 862 | 9.69 | 9.06 | 0.69 | 28.77 | 4.23 | 1.08±0.17 | 0.98±0.02 | 0.78 | -0.38±0.14 | 1.14±0.02 | -0.90 | 2.17 |
| **$PM_{2.5}$_raw S19** | 862 | 12.54 | 10.25 | 0.28 | 46.12 | 8.47 | -3.61±0.41 | 1.84±0.04 | 0.68 | -3.97±0.21 | 1.84±0.04 | -3.75 | 6.85 |
| **$PM_{2.5}$_cor S19** | 862 | 9.94 | 9.18 | 1.45 | 31.59 | 4.35 | 0.80±0.15 | 1.04±0.02 | 0.83 | 0.26±0.10 | 1.09±0.02 | -1.15 | 2.13 |
| **$PM_{2.5}$_raw S20** | 697 | 11.88 | 9.85 | 0.27 | 44.00 | 8.32 | -3.92±0.43 | 1.73±0.04 | 0.69 | -3.37±0.19 | 1.62±0.03 | -2.74 | 6.10 |
| **$PM_{2.5}$_cor S20** | 697 | 11.10 | 10.38 | 1.79 | 33.78 | 5.20 | 0.42±0.21 | 1.17±0.02 | 0.82 | 0.06±0.13 | 1.19±0.02 | -1.97 | 3.05 |
| **$PM_{2.5}$ FIDAS** | 862 | 8.79 | 8.20 | 1.00 | 24.60 | 3.81 | | | | | | | |

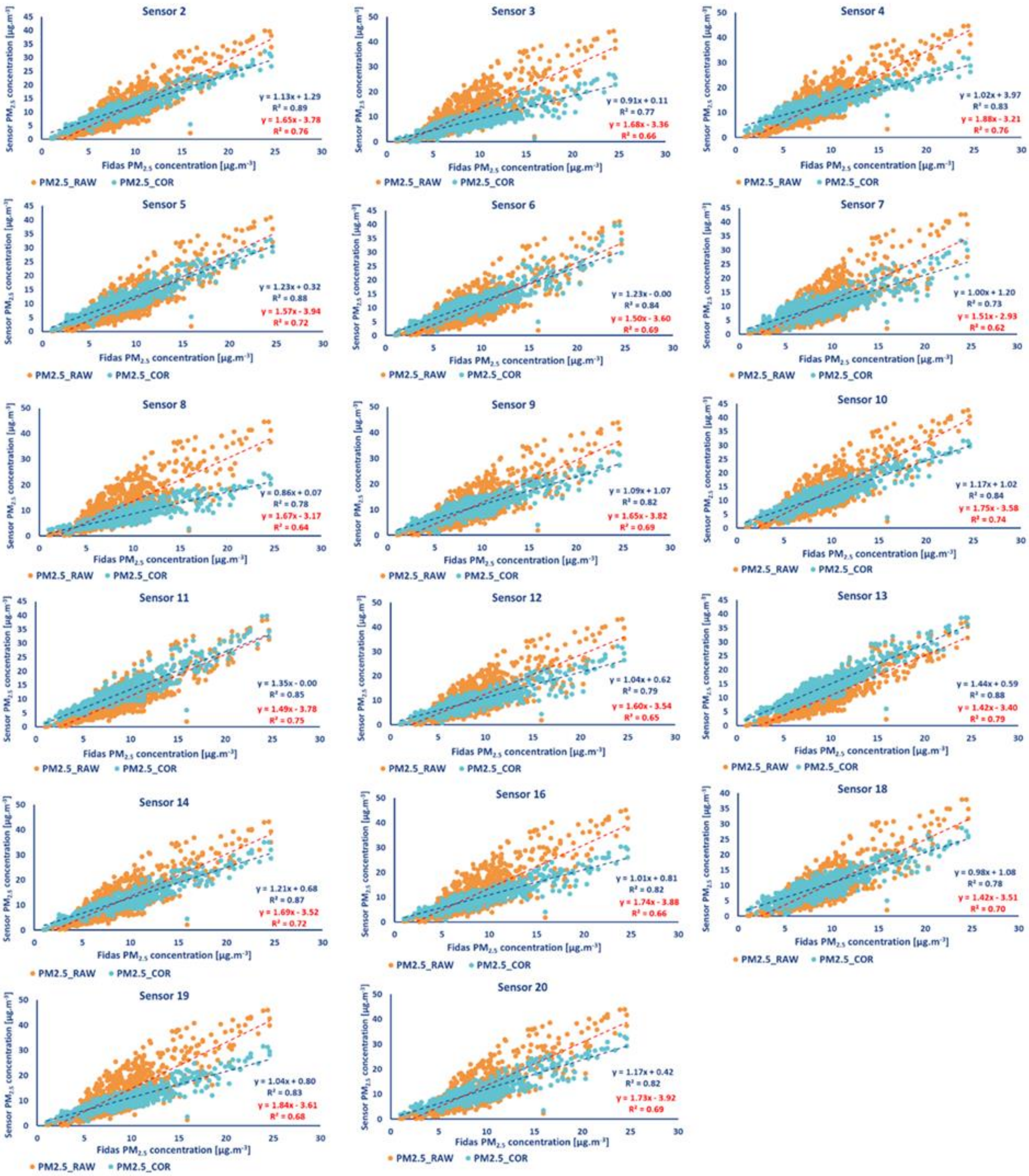


**Figure S32**. Relationship of $PM_{2.5}$ concentrations measured by LCS (the y-axis) and by reference monitor (RM; the x-axis) at the Prague Libuš air quality monitoring (AQM) station during final field comparative measurement. $PM_{2.5}$_RAW = raw concentrations measured by LCSs, $PM_{2.5}$_COR = LCSs concentrations corrected by MARS method.

### S3.1.4 Results of COR2 method taking into account final field comparative measurement at the Prague Libuš AQM station

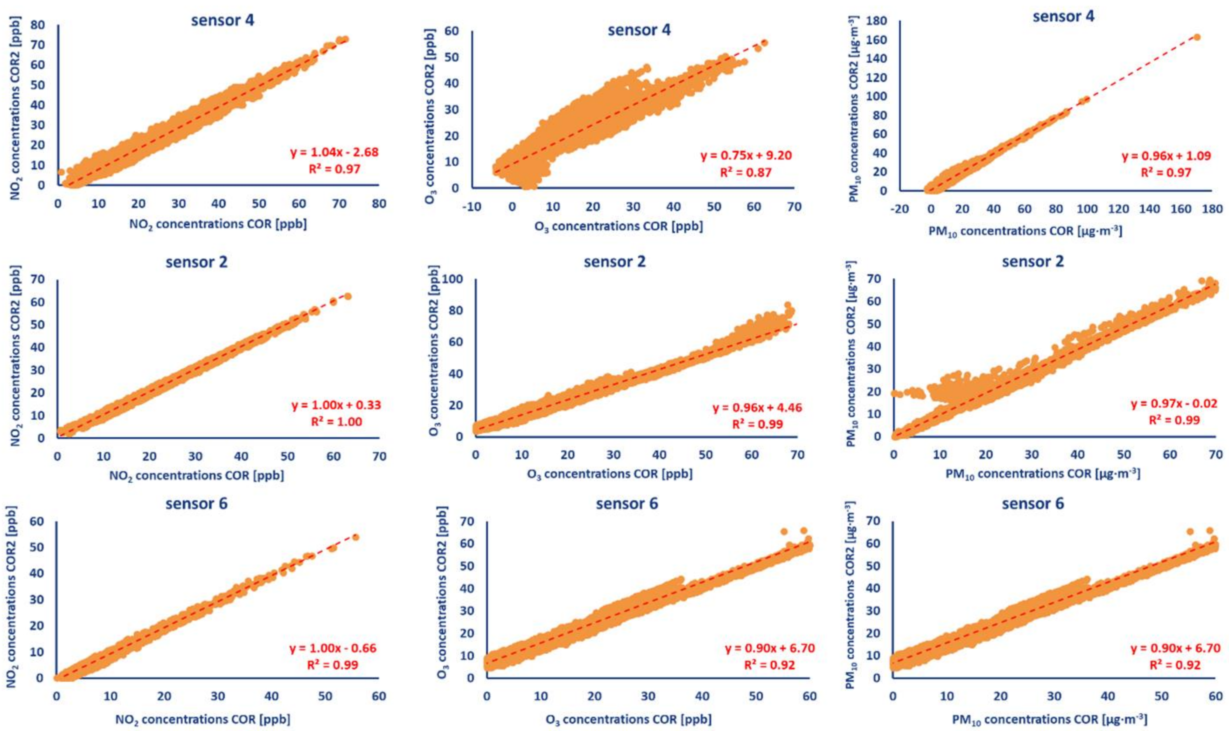


**Figure S33.** Comparison of the results of COR (the x-axis) and COR2 (the y-axis) correction method in case of $NO_2$, $O_3$ and $PM_{10}$ concentrations measured by LCSs S4, S2 and S6. Measurement covering the whole Legerova measurement campaign (from 30 May 2022 to 28 March 2023).

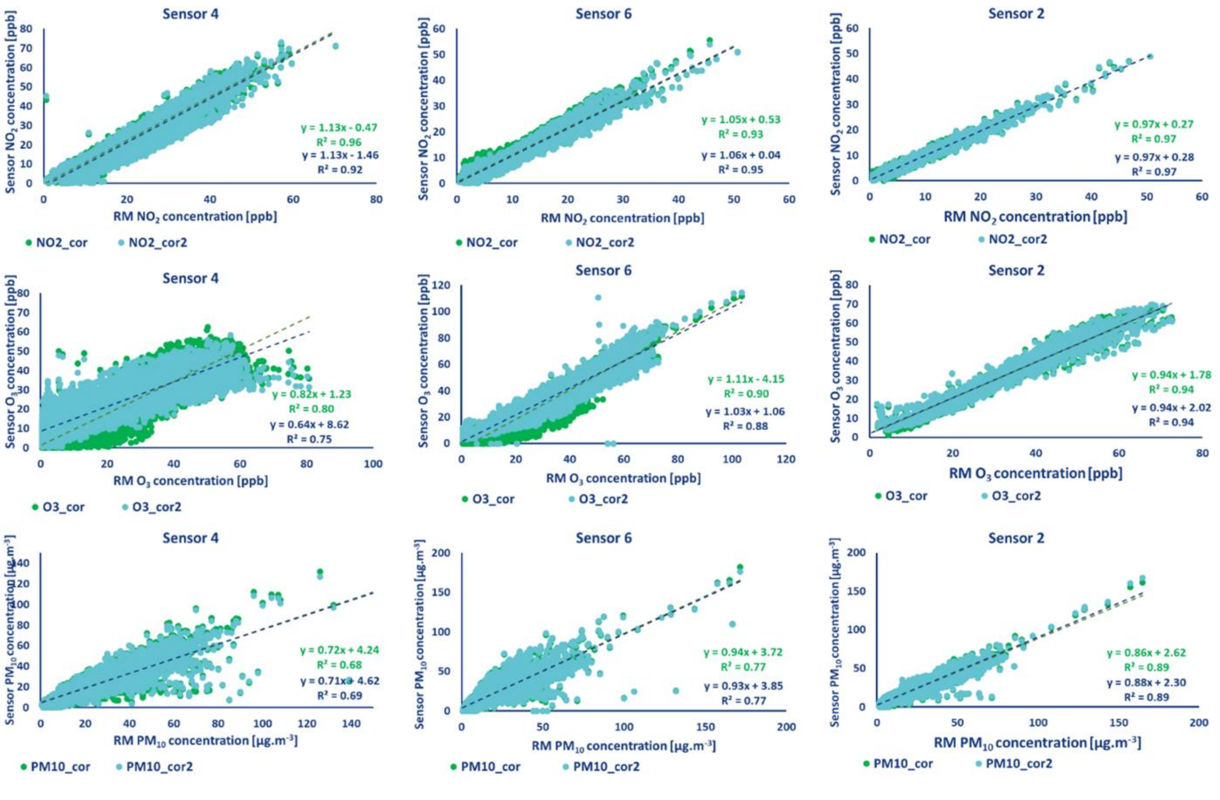


**Figure S34.** Results of linear regression between concentrations of $NO_2$, $O_3$ and $PM_{10}$ measured by RM or EM and by differently corrected LCSs S4, S6 and S2. COR = first correction method based on the initial field comparative measurement; COR2 = alternative correction method based on the combined dataset of initial and final comparison measurements including the addition of sensor age as an additional explanatory variable. In case of LCS S4 and S6 (collocated during the whole measurement campaign at the AQM stations Legerova and Libuš) the whole dataset was used (16 December 2021 – 28 2023), in case of S2 only the period of the first comparative measurement was used (16 December 2021 – 30 May 2022).

### S3.1.5 Meteorological data quality and verification

The data comparison between supplementary meteorological mast measurement and measurement at the reference Prague Karlov MS showed the values of $R^2$ were higher than 0.98 in case of TMP, RH and p, (Fig. S35). The biggest differences were detected in the case of WD and WV measurements (Fig. S35), which is understandable because the wind measurement in the PVK garden location was influenced by the surrounding building blocks (unlike the wind measurement at the Prague Karlov MS located on the roof of the tallest building).

Similarly we found a very good agreement in the case of comparing the TMP measurement by MWR (at the Prague Karlov MS) and by radiosonde (launched at the distant Prague Libuš MS), with resulting $R^2>0.98$ even at the highest level of 1,000 m a.g.l. (Fig. S36). For results of comparisons for particular sounding times under different conditions, including days with precipitation, see Fig. S37-S38. The correctness of the potential TMP profile calculation procedure was also verified on the TMP height profile from the radiosonde output. The resulting difference between the calculated and measured potential TMP did not exceed in absolute value 0.137 % of the value determined according to Arya (2001) and in comparison reached $R^2=0.997$ (see Fig. S39).

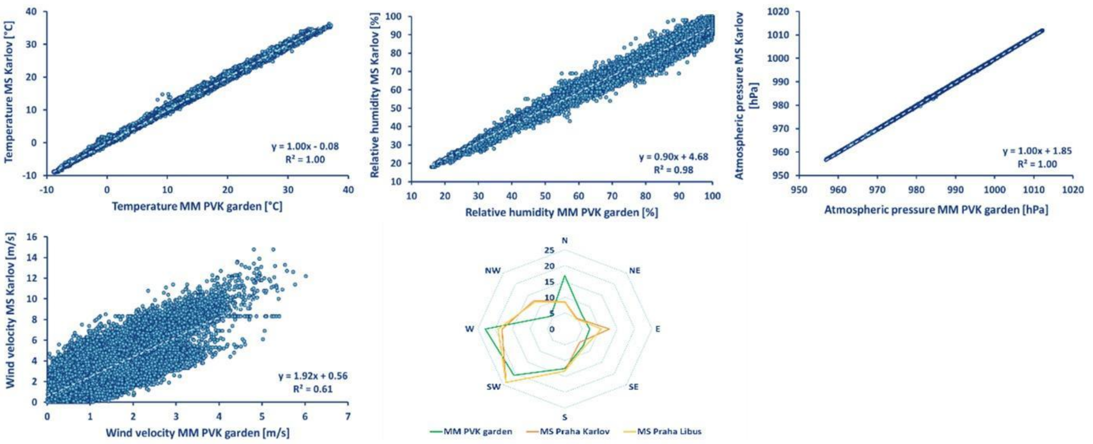


**Figure S35.** Comparison of 10 minute temperature (TMP), relative humidity (RH), atmospheric pressure (p) and wind velocity (WV) data measured by the mobile meteorological mast (MM) placed in PVK garden and by the professional meteorological station (MS) Prague Karlov. The WD comparison is shown in the wind rose with the frequencies of particular directions (last figure). Comparison based on the data measured in the period from 1 June 2022 to 19 April 2023 (n = 46389).

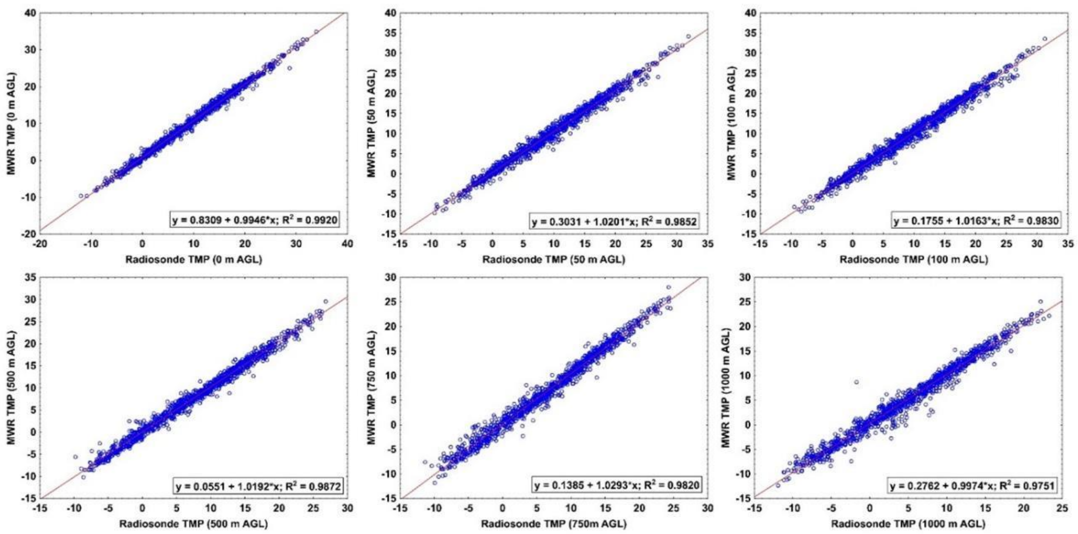


**Figure S36.** Comparison of air temperatures (°C) measured by radiosonde at the Prague Libuš MS and by MWR at the Prague Karlov MS in particular heights above the ground (0, 50, 100, 500 and 1000 m agl). Comparison of data measured in the period from 25 February 2022 to 24 March 2023 (n = 1172).

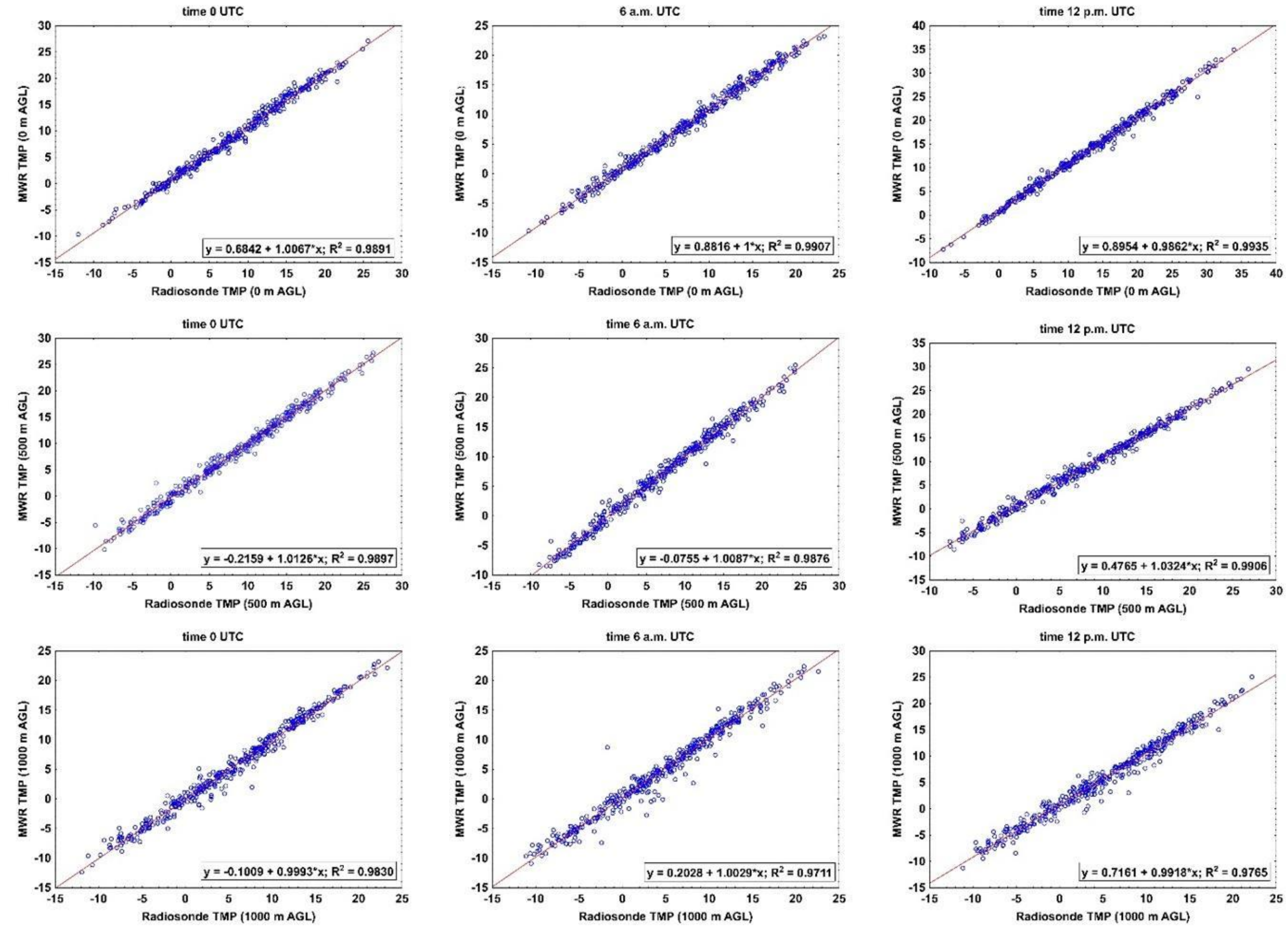


**Figure S37.** Comparison of air temperatures (°C) measured by radiosonde at the Prague Libuš MS and by MWR at the Prague Karlov MS at the 0, 500 and 100 m a.g.l. for particular sounding times (0, 6 and 12 UTC). Comparison of the data measured in the period from 25 February 2022 to 24 March 2023 (n = 1172).

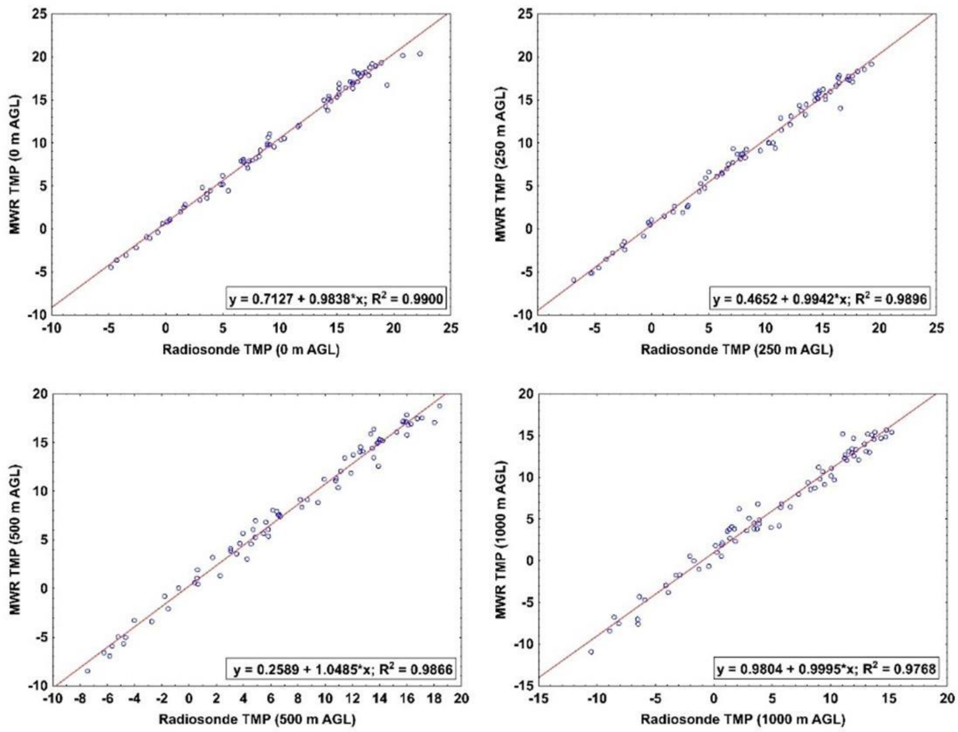


**Figure S38.** Comparison of air temperature (TMP, °C) measured by radiosonde at the Prague Libuš MS and by MWR at the Prague Karlov MS at the height levels 0, 250, 500 and 1000 m a.g.l under rainy conditions. Comparison of data measured within the period from 25 February 2022 to 24 March 2023 (n = 76).

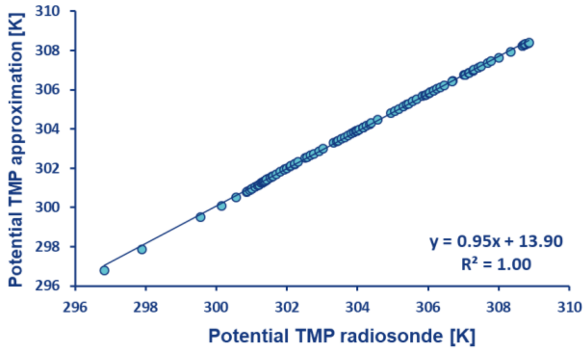


**Figure S39.** Relationship of approximated potential TMPs (K) calculated according to the (Arya, 2001) method (the y-axis) and potential TMPs measured by radiosonde at the Prague Libuš MS.

## S3.2 Results of the Prague Legerova measurement campaign

### S3.2.1 Air quality LCS measurement

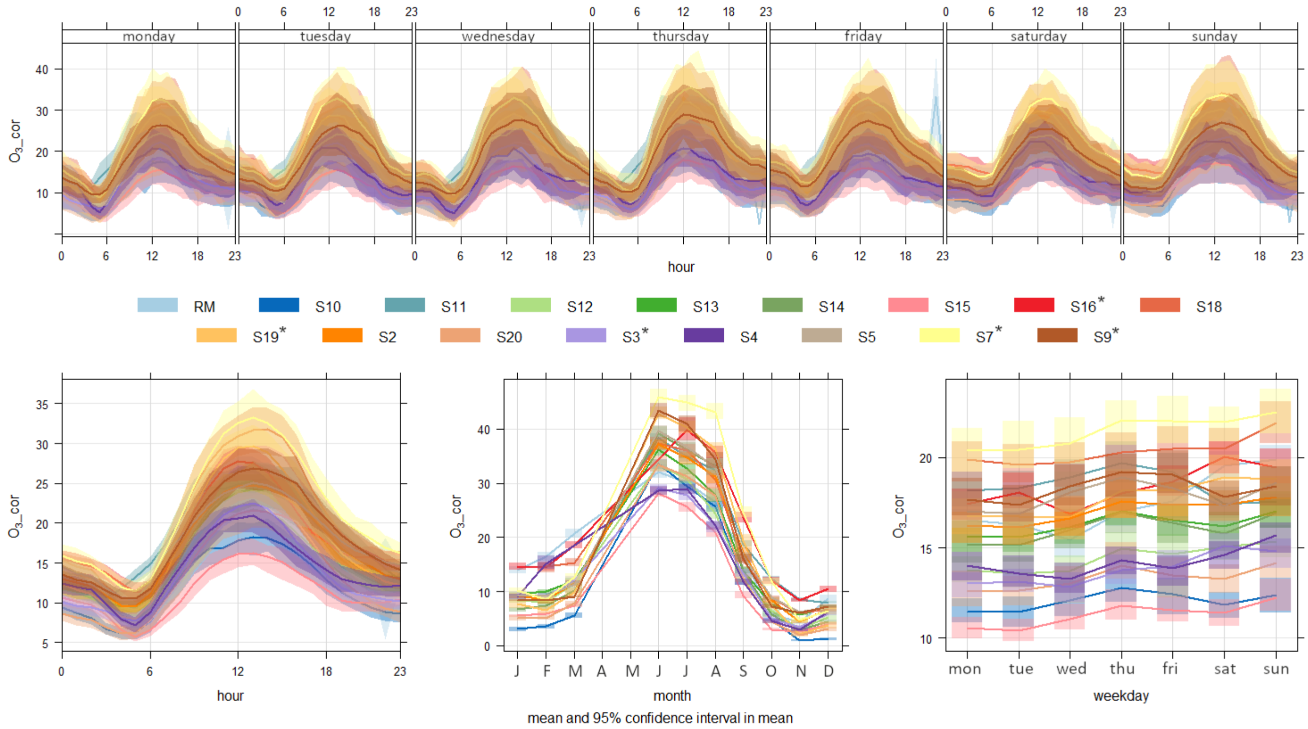


**Figure S40.** Daily (top), hourly (bottom left), monthly (bottom middle) and weekly (bottom right) variations of corrected $O_3$ concentrations (ppb) measured by all low-cost sensor stations (LCSs S2 – S20) within the Legerova domain and by the Prague 9-Vysočany reference monitor (RM) out of the Legerova domain ($O_3$ measurement is not available at Prague 2-Legerova RM). Measuring period from 30 May 2022 to 28 March 2023 (in monthly graph May to December 2022, January to March 2023). LCSs located at background sites are marked with an asterisk.

**Table S20**. Summary statistics of 1-hour average MARS corrected $O_3$ concentrations measured by all LCSs during the Legerova measurement campaign. Valid N = number of valid values, % valid = percentage of valid values in the dataset, CI mean = lower and upper confidence interval of mean, Min = minimum value, Max = maximum value, SD = standard deviation, CI SD = lower and upper confidence interval of standard deviation, SE = standard error of mean. The table is sorted in ascending order according to the mean concentration values. LCSs located at background sites are marked with an asterisk within the ID.

| Measurement ID | Valid N | % Valid | Mean | CI mean (lower) | Ci mean (upper) | Median | Min | Max | SD | CI SD (lower) | CI SD (upper) | SE mean |
|---|---|---|---|---|---|---|---|---|---|---|---|---|
| S15 | 7206 | 99.99 | 11.29 | 11.00 | 11.58 | 5.92 | -4.14 | 66.12 | 12.59 | 12.39 | 12.80 | 0.15 |
| S10 | 7206 | 99.99 | 12.07 | 11.72 | 12.42 | 6.03 | -4.44 | 76.47 | 15.10 | 14.86 | 15.35 | 0.18 |
| S20 | 7206 | 99.99 | 13.32 | 12.94 | 13.70 | 7.88 | -5.04 | 104.29 | 16.44 | 16.18 | 16.72 | 0.19 |
| S3* | 7205 | 99.97 | 13.81 | 13.50 | 14.11 | 10.48 | -5.56 | 96.77 | 13.22 | 13.00 | 13.44 | 0.16 |
| S4 | 5947 | 82.52 | 14.20 | 13.85 | 14.54 | 9.23 | -4.16 | 62.57 | 13.59 | 13.35 | 13.83 | 0.18 |
| S12 | 7206 | 99.99 | 14.44 | 14.10 | 14.77 | 10.12 | -2.41 | 79.18 | 14.38 | 14.14 | 14.61 | 0.17 |
| S14 | 7206 | 99.99 | 16.07 | 15.64 | 16.50 | 8.60 | -2.18 | 109.36 | 18.58 | 18.28 | 18.89 | 0.22 |
| S13 | 7206 | 99.99 | 16.32 | 15.97 | 16.67 | 10.80 | 0.82 | 90.16 | 15.02 | 14.78 | 15.27 | 0.18 |
| S2 | 7206 | 99.99 | 17.02 | 16.65 | 17.40 | 12.00 | -3.29 | 75.24 | 16.32 | 16.06 | 16.59 | 0.19 |
| RM[a] | 6854 | 95.10 | 17.49 | 17.14 | 17.84 | 15.38 | 0.50 | 80.67 | 14.89 | 14.65 | 15.14 | 0.18 |
| S19* | 7198 | 99.88 | 17.76 | 17.29 | 18.24 | 12.97 | -8.66 | 100.85 | 20.48 | 20.15 | 20.82 | 0.24 |
| S5 | 7206 | 99.99 | 17.89 | 17.50 | 18.28 | 10.64 | 0.06 | 99.73 | 16.79 | 16.52 | 17.07 | 0.20 |
| S9* | 7204 | 99.96 | 18.29 | 17.87 | 18.72 | 9.39 | 1.87 | 103.82 | 18.48 | 18.19 | 18.79 | 0.22 |
| S16* | 6036 | 83.75 | 18.37 | 18.00 | 18.74 | 14.24 | -2.39 | 76.70 | 14.60 | 14.34 | 14.86 | 0.19 |
| S11 | 7206 | 99.99 | 18.48 | 18.13 | 18.82 | 12.98 | 0.63 | 86.63 | 14.85 | 14.61 | 15.10 | 0.17 |
| S18 | 5665 | 78.60 | 20.36 | 19.90 | 20.81 | 15.60 | -5.09 | 97.22 | 17.46 | 17.15 | 17.79 | 0.23 |
| S7* | 7205 | 99.97 | 21.46 | 20.97 | 21.95 | 15.35 | -4.66 | 104.14 | 21.14 | 20.80 | 21.49 | 0.25 |

[a]In case of $O_3$ the Prague Vysočany AQM station used as RM for indicative comparison.

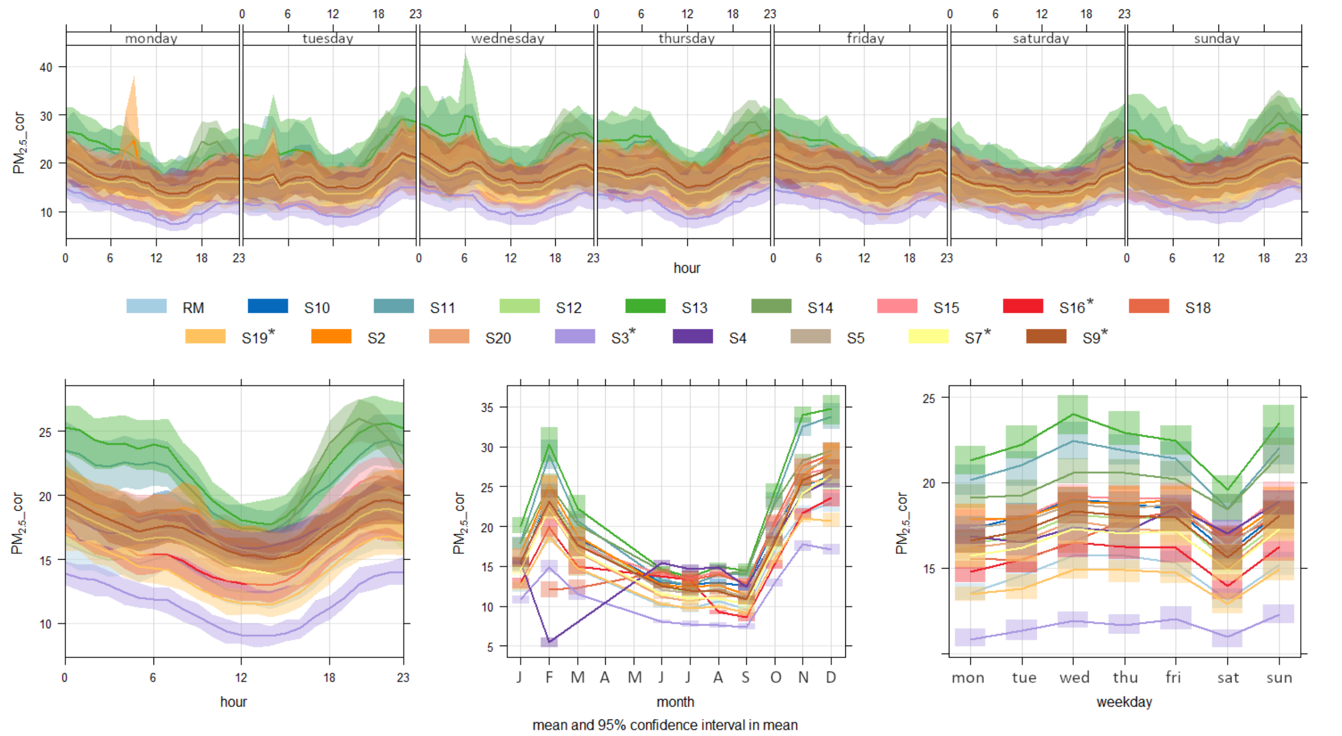


**Figure S41.** Daily (top), hourly (bottom left), monthly (bottom middle) and weekly (bottom right) variations of corrected $PM_{2.5}$ concentrations ($\mu g \cdot m^{-3}$) measured by all low-cost sensor stations (LCSs S2 – S20) and by equivalent monitor the Prague 2-Legerova within the Legerova domain. Measuring period from 30 May 2022 to 28 March 2023 (in monthly graph May to December 2022, January to March 2023). LCSs located at background sites are marked with an asterisk.

**Table S21.** Summary statistics of 1-hour average MARS corrected $PM_{2.5}$ concentrations measured by all LCSs during the Legerova measurement campaign. Valid N = number of valid values, % valid = percentage of valid values in the dataset, CI mean = lower and upper confidence interval of mean, Min = minimum value, Max = maximum value, SD = standard deviation, CI SD = lower and upper confidence interval of standard deviation, SE = standard error of mean. The table is sorted in ascending order according to the mean concentration values. The RM and LCS S4 highlighted in bold were collocated during the campaign. LCSs located at background sites are marked with an asterisk within the ID.

| Measurement ID | Valid N | % Valid | Mean | CI mean (lower) | CI mean (upper) | Median | Min | Max | SD | CI SD (lower) | CI SD (upper) | SE mean |
|---|---|---|---|---|---|---|---|---|---|---|---|---|
| S3* | 7195 | 99.83 | 11.57 | 11.36 | 11.78 | 9.14 | -5.00 | 95.31 | 9.00 | 8.85 | 9.15 | 0.11 |
| S19* | 7197 | 99.86 | 14.23 | 13.97 | 14.48 | 11.36 | -3.67 | 112.76 | 11.00 | 10.83 | 11.18 | 0.13 |
| **RM** | **7090** | **98.38** | **14.73** | **14.46** | **15.01** | **12.00** | **1.00** | **168.00** | **11.73** | **11.54** | **11.93** | **0.14** |
| S16* | 6046 | 83.89 | 15.62 | 15.31 | 15.94 | 12.52 | -5.07 | 122.40 | 12.56 | 12.34 | 12.79 | 0.16 |
| S7* | 7205 | 99.97 | 16.51 | 16.20 | 16.81 | 12.88 | -4.80 | 148.00 | 13.14 | 12.93 | 13.35 | 0.15 |
| S20 | 7206 | 99.99 | 16.77 | 16.49 | 17.05 | 13.39 | -3.03 | 83.17 | 12.25 | 12.05 | 12.45 | 0.14 |
| S18 | 5665 | 78.60 | 16.91 | 16.63 | 17.20 | 14.71 | -3.18 | 137.76 | 10.81 | 10.61 | 11.01 | 0.14 |
| S12 | 7205 | 99.97 | 17.18 | 16.89 | 17.47 | 13.93 | -2.63 | 139.93 | 12.61 | 12.40 | 12.81 | 0.15 |
| S9* | 7202 | 99.93 | 17.40 | 17.10 | 17.71 | 13.99 | -5.03 | 128.83 | 13.30 | 13.09 | 13.52 | 0.16 |
| **S4** | **5947** | **82.52** | **17.47** | **17.21** | **17.73** | **15.70** | **-5.08** | **75.20** | **10.35** | **10.16** | **10.53** | **0.13** |
| S10 | 7206 | 99.99 | 17.94 | 17.65 | 18.23 | 15.04 | -2.49 | 156.26 | 12.61 | 12.41 | 12.82 | 0.15 |
| S5 | 7206 | 99.99 | 17.97 | 17.65 | 18.30 | 14.09 | -3.09 | 199.87 | 14.17 | 13.94 | 14.40 | 0.17 |
| S2 | 7206 | 99.99 | 18.24 | 17.91 | 18.58 | 14.07 | -2.79 | 311.90 | 14.37 | 14.14 | 14.61 | 0.17 |
| S15 | 7206 | 99.99 | 18.44 | 18.15 | 18.73 | 15.46 | -2.85 | 77.69 | 12.45 | 12.25 | 12.66 | 0.15 |
| S14 | 7206 | 99.99 | 19.97 | 19.65 | 20.28 | 16.50 | -12.46 | 127.27 | 13.71 | 13.49 | 13.94 | 0.16 |
| S11 | 7205 | 99.97 | 21.06 | 20.67 | 21.45 | 16.00 | -2.40 | 161.40 | 16.79 | 16.52 | 17.07 | 0.20 |
| S13 | 7206 | 99.99 | 22.28 | 21.87 | 22.69 | 17.76 | -3.74 | 181.88 | 17.76 | 17.47 | 18.05 | 0.21 |

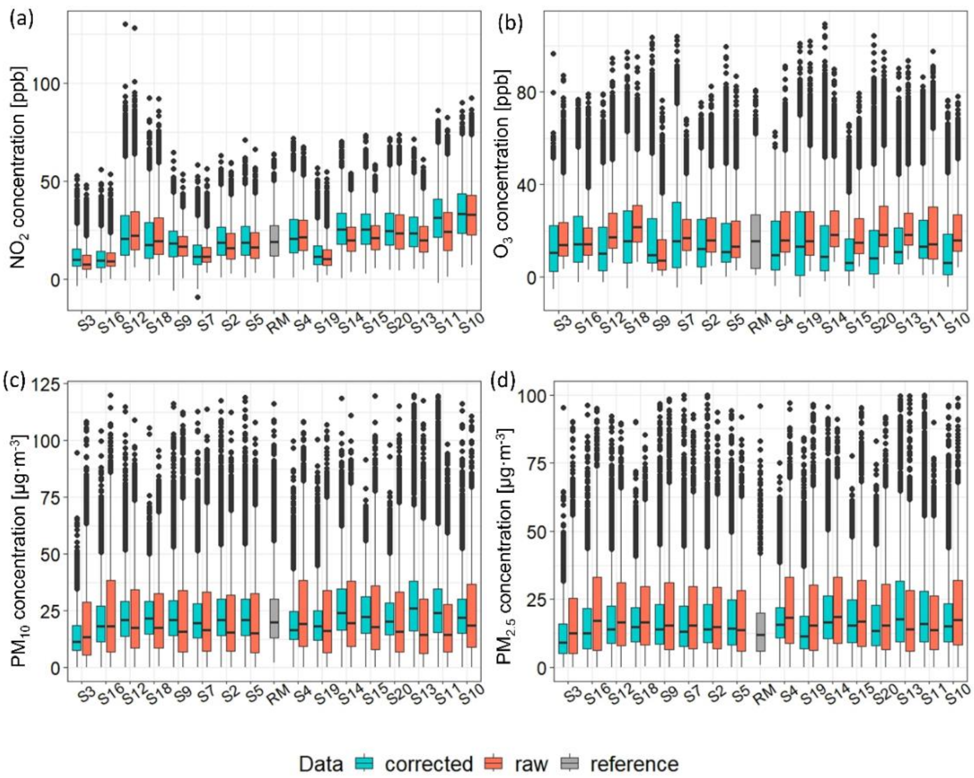


**Figure S42.** Boxplot showing medians and ranges of (a) $NO_2$, (b) $O_3$, (c) $PM_{10}$ and (d) $PM_{2.5}$ hourly averaged concentrations originally measured by LCSs (raw; red colour), corrected by the MARS method (corrected; blue colour) and by reference or equivalent method (RM; grey colour) during the Praha Legerova measurement campaign lasting from 30 May 2022 to 28 March 2023. The X-axis is sorted according to the measurement deployment sites. Black dots show the deviated concentrations. Some weakly negative values are shown in MARS corrected data (less than 1 % of the whole dataset for gases and less than 3 % for aerosols).

### S3.2.2 Episodes with temporarily increased air pollution

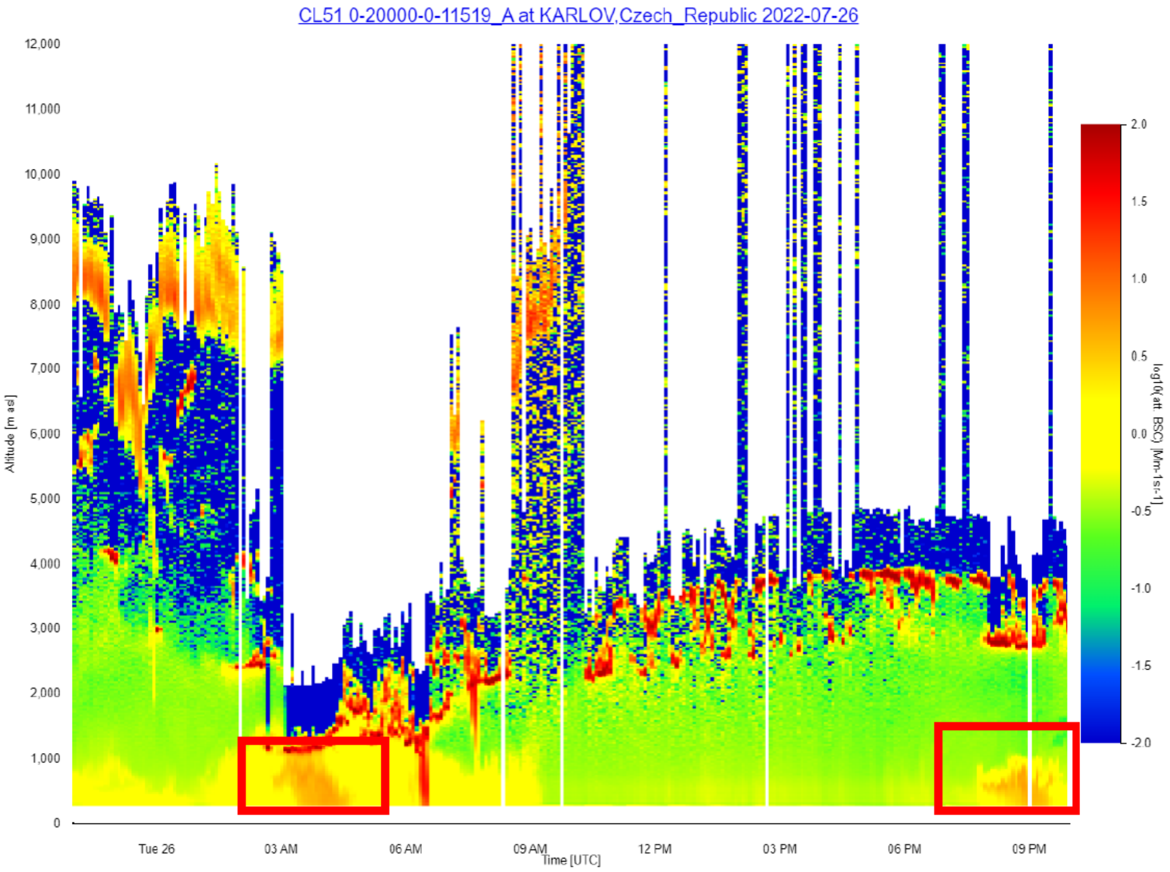


**Figure S43.** Aerosol pollution (orange-red colour; highlighted in red rectangles) detected in attenuated backscatter profile up to the height approximately 1,000 m a.g.l. Measured by Vaisala ceilometer CL51 at the Prague Karlov MS during the Legerova campaign on 26 July 2022 between 2 a.m. and 5 a.m. UTC and between 8 p.m. and 11 p.m. UTC. The increased backscatter intensity (strong red colour) in between 800 and 1,000 m a.g.l. at 3 a.m. was caused by low clouds above the aerosol layer.

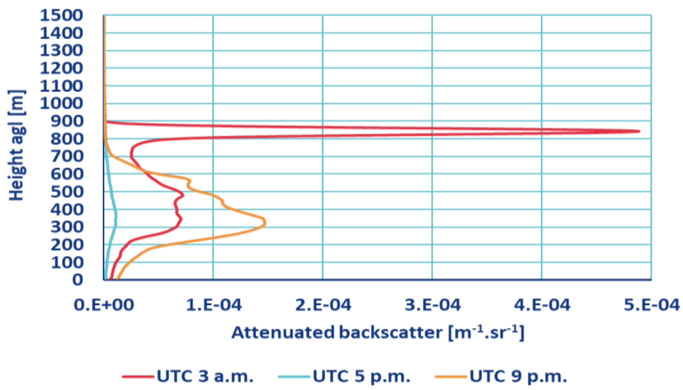


**Figure S44.** The attenuated backscatter intensity [$m^{-1}\cdot sr^{-1}$] measured by doppler LIDAR placed in PVK roof on 26 July 2022 during the Legerova campaign. Increased backscatter intensity detected in between 200 and 600 m height a.g.l. at 3 a.m. and 9 p.m. was caused by aerosol pollution transported from forest fire in Hřensko. The increased backscatter intensity in between 800 and 1000 m a.g.l. at 3 a.m. was caused by low clouds above the aerosol layer.

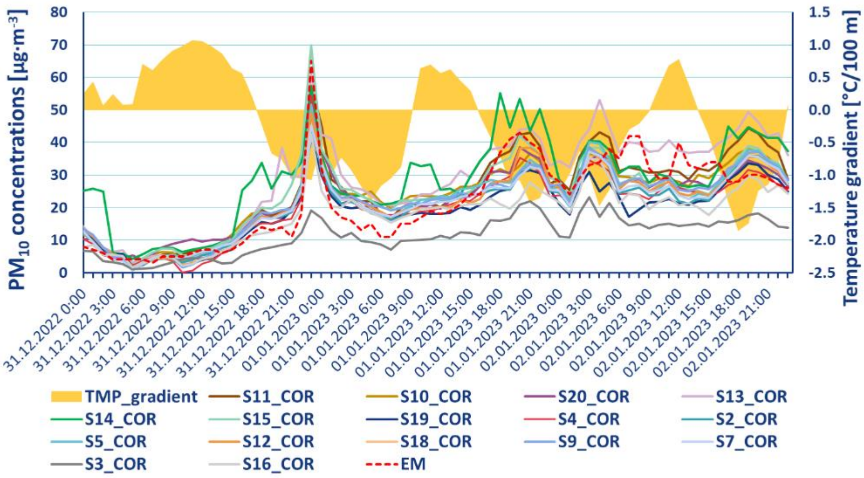


**Figure S45.** The course of MARS corrected 1-hour average $PM_{10}$ concentrations (µg·m$^{-3}$) during the New Year's Eve (31 December 2022). The temperature gradient (°C/100 m) is shown for the continuity with TMP inversion conditions.

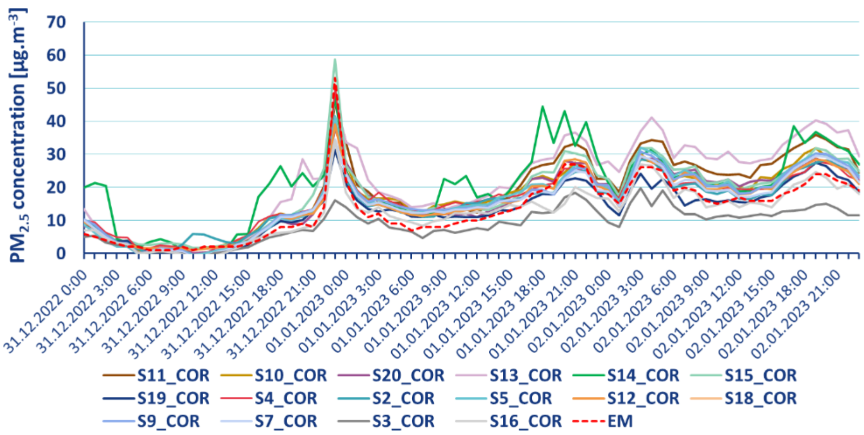


**Figure S46.** The course of MARS corrected 1-hour average $PM_{2.5}$ concentrations (µg·m$^{-3}$) during the New Year's Eve (31 December 2022).

### S3.2.3 The association between atmospheric temperature stratification and air pollution (examples of particular days)

Here is an example of fast reconstruction of TMP stratification in the atmospheric boundary layer, which corresponds well to the pollution situation, especially in the case of aerosol ($NO_2$ concentrations were driven more by traffic patterns on the streets) during 24 September 2022. Figure S47 shows the change of atmospheric stability according to the potential TMP gradient. On this day the vertical profile measurements showed the TMP inversion with a peak at the height of 400-450 m a.g.l. at 3 and 6 a.m. UTC (with the TMP difference of 2.56 °C between 0 and 400 m height a.g.l. at 3 a.m. UTC and 2.76 °C between 0 and 450 m height a.g.l. at 6 a.m. UTC; see Fig. S48a). At the same times (3 and 6 a.m. UTC), two layers with evident low-level jet were noted in the wind profile within this nocturnal inversion (at height 46.6 m a.g.l. WV around 1.5 m·s$^{-1}$ and at 226 m a.g.l. 6.49 m·s$^{-1}$ at 3 a.m. UTC and at 173 m a.g.l. 4.58 m·s$^{-1}$ at 6 a.m. UTC with a rapid decrease of the WV with height in both cases) including a partial change in WD between 46.4 m and 200 m a.g.l. (see Fig. S48b and Fig. S48c). At 8 a.m. UTC, the TMP inversion was no longer occurring and at 3 p.m. UTC the profile was already almost adiabatic (see Fig. S48a and Fig. S48d). During non-inversion conditions, the WV and WD were much more variable in lower heights (i.e. between 46.4 m and 100 m a.g.l.; see 8 a.m. and 3 p.m. UTC cases in Figures S48e and S48f). Then at 10 p.m. UTC, the nocturnal temperature inversion was again noted (Fig. S48d). This change in atmospheric stratification corresponded well with the pollution situation, especially in the case of aerosol ($NO_2$ concentrations followed more the traffic regime on the streets; see Fig. S49). An example of slower and less intense change in stratification including low-level jets and the follow-up to the air pollution changes is shown on 13 February 2023 in Fig. S50 and Fig. S51.

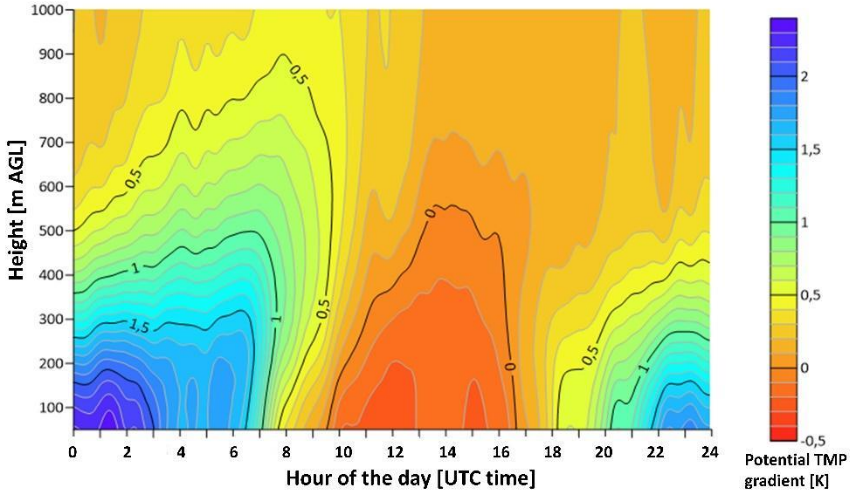


**Figure S47.** Evolution of the stability of the atmospheric boundary layer according to the potential temperature gradient measured by microwave radiometer on the Prague Karlov MS roof on 24 September 2022.

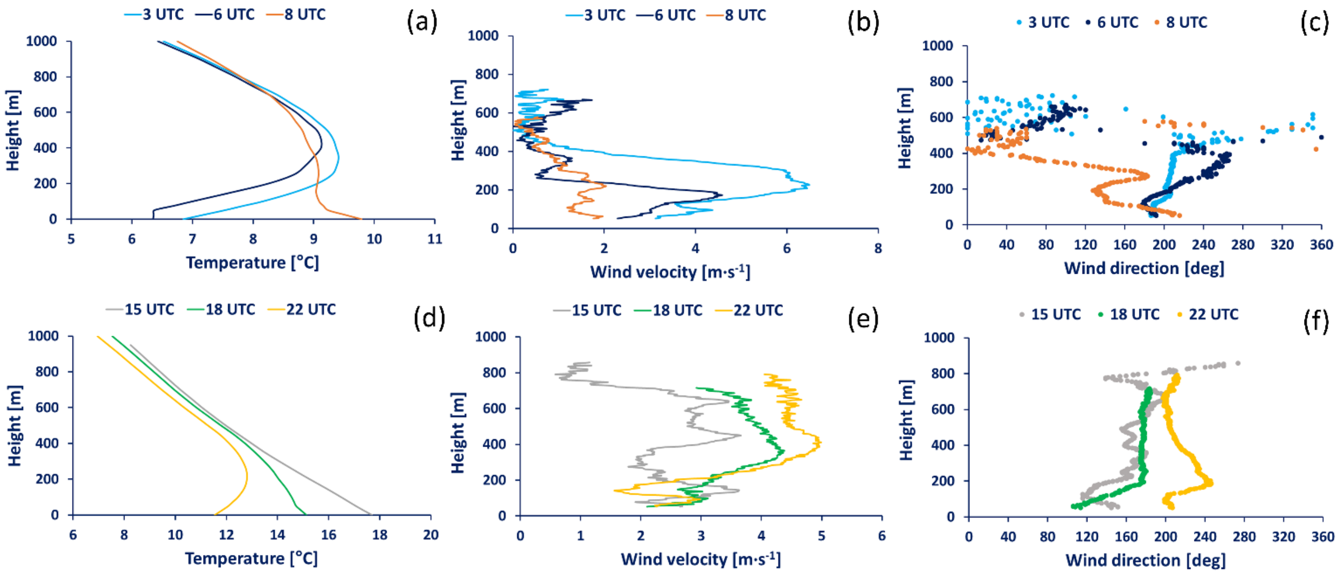


**Figure S48.** Example of temperature (TMP), wind velocity (WV) and wind direction (WD) profiles during 24 September 2022 with a fast reconstruction of TMP stratification within the lower boundary layer. The TMP profiles were measured by MWR at the Prague Karlov MS at (a) 3:00, 6:00 and 8:00 UTC time and at (d) 15:00, 18:00 and 22:00 UTC time; WV and WD profiles were measured by LIDAR at the PVK roof at (b+c) 3:00, 6:00 and 8:00 UTC time and at (e+f) 15:00, 18:00 and 22:00 UTC time.

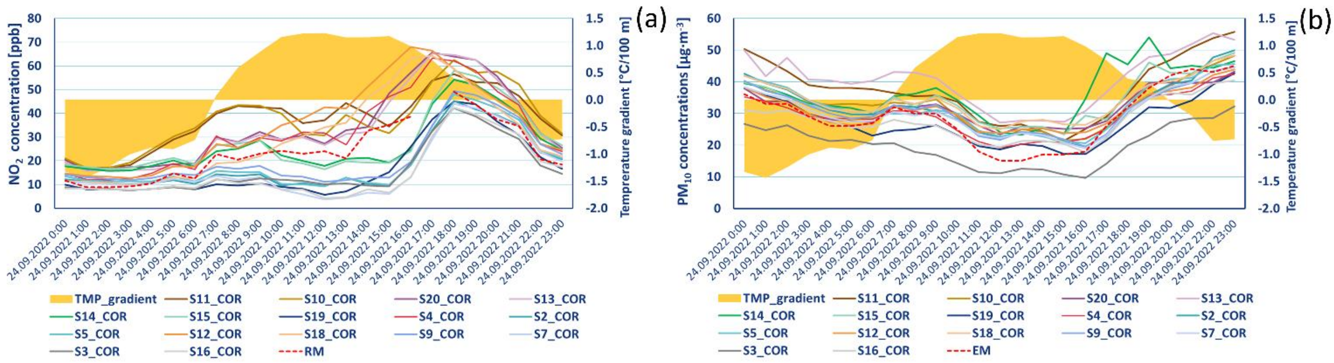


**Figure S49.** The course of 1-hour average (a) $NO_2$ and (b) $PM_{10}$ concentrations measured by low-cost sensors at different locations within the Legerova campaign on 24 September 2022. The temperature inversion and non-inversion conditions are shown by the temperature gradient (°C/100 m).

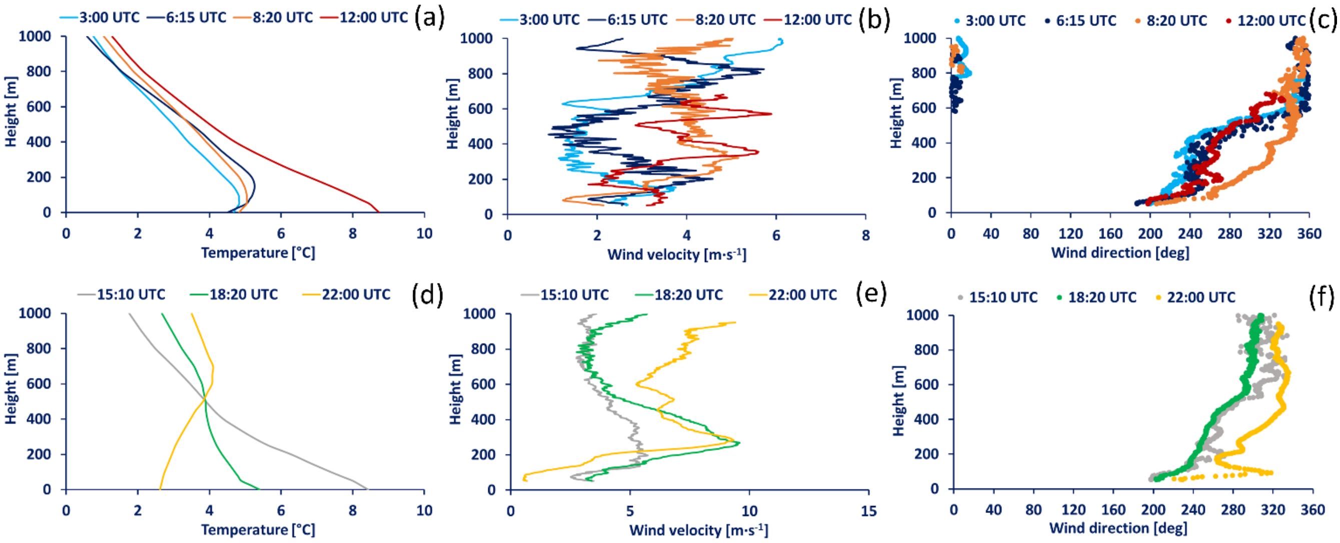


**Figure S50.** Example of temperature (TMP), wind velocity (WV) and wind direction (WD) profiles during 13 February 2023 with change in TMP stratification within the lower boundary layer. The TMP profiles were measured by MWR at the Prague Karlov MS at (a) 3:00, 6:15, 8:20, 12:00 UTC and at (d) 15:10, 18:20 and 22:00 UTC; WV and WD profiles measured by LIDAR at the PVK roof at (b+c) 3:00, 6:15, 8:20, 12:00 UTC, and at (e+f) 15:10, 18:20 and 22:00 UTC.

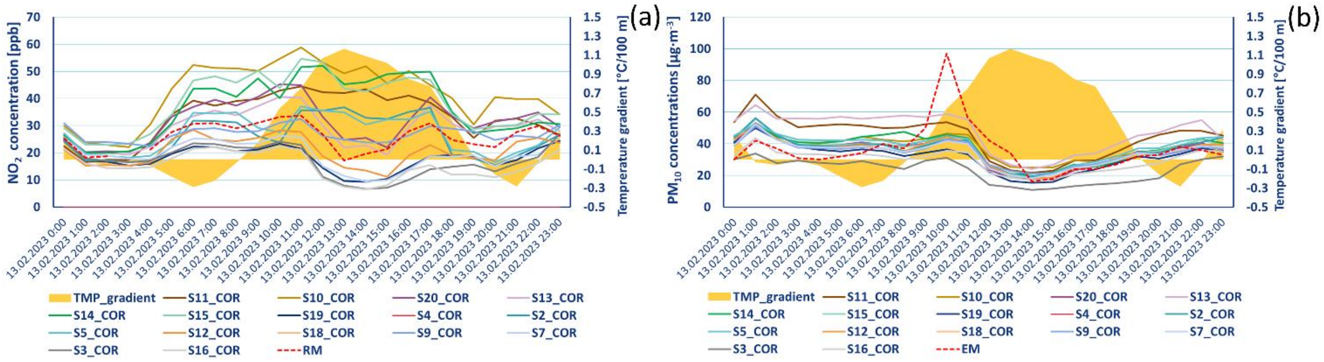


**Figure S51.** The course of 1-hour average (a) $NO_2$ and (b) $PM_{10}$ concentrations measured by low-cost sensors at different locations within the Legerova campaign on 13 February 2023. The temperature inversion and non-inversion conditions are shown by the temperature gradient (°C/100 m).

### S3.2.4 Meteorological measurement in Legerova campaign

The results of meteorological mast measurement in the PVK garden between 1 June 2022 and 19 April 2023 showed quite normal (expected) courses of TMP, RH and WV (Figs. S52-S54 and summary statistics in Tables S22-S24 below). In the case of TMP, the threshold of 30 °C was exceeded for a total of 11 days during June and July 2022 (maximum TMP 37.13 °C on 19 June 2022; the longest period of TMPs over 30 °C lasted four consecutive days during 19-22 July 2022). Conversely, TMPs below 0 °C were measured in nine consecutive days during 10-19 December 2022. The coldest 1-hour average TMP of −8.88 °C was observed during the cold period of 12-14 December 2022. The TMP gradients calculated from the lowest 200 m of TMP profiles showed that in the period between 23 February 2022 and 28 March 2023 (398 days) there were a total of 279 days with the occurrence of TMP inversion conditions. The deepest inversion (TMP gradient higher than −3.5 °C/100 m) was detected on 24 March 2022 between 3 a.m. and 5 a.m. UTC (Fig. S55).

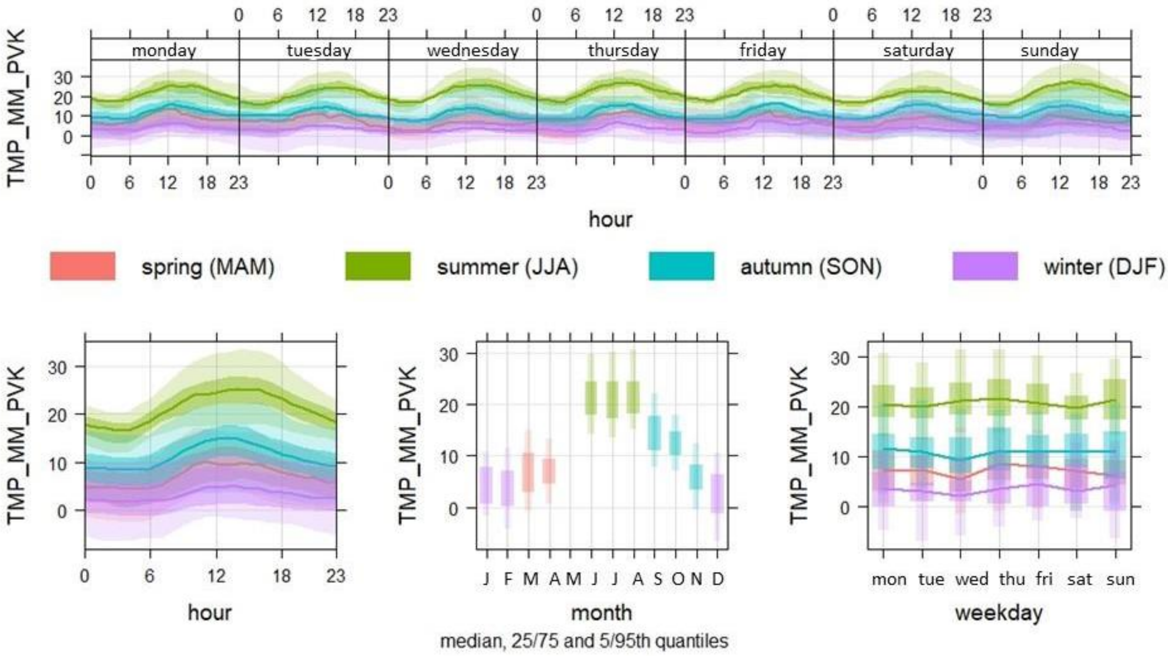


**Figure S52.** Daily (top), hourly (bottom left), monthly (bottom middle) and weekly (bottom right) variations of temperatures (°C) measured by meteorological mast at PVK garden, all sorted by particular seasons. Measuring period from 1 June 2022 to 19 April 2023 (in monthly graph May to December 2022, January to April 2023).

**Table S22.** The summary statistics of temperature (TMP, °C) measured by meteorological mast (MM) at PVK garden during the whole measurement campaign (from June 2022 to April 2023). Valid N = number of valid 1-hour averaged values, CI mean lower and upper = confidence interval of mean -95 % and 95 %; SD = standard deviation; CI SD lower and upper = confidence interval of standard deviation - 95 % and 95 %; SE mean = standard error of mean.

| Month / Year | Valid N | % Valid | Mean | CI mean (lower) | CI mean (upper) | Median | Min | Max | SD | CI SD (lower) | CI SD (upper) | SE mean |
|---|---|---|---|---|---|---|---|---|---|---|---|---|
| 6/22 | 4262 | 99.95 | 21.36 | 21.22 | 21.50 | 20.89 | 11.21 | 37.13 | 4.76 | 4.66 | 4.86 | 0.07 |
| 7/22 | 4462 | 99.96 | 20.93 | 20.78 | 21.07 | 20.41 | 10.40 | 35.49 | 5.00 | 4.90 | 5.11 | 0.07 |
| 8/22 | 4462 | 99.96 | 21.49 | 21.35 | 21.62 | 20.78 | 11.88 | 33.99 | 4.56 | 4.46 | 4.65 | 0.07 |
| 9/22 | 4320 | 100.00 | 14.45 | 14.31 | 14.58 | 14.47 | 4.19 | 26.84 | 4.49 | 4.40 | 4.59 | 0.07 |
| 10/22 | 4462 | 99.96 | 12.39 | 12.29 | 12.48 | 12.23 | 2.97 | 23.07 | 3.35 | 3.28 | 3.42 | 0.05 |
| 11/22 | 4320 | 100.00 | 5.57 | 5.46 | 5.69 | 5.09 | -3.48 | 16.15 | 3.71 | 3.63 | 3.79 | 0.06 |
| 12/22 | 4464 | 100.00 | 2.39 | 2.24 | 2.55 | 1.95 | -8.88 | 17.50 | 5.34 | 5.23 | 5.45 | 0.08 |
| 1/23 | 4462 | 99.96 | 4.27 | 4.15 | 4.39 | 3.80 | -3.62 | 16.20 | 4.13 | 4.04 | 4.21 | 0.06 |
| 2/23 | 3965 | 98.34 | 3.61 | 3.46 | 3.76 | 3.52 | -8.01 | 13.50 | 4.72 | 4.62 | 4.83 | 0.07 |
| 3/23 | 4464 | 100.00 | 6.91 | 6.76 | 7.05 | 6.76 | -3.53 | 20.03 | 4.88 | 4.78 | 4.98 | 0.07 |
| 4/23 | 2669 | 100.00 | 7.15 | 7.01 | 7.29 | 7.40 | -2.87 | 15.61 | 3.65 | 3.56 | 3.75 | 0.07 |

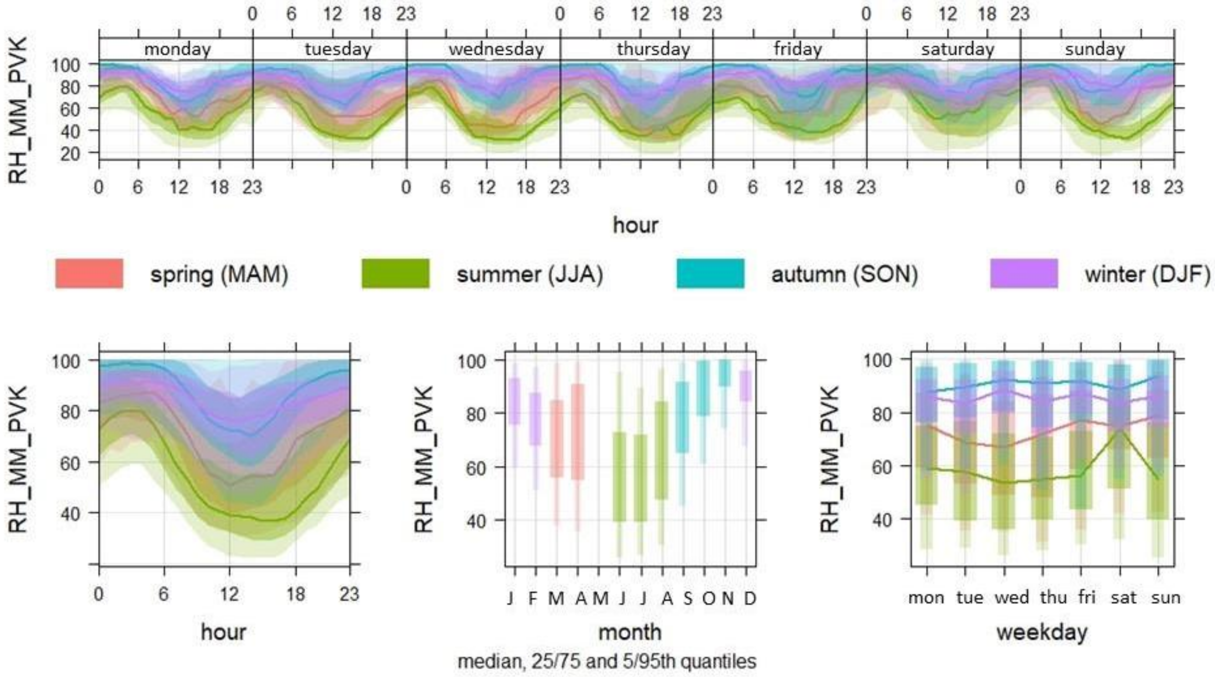


**Figure S53.** Daily (top), hourly (bottom left), monthly (bottom middle) and weekly (bottom right) variations of relative humidity (%) measured by meteorological mast at PVK garden, all sorted by particular seasons. Measuring period from 1 June 2022 to 19 April 19 2023 (in monthly graph May to December 2022, January to April 2023).

**Table S23.** The summary statistics of relative humidity (RH, %) measured by meteorological mast (MM) at PVK garden during the whole measurement campaign (from June 2022 to April 2023). Valid N = number of valid 1-hour averaged values, CI mean lower and upper = confidence interval of mean -95% and 95%; SD = standard deviation; CI SD lower and upper = confidence interval of standard deviation - 95% and 95%; SE mean = standard error of mean.

| Month / Year | Valid N | % Valid | Mean | CI mean (lower) | CI mean (upper) | Median | Min | Max | SD | CI SD (lower) | CI SD (upper) | SE mean |
|---|---|---|---|---|---|---|---|---|---|---|---|---|
| 6/22 | 4262 | 99.95 | 57.21 | 56.57 | 57.86 | 55.52 | 15.94 | 100.00 | 21.52 | 21.07 | 21.98 | 0.33 |
| 7/22 | 4462 | 99.96 | 55.84 | 55.26 | 56.42 | 53.90 | 18.63 | 100.00 | 19.80 | 19.39 | 20.22 | 0.30 |
| 8/22 | 4462 | 99.96 | 65.07 | 64.44 | 65.71 | 65.56 | 26.15 | 100.00 | 21.60 | 21.17 | 22.06 | 0.32 |
| 9/22 | 4320 | 100.00 | 76.98 | 76.48 | 77.47 | 79.22 | 32.36 | 100.00 | 16.65 | 16.30 | 17.01 | 0.25 |
| 10/22 | 4462 | 99.96 | 86.89 | 86.50 | 87.28 | 90.27 | 42.30 | 100.00 | 13.36 | 13.09 | 13.64 | 0.20 |
| 11/22 | 4320 | 100.00 | 93.43 | 93.18 | 93.69 | 97.29 | 57.87 | 100.00 | 8.52 | 8.35 | 8.71 | 0.13 |
| 12/22 | 4464 | 100.00 | 88.49 | 88.19 | 88.78 | 90.40 | 47.53 | 100.00 | 10.00 | 9.80 | 10.21 | 0.15 |
| 1/23 | 4462 | 99.96 | 82.81 | 82.45 | 83.17 | 84.45 | 39.98 | 100.00 | 12.29 | 12.04 | 12.55 | 0.18 |
| 2/23 | 3965 | 98.34 | 76.61 | 76.18 | 77.04 | 78.04 | 31.29 | 100.00 | 13.82 | 13.53 | 14.13 | 0.22 |
| 3/23 | 4464 | 100.00 | 70.21 | 69.68 | 70.74 | 72.29 | 27.54 | 100.00 | 18.05 | 17.68 | 18.43 | 0.27 |
| 4/23 | 2669 | 100.00 | 72.35 | 71.57 | 73.13 | 76.95 | 28.45 | 100.00 | 20.64 | 20.10 | 21.21 | 0.40 |

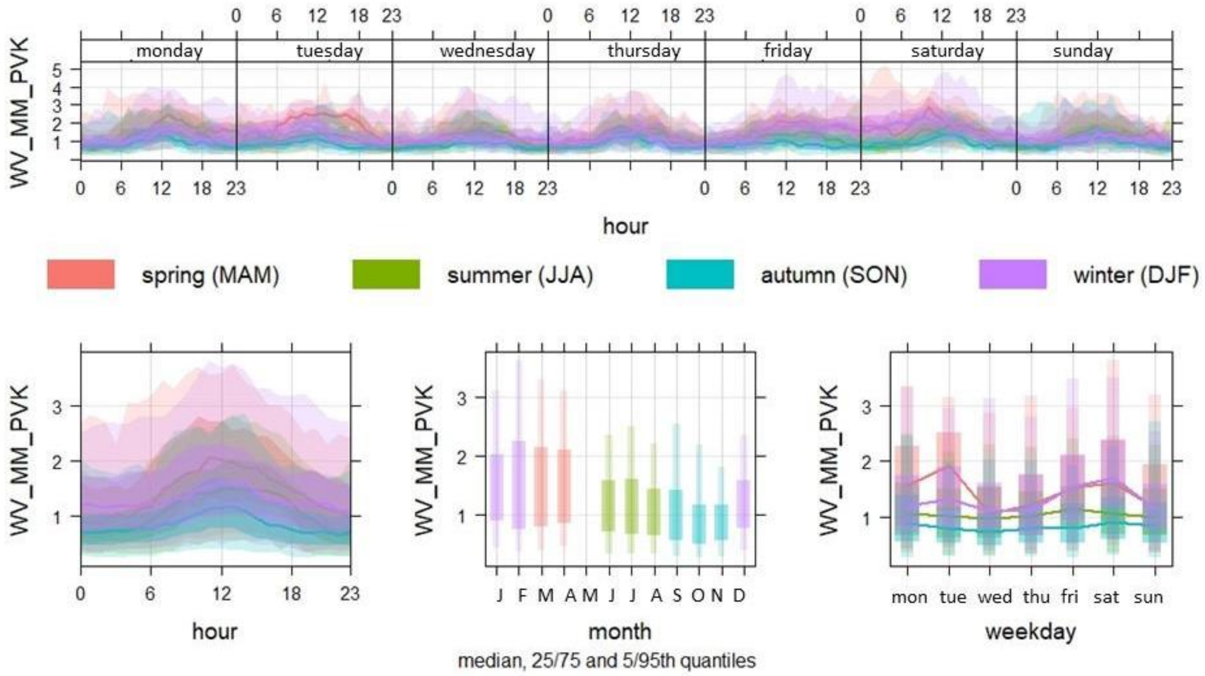


**Figure S54.** Daily (top), hourly (bottom left), monthly (bottom middle) and weekly (bottom right) variations of wind velocity ($m \cdot s^{-1}$) measured by meteorological mast at PVK garden, all sorted by particular seasons. Measuring period from 1 June 2022 to 19 April 2023 (in monthly graph May to December 2022, January to April 2023).

**Table S24.** The summary statistics of wind velocity (WV, $m \cdot s^{-1}$) measured by meteorological mast (MM) at PVK garden during the whole measurement campaign (from June 2022 to April 2023). Valid N = number of valid 1-hour averaged values, CI mean lower and upper = confidence interval of mean -95% and 95%; SD = standard deviation; CI SD lower and upper = confidence interval of standard deviation - 95% and 95%; SE mean = standard error of mean.

| Month Year | Valid N | % Valid | Mean | CI mean (lower) | CI mean (upper) | Median | Min | Max | SD | CI SD (lower) | CI SD (upper) | SE mean |
|---|---|---|---|---|---|---|---|---|---|---|---|---|
| 6/22 | 4262 | 99.95 | 1.18 | 1.16 | 1.20 | 1.10 | 0.00 | 3.74 | 0.62 | 0.61 | 0.64 | 0.01 |
| 7/22 | 4462 | 99.96 | 1.19 | 1.17 | 1.21 | 1.06 | 0.05 | 5.02 | 0.67 | 0.66 | 0.68 | 0.01 |
| 8/22 | 4462 | 99.96 | 1.08 | 1.07 | 1.10 | 0.97 | 0.01 | 4.55 | 0.59 | 0.58 | 0.60 | 0.01 |
| 9/22 | 4320 | 100.00 | 1.08 | 1.05 | 1.10 | 0.87 | 0.03 | 4.22 | 0.71 | 0.69 | 0.72 | 0.01 |
| 10/22 | 4462 | 99.96 | 0.91 | 0.89 | 0.93 | 0.75 | 0.03 | 3.64 | 0.59 | 0.57 | 0.60 | 0.01 |
| 11/22 | 4320 | 100.00 | 0.90 | 0.89 | 0.92 | 0.82 | 0.01 | 3.52 | 0.49 | 0.48 | 0.50 | 0.01 |
| 12/22 | 4464 | 100.00 | 1.25 | 1.23 | 1.26 | 1.17 | 0.02 | 4.56 | 0.63 | 0.62 | 0.64 | 0.01 |
| 1/23 | 4462 | 99.96 | 1.53 | 1.51 | 1.56 | 1.42 | 0.05 | 4.79 | 0.83 | 0.81 | 0.84 | 0.01 |
| 2/23 | 3965 | 98.34 | 1.59 | 1.55 | 1.62 | 1.29 | 0.03 | 6.02 | 1.06 | 1.03 | 1.08 | 0.02 |
| 3/23 | 4464 | 100.00 | 1.55 | 1.52 | 1.58 | 1.36 | 0.00 | 5.77 | 0.94 | 0.92 | 0.96 | 0.01 |
| 4/23 | 2669 | 100.00 | 1.55 | 1.52 | 1.59 | 1.43 | 0.06 | 5.06 | 0.84 | 0.82 | 0.87 | 0.02 |

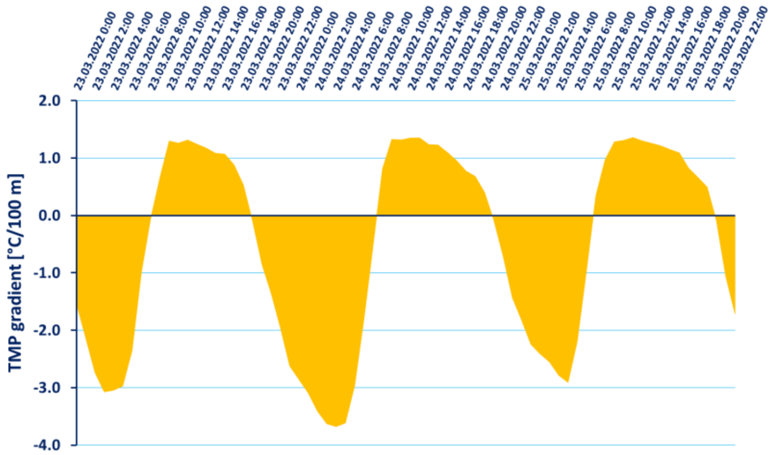


**Figure S55.** Temperature gradient (°C/100 m) calculated from 200 m profile of microwave radiometer temperature measurement at the Prague Karlov MS during 23 – 25 March 2022.

## S4 Discussion

### S4.1 Data quality of supplementary meteorological measurement

The supplementary meteorological measurement by the meteorological mast placed in the PVK garden performed very well in comparison with the adjacent Prague Karlov MS placed on the roof of the university building ($R^2$>0.98 in TMP, RH and p). The biggest differences were in WV and WD which are typical in complex urban environments (Zou et al., 2021). The TMP profile measurement with the MTP-5-He microwave radiometer also reached very high data quality in comparison with the TMP profiles measured by radiosonde from the Prague Libuš MS. The resulting performance was $R^2$>0.98 across different height levels and different launching times (0, 6, 12 UTC). High measurement quality (with mentioned maximum accuracy between 0.5-0.8 °C) was also described in Kadygrov et al. (2015), Kadygrov and Pick (1998) and Pietroni et al. (2014) during the comparison of the MTP-5 measurement against *in situ* measurements. Although for example Argentini et al. (2009) described that this type of radiometer has difficulties in detecting and measuring elevated temperature inversions, we did not observe this pattern. Although it should be noted that our data verification was not within the co-location of the instruments, but they were about 8 km apart by air. Other uncertainties were described by Ezau et al. (2013), who discovered that the formation of a thin water film (of ice or, to a smaller degree, of sleet) on the surface of the older type MTP-5 sensor cover has a significant impact on the data quality of the TMP monitoring. Therefore, we have additionally included the comparison of MTP-5 measurements with a radiosonde in dates and times with recorded precipitations at the Prague Karlov MS. The resulting $R^2$ under rainy conditions was in our case 0.97 and higher at different height levels (with sample size n = 1172). The wind profile data measured by the Doppler LIDAR StreamLine XR placed on the PVK roof with the VAD 6 scan mode setting were not verified within this study (against radiosonde or in situ measurement) because the different spatial conditions (and distance) in the deployment locations of the measurements in this case had a disturbing effect and such a comparison would not be representative. Nevertheless, the quality of wind profiles and root-mean-square deviations (RMSDs) from different VAD scanning programs were tested several times in comparison with radiosondes and meteorological masts, overall with the resulting $R^2$>0.80 (e.g. studies by Newsom and Krishnamurthy, 2022; Newsom et al., 2017; Tzadok et al., 2022). Moreover, Rahlves et al. (2022) demonstrated that the VAD 6 scanning program performs more accurately in the case of WV than the VAD 24 program. Within the framework of WV profile data pre-processing, the method using the standard deviations of WV calculated in the sliding high-range window and the DMC visualisation was tested for possible flexible identification of sudden changes within the profiles. Although this method appears to be usable in most cases (with the occurrence of a few exceptions in erroneous determination), it needs to be subjected to further investigation and testing in future.

## S4.2 Air quality and meteorological measurement within Legerova campaign

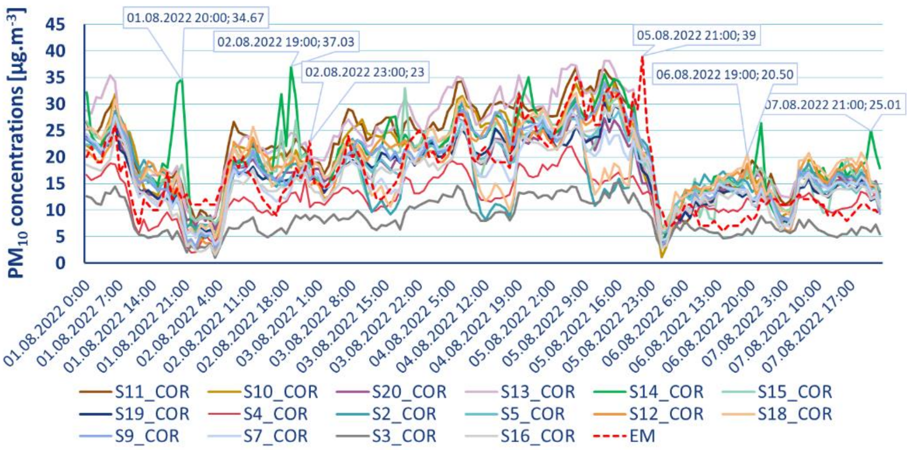


**Figure S56.** The course of the MARS corrected $PM_{10}$ concentrations ($\mu g \cdot m^{-3}$) measured by different LCSs and EM (Fidas at Prague Legerova RM) during the Prague Legerova campaign. Showed data from the period 1–7 August 2022. The afternoon concentration peaks are pointed out.

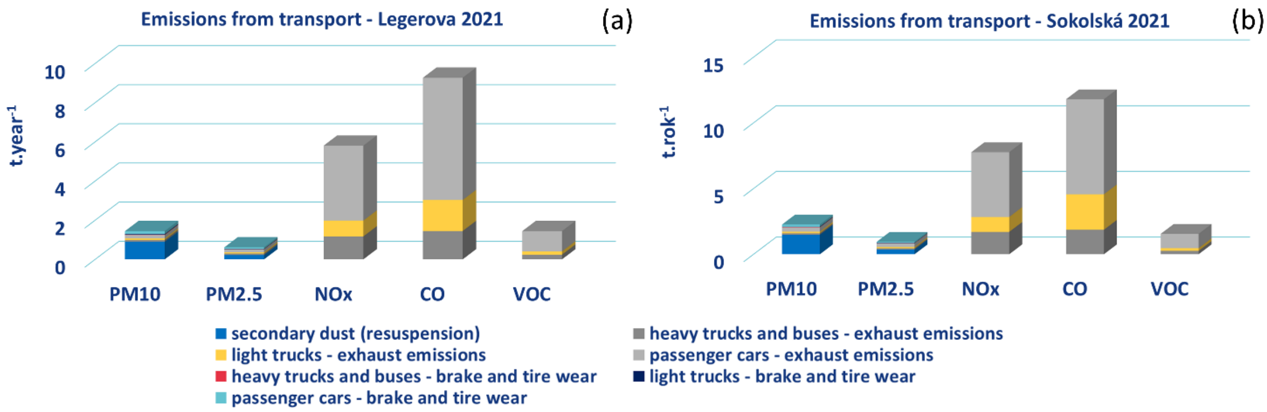


**Figure S57.** Representation of various types of transport emissions of selected pollutants ($PM_{10}$, $PM_{2.5}$, $NO_x$, CO and VOC) in (a) Legerova and (b) Sokolská street (Prague), both year 2021. Exhaust and tyre and break wear emissions were calculated by the MEFA 13 model (ATEM, 2013), resuspension according to the methodology approved by the Czech Ministry of Environment (CESNET, 2015).

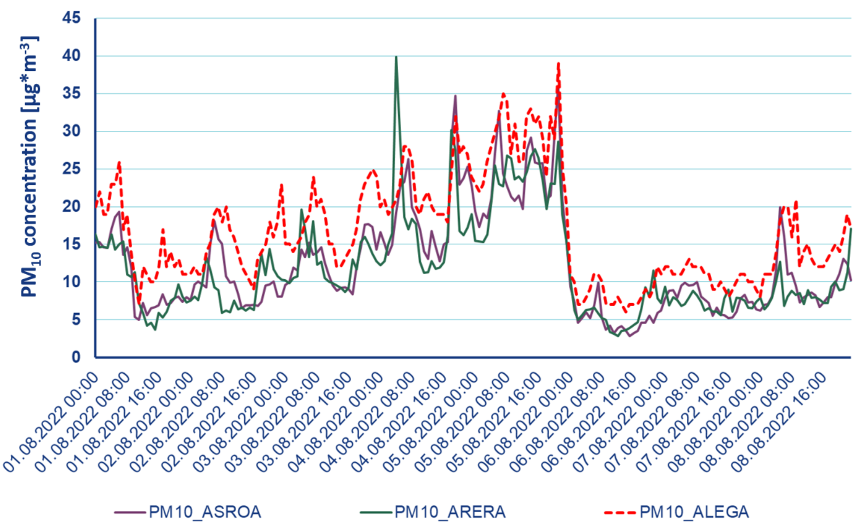


**Figure S58.** The course of $PM_{10}$ concentrations ($\mu g \cdot m^{-3}$) measured during 1-8 August 2022 (Monday-Sunday) at the reference transport station Prague Legerova (ALEGA), at the urban background station Prague Šrobárova (ASROA) and at the suburban background station Prague Řeporyje (ARERA). All stations measure with the optoelectronic equivalent monitor FIDAS200, Palas.

## References


Argentini, S., Pietroni, I., Gariazzo, C., Amicarelli, A., Mastrantonio, G., Pelliccioni, A., Petenko, I., and Viola, A.: Boundary layer temperature profiles by a RASS and a microwave radiometer: Differences, limits and advantages, Il Nuovo Cimento B, 124, 549–564, https://doi.org/10.1393/ncb/i2009-10791-9, 2009.

Arya, S. P.: Introduction to Micrometeorology, Academic Press, San Diego, 420 pp., ISBN 0-12-059354-8, 2001.

ATEM, 2013. MEFA 13 - software for calculation of emissions from road vehicles, https://www.atem.cz/mefa.php, last access: 20. January 2025.

CESNET, 2015. Metodika pro výpočet emisí částic pocházejících z resuspenze ze silniční dopravy. https://www.mzp.cz/C1257458002F0DC7/cz/doprava/$FILE/OOO-resuspenze_metodika-20190708.pdf, last access: 20 January 2025

Everingham, Y.L., Sexton, J., and White, J.: An introduction to multivariate adaptive regression splines for the cane industry. In: Proceedings of the 2011 Conference of the Australian Society of Sugar Cane Technologists. pp. 1-22. From: 2011 Conference of the Australian Society of Sugar Cane Technologists, 4-6 May 2011, Mackay, QLD, Australia, 2011.

Ezau, I. N., Wolf, T., Miller, E. A., Repina, I. A., Troitskaya, Yu. I., and Zilitinkevich, S. S.: The analysis of results of remote sensing monitoring of the temperature profile in lower atmosphere in Bergen (Norway), Russ. Meteorol. Hydro., 38, 715–722, https://doi.org/10.3103/S1068373913100099, 2013.

Friedman, J. H.: Estimating Functions of Mixed Ordinal and Categorical Variables Using Adaptive Splines, Department of Statistics, Standford University, Stanford, California, 49 pp, 1991a.

Friedman, J. H.: Multivariate Adaptive Regression Splines. The Annals of Statistics, 19(1), 1-67, 1991b.

Gill: WindSonic, Wind Speed & Direction Sensor. Datasheet: https://gillinstruments.com/compare-2-axis-anemometers/windsonic-2axis/, last access: 13 December 2023, 2023a.

Gill: MetConnect THP, Professional Weather Station. Datasheet: https://gillinstruments.com/compare-weather-stations/metconnect-weather-station/, last access: 13 December 2023, 2023b.

IFU: MTP-5 Microwave radiometer. Datasheet: https://www.temperaturprofile.de/PRODUKTE/MTP-5/, last access: 20 December 2023, 2023.

Kadygrov, E. N. and Pick, D. R.: The potential for temperature retrieval from an angular-scanning single-channel microwave radiometer and some comparisons within situ observations, Met. Apps, 5, 393–404, https://doi.org/10.1017/S1350482798001054, 1998.

Kadygrov, E. N., Ganshin, E. V., Miller, E. A., and Tochilkina, T. A.: Ground-based microwave temperature profilers: Potential and experimental data, Atmos Ocean Opt, 28, 598–605, https://doi.org/10.1134/S102485601506007X, 2015.

Leathwick, J. R., Elith, J., and Hastie, T.: Comparative performance of generalized additive models and multivariate adaptive regression splines for statistical modelling of species distributions, Ecological Modelling, 199, 188–196, https://doi.org/10.1016/j.ecolmodel.2006.05.022, 2006.

Metek: Doppler Lidar Streamline AllSky XR, METEK. Datasheet: https://metek.de/product/streamline-xr/, last access: 10 December 2023, 2023.

Newsom, R. and Krishnamurthy, R.: Doppler Lidar (DL) Instrument Handbook, https://doi.org/10.2172/1034640, 2022.

Newsom, R. K., Brewer, W. A., Wilczak, J. M., Wolfe, D. E., Oncley, S. P., and Lundquist, J. K.: Validating precision estimates in horizontal wind measurements from a Doppler lidar, Atmos. Meas. Tech., 10, 1229–1240, https://doi.org/10.5194/amt-10-1229-2017, 2017.

Pietroni, I., Argentini, S., and Petenko, I.: One year of surface-based temperature inversions at Dome C, Antarctica, Boundary-Layer Meteorol, 150, 131–151, https://doi.org/10.1007/s10546-013-9861-7, 2014.

Rahlves, C., Beyrich, F., and Raasch, S.: Scan strategies for wind profiling with Doppler lidar – an large-eddy simulation (LES)-based evaluation, Atmos. Meas. Tech., 15, 2839–2856, https://doi.org/10.5194/amt-15-2839-2022, 2022.

Smalikho, I. N. and Banakh, V. A.: Measurements of wind turbulence parameters by a conically scanning coherent Doppler lidar in the atmospheric boundary layer, Atmos. Meas. Tech., 10, 4191–4208, https://doi.org/10.5194/amt-10-4191-2017, 2017.

Surfer: Golden Software Surfer, sotware, https://shop.goldensoftware.com/surfer, 2022.

TIBCO: TIBCO Statistica® Software, https://docs.tibco.com/pub/stat/14.1.0/TIB_stat_14.1.0_relnotes.pdf?id=1, 2020.

Tzadok, T., Ronen, A., Rostkier-Edelstein, D., Agassi, E., Avisar, D., Berkovic, S., and Manor, A.: Profiling the Planetary Boundary Layer Wind with a StreamLine XR Doppler LiDAR: Comparison to In-Situ Observations and WRF Model Simulations, Remote Sensing, 14, 4264, https://doi.org/10.3390/rs14174264, 2022.

Vaisala: Ceilometer CL51 for high-range cloud height detection, Vaisala. Datasheet, https://www.vaisala.com/en/products/weather-environmental-sensors/ceilometers-CL31-CL51-meteorology, 2022.

Zou, J., Yu, Y., Liu, J., Niu, J., Chauhan, K., and Lei, C.: Field measurement of the urban pedestrian level wind turbulence, Building and Environment, 194, 107713, https://doi.org/10.1016/j.buildenv.2021.107713, 2021.